



# MONASH University

**Temporal neuronal activity patterns in barrel cortex to simple and complex stimuli and the effects of traumatic brain injury**

*Thomas Francis Burns*

*Bachelor of Science (Honours), Master of Bioethics*

A thesis submitted for the degree of Master of Philosophy at  
Monash University in 2018  
Department of Physiology

## **Copyright notice**

© Thomas Francis Burns 2018.

*I certify that I have made all reasonable efforts to secure copyright permissions for third-party content included in this thesis and have not knowingly added copyright content to my work without the owner's permission.*

This thesis contains no material which has been accepted for the award of any other degree or diploma at any university or equivalent institution and that, to the best of my knowledge and belief, this thesis contains no material previously published or written by another person, except where due reference is made in the text of the thesis.

Signature



Print Name Thomas Francis Burns

Date 16/05/2018

## Abstract

Traumatic brain injury (TBI) is a serious and debilitating health problem worldwide. In this study, an animal model of diffuse TBI (the most common form of TBI) in rat barrel cortex was studied using an established database of in vivo extracellular electrophysiology while naturalistic stimuli were applied to whiskers under anesthesia. Using this database, we characterised and compared the stimulus-evoked activity in cortical layers II and IV. Wistar rats were subjected to a sham surgery (n=13) or TBI (n=23) caused by an established weight-drop method. TBI animals were studied at three time-points after injury: 4-days (n=6), 2-weeks (n=9), and 8-12-weeks (n=8). Past studies indicate some functional recovery across these time-points, however have focused on broad, population-level spike statistics. In this study, we used an algorithm based on local maxima and another using graph theory to identify major temporal neuronal activity components on a unit-by-unit basis in 50ms post-stimulus recording windows for 1,210 online-sorted units. Units were either non-responsive or contained 1-3 major components. Using these components and the categorization of units as non-responsive or containing major components, we analysed the timing of components with respect to the stimulus, the change of proportions in unit categories across conditions and between layers, as well as the temporal regularity of components occurring within the same units. We also analysed how non-stationary units' components were and whether the activity of components within the same units were correlated. We found that the proportions of unit categories were significantly different between layers II and IV for some conditions, especially at the 4-days TBI timepoint where there was a marked increase in the proportion of non-responders and a general reduction in the number of temporal components. For both stimuli, it was possible to clearly associate component timings with prominent features in the stimulus, such as the stimuli's maximum amplitude. Temporal regularity of components within the same units was consistent and significant for the sham condition but such relationships broke down after TBI, especially in the 2-weeks condition. Regularity did reappear, however, in the 8-12-weeks condition. Components were more stationary in layer IV in the 2-week condition compared to sham, and layer II components for both the sham and 2-weeks condition were significantly different than those in layer IV, perhaps indicating a compensatory mechanism. We conclude that microcircuits functionally maladapt and/or reorganize in barrel cortex after diffuse TBI, affecting its ability to encode naturalistic stimuli. Such maladaptation/reorganization is layer-dependent, perhaps due to differences in inhibitory neuronal makeup.

## Contents

Abstract.....	4
Contents.....	5
I. Acknowledgements.....	6
II. Abbreviations .....	7
1. Literature review: Neurophysiology of barrel cortex and traumatic brain injury .....	8
1.1 Whisker-sensing pathways to barrel cortex .....	9
1.2 Barrel cortex somatotopy and microcircuitry.....	11
1.3 Encoding of whisker movement .....	23
1.4 Animal models of brain injury and their effects on cortical inhibition .....	23
1.5 Computational methods .....	27
2. Project summary.....	29
3. Temporal neuronal activity patterns in layers II and IV of rat barrel cortex in response to simple and complex stimuli and the effects of traumatic brain injury .....	31
3.1 Aims and hypotheses .....	31
3.2 Methods .....	32
3.3 Data Analyses and Results .....	37
3.4 Discussion.....	64
4. Bibliography .....	73
5. Appendices.....	86
5.1 Appendix I - Evaluating PCA as a method for identifying and distinguishing between unit activity patterns.....	86
5.2 Appendix II – Time distributions of peak-based TBI components .....	96
5.1 Appendix III – MATLAB implementation of graph theoretic analysis .....	98

## I. Acknowledgements

I wish to thank my many academic mentors and teachers for their assistance throughout my studies at Monash University. I wish to especially thank my academic supervisors for this MPhil project, Prof Ramesh Rajan and Dr Dasuni Alwis, as well as my academic review panel members, postgraduate research coordinators, and examiners. I am also very grateful for the support offered to me by various technical, research, and administration staff within the Department of Physiology. I am also thankful for the support of staff from the Monash Graduate Research Office and Monash Postgraduate Association. The friendship and support of fellow students has also been of tremendous value throughout my studies, as well as the continual support of my family.

## II. Abbreviations

TBI	traumatic brain injury
VPM	ventroposterior medial nucleus
POm	medial posterior nucleus
NRT	nucleus of the thalamus
PMBSF	posteromedial barrel subfield
PW	principal whisker
CBP	calcium-binding protein
PV	parvalbumin
SOM	somatostatin
5-HT <sub>3A</sub> R	5-HT <sub>3A</sub> receptors
GABA	gamma-aminobutyric acid
FS	fast-spiking
BC	basket cell
MC	Martinotti cell
ChC	chandelier cell
NGFC	neurogliaform cell
DBC	double bouquet cell
BTC	bitufted cell
BPC	bipolar cell
vM1	vibrassal motor cortex
CR	calretinin
MPBC	multipolar bursting cell
MPC	multipolar cell
SSC	spiny stellate cell
LBC	large basket cell
SBC	small basket cell
NBC	nest basket cell
DBoC	double bouquet cell
SBoC	single bouquet cell
ENGFC	elongated neurogliaform cell
EE	environmental enrichment
CSD	cortical spreading depression
PSTH	peristimulus time histogram
4d TBI	TBI four-days post-injury
2w TBI	TBI two-weeks post-injury
8-12w TBI	TBI 8-12-weeks post-injury
KS	Kolmogorov–Smirnov
Basic	the trapezoid stimulus
Contact	the naturalistic object contact stimulus
SE	standard error
PCA	principle components analysis
PC	principle component

## 1. Literature review: Neurophysiology of barrel cortex and traumatic brain injury

Sensory information is vital for interacting with the world and fulfilling the basic requirements for human survival, socialization, and cooperation. We use combinations of sensory data streams – auditory, visual, touch, etc. – to interpret and form internal maps of the outside world. It is therefore often debilitating for humans to experience minor or major sensory deficits or perturbations in sensory processing pathways, and such debilitations come at broader social and economic costs <sup>1,2</sup>. Thus, the study of such sensory systems and their deficits is important for human health and wellbeing. Sensory systems are also ideal for basic neuroscience study because sensory information is processed in dedicated, known and highly-structured neural pathways from periphery to cortex and, for the purposes of experimentation, sensory input can be easily manipulated over scales from reductionist through to complex naturalistic stimuli. This allows detailed study of broad questions about how neurons connect and form networks to carry out computations, as well as how different alterations in health states affect these networks. This combination of reasons – understanding the brain in health and in injury with a view to creating the basic neuroscience knowledge base for improving human health – motivates the current thesis.

For bioethical and practical reasons, it is not always preferable or possible to study neural tissues from humans. However, ethical guidelines have been developed for the use of non-human animals <sup>3</sup>, and brain development and likeness to human brains in this context has been studied in detail in relevant non-human animals, particularly rodents <sup>4</sup> which have become popular models for studying brain injury <sup>5</sup> and for basic neuroscience generally <sup>6</sup>. Given the ecological niche they occupy, the rodent face whiskers act as important sensing organs to probe the environment and to interact with conspecifics, especially in the low-light nocturnal conditions when rodents are most active. The whiskers are readily manipulated and the relevant parts of somatosensory cortex are easily accessed via surgery; hence, study of whisker-sensation in rodents has been ongoing in basic and sensory neuroscience for many years <sup>7-11</sup>, including to test the effects of deficit or damage on neural function and structure <sup>5,12,13</sup>.

In this review, I will outline the basic state of knowledge of rodent whisker-sensation physiology and how this system is affected by animal models of traumatic brain injury (TBI). I will first outline the general structural elements in the pathways which allow rats to receive information about the world from their whisker movements. Next, I will discuss the importance of different neuron subtypes in the microcircuits of the somatosensory cortex, where perception occurs. I will then briefly introduce the concept of population coding, especially temporal coding, in the context of barrel cortex. I will summarise

findings from animal models of brain injury and the effect this perturbation has on different neuron subtypes, again with emphasis on the somatosensory cortex. Lastly, I will provide a short introduction to computational methods and concepts utilized in this thesis.

## 1.1 Whisker-sensing pathways to barrel cortex

Sensory whiskers, or vibrissae, are composed of a keratin shaft which extends out from a mammal's body. The shaft itself does not contain nerve fibres but its mechanical manipulation activates mechanoreceptors at its base<sup>14-19</sup>. In the case of the rat, first-order bipolar afferent neurons with terminals contacting the whisker base send axons to synapse in the trigeminal ganglion and the sensory trigeminal nuclei<sup>20</sup>. From here, second-order afferents project to various subcortical nuclei in the brain<sup>21</sup> in complex, detailed arrangements<sup>22-24</sup> (see Figure 1 for a summary of these pathways). This leads to independent levels of activation of the ventroposterior medial nucleus (VPM) and the medial posterior nucleus (POm), the two major thalamic nuclei which will relay the information to cortex. The connection patterns of second-order afferents to VPM and POm achieve two things: (1) it establishes VPM and POm as distinct, specialised information streams relaying different types of information to cortex (see Figure 1); and (2) it maintains a highly organised and systematic representation of information sent by the individual whiskers<sup>25-27</sup>.

The reticular nucleus of the thalamus (NRT) is a common source of inhibition to both VPM and POm. It is activated by corticothalamic feedback and can provide lateral inhibition to neighbouring segments of thalamus representing other, nearby whiskers to inhibit the primary whisker represented by another given segment of thalamus<sup>28-31</sup>. VPM primarily receives inhibition via NRT whereas POm receives additional, intra- and extra-thalamic inhibition<sup>32</sup>. These additional sources of inhibition normally silence POm activity during regular whisker activation<sup>33-35</sup>. The activity of VPM and POm are also susceptible to corticothalamic feedback, especially from cortical layers V and VI<sup>36-42</sup>. Corticothalamic fibres sent to POm are thought to be the main drivers of POm, and fibres sent to VPM help modulate incoming activity. Corticothalamic fibres originating from cortical layer VI have especially strong synapses<sup>43</sup> and are similar in strength to second-order afferent synapses<sup>44</sup> (while most other corticothalamic synapses are relatively weak). In addition to these cortical feedback mechanisms, VPM is additionally modulated by the brainstem<sup>24</sup>. In combination, these sources of inhibition, feedback, and modulation (see Figure 1 for diagrammatic summary) therefore shape the responses of intrinsically excitable thalamocortical cells<sup>22,45</sup> in VPM and POm, which receive sensory information from second-order afferents. This results in the cortex, specifically barrel cortex, receiving a partially filtered sensory signal and not the raw sensory signal itself.

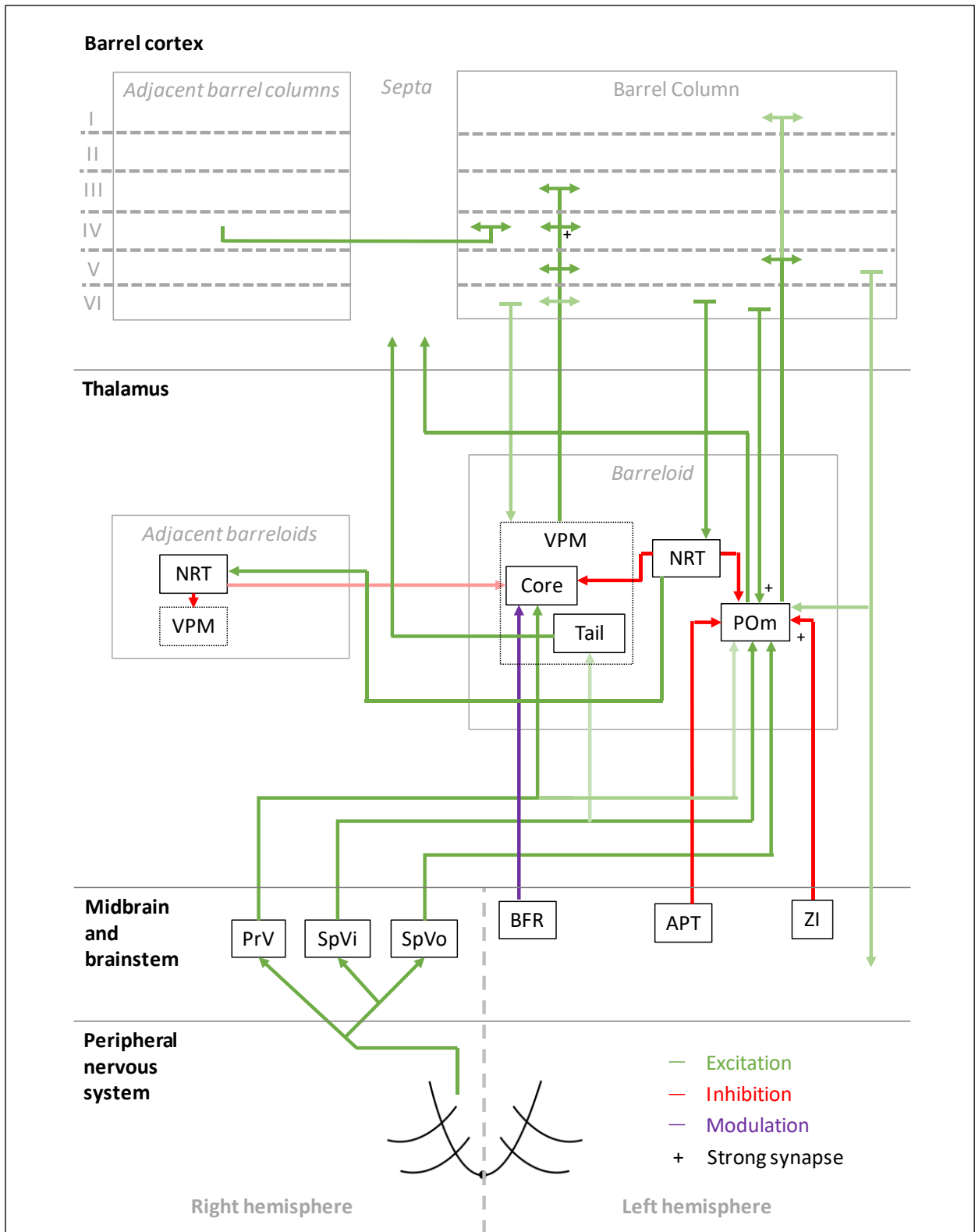
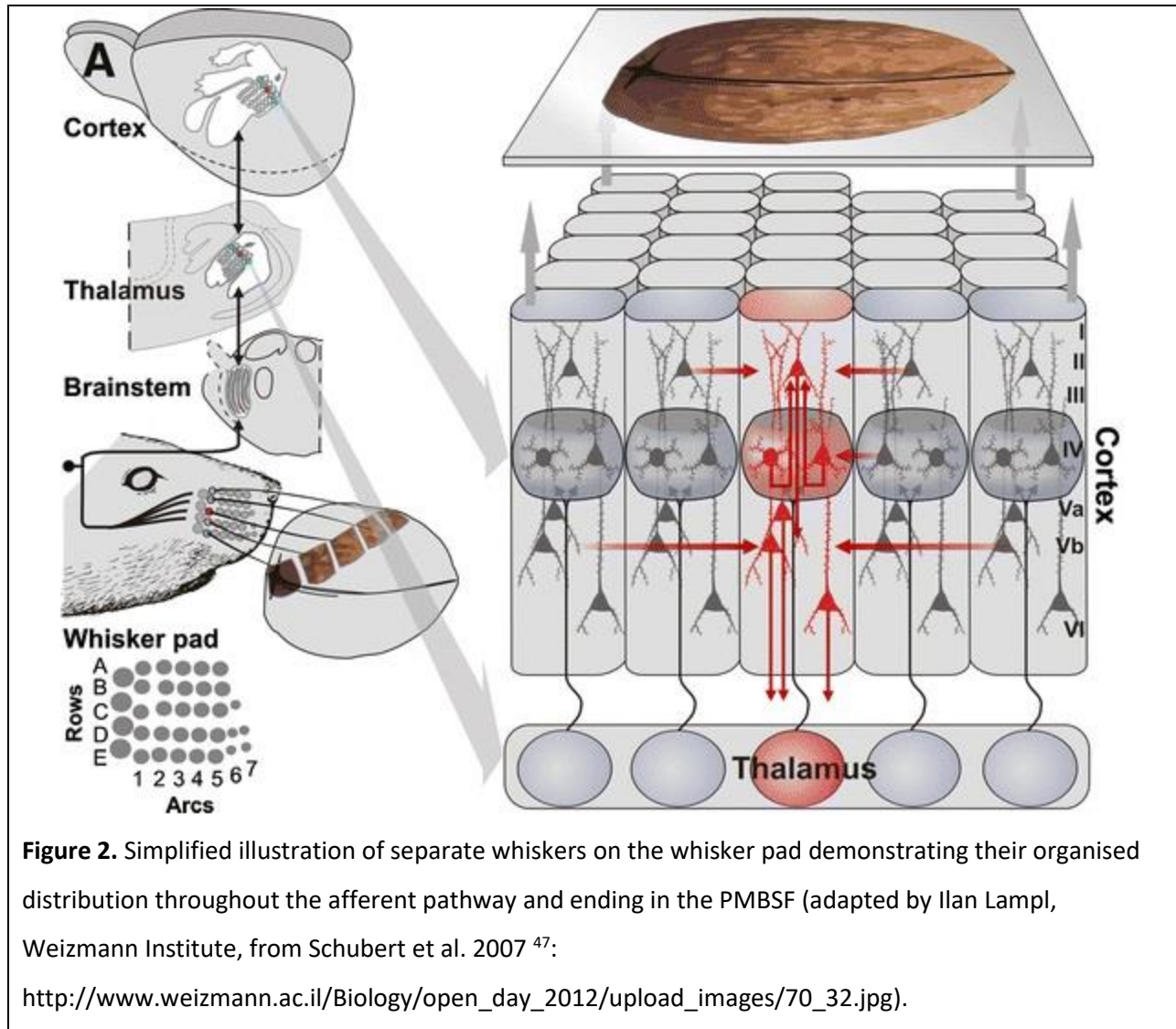


**Figure 1.** Simplified summary of connections of the whisker-sensing thalamus.

Abbreviations: PrV = principal trigeminal nuclei; SpVi = interpolaris subnucleus of the spinal trigeminal nuclei; SpVo = oralis subnucleus of the spinal trigeminal nuclei; BFR = brainstem reticular formation; APT = anterior pretectal nucleus; ZI = zona incerta; other abbreviations same as text. Based on review by Castro-Alamancos<sup>24</sup>.

## 1.2 Barrel cortex somatotopy and microcircuitry

In rodents, whisker sensation is represented in the posteromedial barrel subfield (PMBSF) region of somatosensory cortex, commonly known as *barrel cortex* due to specializations in the organization of neurons in the input layer IV as described below. The PMBSF occupies approximately 70% of primary somatosensory cortex and 13% of the cortical surface<sup>46</sup>, a disproportionately large part of cortex relative to the small external physical size of the whiskers when compared to other parts of the rodent body. This indicates the ecological importance of whisker somatosensation in comparison to other tactile inputs. The PMBSF is organised somatotopically, meaning each of the major facial whiskers is represented, whisker for whisker, in separate columns of neurons extending from the surface to the white matter. Each of these regions which receives a dominant *principal whisker* (PW) input is defined anatomically by the organization of layer IV neurons into 'barrel' like structures with a relatively hollow interior. They are laid out in a grid formation in the PMBSF. The cortical layers above and below a layer IV barrel are often referred to as a 'barrel column' and together represent the cortical column responsible for processing the sensory input from one whisker. The grid formation in PMBSF consists of arcs (columns) and rows of whisker barrels, each representing the same arcs and rows of whiskers found in the whisker pad on the rat face (see bottom-left panel of Figure 2 – notice that this organisation is maintained through the brainstem, thalamus, and cortex). A1 represents the top-most whisker at the nose bridge end, A2 the whisker one closer to the nose in the same row, and so on, right through to E8, which represents the bottom-most whisker at the nose end (n.b. some species-, individual-, and reporting-specific differences will mean a slightly different end whisker count, e.g. E7 as in Figure 2).



Classically, each whisker barrel receives its primary thalamic input mainly at layer IV (Figure 2). This sensory information is then projected up to layers II and III for further processing (along with other local cortical areas), then down to layers V and VI for final output to more distant cortical areas, such as motor cortex (as well as sending feedback to sub-cortical areas) <sup>48</sup>. Layer IV excitatory cells typically have strong, narrow tuning to single whiskers while cells in supra- and infra-granular layers typically show broader, mixed-strength tuning (indicating tuning to more precise, higher-order features, and possibly common to multiple whiskers). Neurons across all layers, but particularly infragranular layers, can be tuned to temporal or qualitative features of whisker deflection, e.g. directional sensitivity or initial versus sustained parts of deflection. Such differences are the result of interaction between the increasing number of complex microcircuits being identified <sup>49-51</sup> both within and between layers, and within and

between barrels<sup>52</sup>. For instance, the septa are innervated by a separate thalamic pathway to the barrels (see Figure 1), and their lateral connections between barrels<sup>51</sup> likely modulate individual barrels' activity. Where<sup>49</sup> and how<sup>53</sup> thalamocortical cells connect within the cortical layers is another source of these differences. And while the VPM and POm pathways appear to target cortex in complementary ways, the relevant feedforward<sup>34,54,55</sup> and feedback<sup>49,56</sup> systems within cortex make the subsequent interlaminar interactions all the more complex, thus interesting and important for sensory processing. For these reasons, the classical, simple view of information flowing neatly and wholly from layer IV, up to II/III, then down to V is increasingly being reinforced in general principle while also undermined by long lists of special cases. In the following sub-sections, we will attempt to follow the general principle view in detail, layer-by-layer, and discuss the implications of relevant special cases.

## Layer IV

Layer IV is the primary input layer from the thalamus and typically has narrow, strong tuning to a single PW. It helps to amplify and further filter the thalamic signal and distribute its activity to other cortical layers, primarily the supragranular layers<sup>49,57,58</sup>.

In the classical pathway, VPM afferents first synapse onto both excitatory and inhibitory cells in layer IV<sup>59</sup>, with more synapses onto excitatory than inhibitory cells as the ratio of excitatory to inhibitory cells in layer IV is approximately 9:1<sup>60</sup>. That said, the vast majority (approximately 85%) of synaptic contacts in layer IV are intracortical<sup>59</sup>, i.e. from other areas of (mostly barrel) cortex. Thalamocortical synapses are only slightly more efficacious than intracortical synapses, with evidence that the relative strength of thalamocortical synapses is due to coincident activation of a number of such inputs rather than significantly stronger synapses<sup>61</sup> (although their synapses are slightly more proximal to somas of layer IV spiny stellate, excitatory cells than are intracortical synapses).

The excitatory cells in layer IV are predominantly spiny stellates, star pyramids, and non-star pyramids<sup>62-67</sup>, all innervated by VPM afferents. There are some morphological and functional differences between them<sup>57,68</sup>, but they most differ in connectivity to other layers and columns<sup>58,65,66,68</sup>: spiny stellates axons' project almost exclusively within layer IV and to layer II and III, and very rarely to infragranular layers; star pyramids have dendrites which extend from layer IV into II and III and axons which project to layer II, III, within IV, and to infragranular layers; and non-star pyramids are very similar to star pyramids although can also project to neighbouring columns. Despite these differences, excitatory cells in layer IV mainly target layers II and III in the same column (with an overall connectivity probability of ~10-15% with layer II/III pyramidal cells;<sup>60,69</sup>). Within layer IV, excitatory cells appear to form excitatory

clusters of  $\leq \sim 10$  cells in which the cells are highly interconnected<sup>60</sup>, making individual cells in these clusters highly efficacious in causing action potentials in other cells of the same cluster<sup>11</sup>.

Excitatory cell activity in all cortical layers is modulated by interneuron cells located locally (from within the same layer of the same column), trans laminarily (from other layers within the same column), and laterally (from layers within other columns). These interneurons come in different and complex morphological and electrical varieties, are present and connected in different proportions and manners throughout cortex, and can have inhibitory or excitatory synapses with other cells (though most are inhibitory)<sup>70-72</sup>. This diversity can make precise identification of interneuron subtypes difficult under experimental conditions, and in many reports of microcircuits, only some features of the interneurons are known. However, a common technique to identify them takes advantage of their differential expressions of calcium-binding proteins (CBPs), neuropeptides, and other molecular markers<sup>70,73,74</sup> (see Table 1). In the case of layer IV interneurons, VPM afferents activate cells positive for parvalbumin (PV<sup>+</sup>), somatostatin (SOM<sup>+</sup>), and 5-HT<sub>3A</sub> receptors (5-HT<sub>3A</sub>R<sup>+</sup>)<sup>75-77</sup>. PV<sup>+</sup> interneurons are also driven by layer IV excitatory cells<sup>52,78</sup> and layer VI corticothalamic pyramidal cells<sup>56</sup>. Together, these excitatory connections onto inhibitory cells can be considered *feedforward inhibition*, as they drive inhibitory interneurons' activity forward onto other cells. *Feedback inhibition* occurs when inhibitory cells synapse back onto excitatory cells, typically releasing gamma-aminobutyric acid (GABA). PV<sup>+</sup>, SOM<sup>+</sup>, and 5-HT<sub>3A</sub>R<sup>+</sup> layer IV interneurons cause feedback inhibition on layer IV excitatory cells<sup>78-80</sup> and SOM<sup>+</sup> interneurons cause *disinhibition* (inhibiting other inhibitory cells, thus reducing their inhibition onto excitatory cells) on PV<sup>+</sup> interneurons<sup>80</sup>.

Functionally, PV<sup>+</sup> interneurons appear to be mostly fast-spiking (FS) and can produce very high, non-adapting firing rates (>100 Hz). They synapse almost exclusively onto excitatory cells in layer IV and are likely to be basket cells (BCs; see Table 1) which typically possess a dense axonal plexus that projects within a small area<sup>75,78</sup>. These PV<sup>+</sup>-FS cells have very short latencies to cortical activation (0.6 ms), high release probabilities, and make an average of 3.5 synapses onto excitatory cell dendrites at proximal and distal locations<sup>78</sup>. It has therefore been suggested<sup>48</sup> that as these PV<sup>+</sup>-FS cells are rapidly recruited by thalamocortical afferents and further driven by local excitatory cells, they may act to quickly 'reset' layer IV excitation and increase temporal resolution in that layer. Relatively FS (70-150 Hz), adaptive firing from SOM<sup>+</sup> cells likely provides the required disinhibitory control of PV<sup>+</sup>-FS cells<sup>81</sup>; synapses from SOM<sup>+</sup> to PV<sup>+</sup>-FS cells are much stronger than those from SOM<sup>+</sup> to excitatory cells within layer IV<sup>80</sup>. However, a different subtype of SOM<sup>+</sup> interneuron in layer IV are likely to be the Martinotti cells which are identifiable by axons projecting to layer I<sup>81</sup> and provide widespread cortical dampening to pyramidal neurons<sup>82</sup> (Table 1). Then, 5-HT<sub>3A</sub>R<sup>+</sup> interneurons – which appear in comparatively low numbers in this layer – show long firing

latencies and result in slow inhibition on excitatory cells within layer IV <sup>77,79,83</sup>, acting weakly but surely against PV<sup>+</sup>-FS cells' temporal sharpening. This could counteract excitation-inhibition imbalances or provide the wider temporal integration necessary for long-term neuroplasticity <sup>48</sup>.

### Layer II and III

The main layer IV excitatory output is to layers II and III, where it combines with additional VPM input to layer III pyramidal cells <sup>10,53,84,85</sup> and P<sub>Om</sub> input to apical tufts of layer II pyramidal cells <sup>48,86</sup>. Together, layers II and III act as the first and major integrative processing cortical layers. Pyramidal cells in layer II and III typically project their axons over several barrel columns in layers II, III, and V, and to secondary somatosensory and motor cortices <sup>87,88</sup>. However, layer II pyramidal cells near the border of layers I and II have highly lateralized apical dendrites, and a small subset of layer III pyramidal cells restrict their projections to mostly within one barrel <sup>89,90</sup>. Within layer II and III, pyramidal neurons form excitatory connections to one another with a probability of ~10-20%, as layer IV excitatory cells connect to layer II and III pyramidal cells <sup>88,91</sup>. These intralayer connections between layer II and III pyramidal cells are typically on the order of ~3 synaptic connections per neuron (to mostly basal dendrites) <sup>88,92</sup>, however the strength of these connections depends on sensory experience <sup>93</sup>. Axons from layer II and III pyramidal neurons also project to layer V pyramidal neurons, typically forming weak synapses on basal dendrites <sup>94-96</sup>, and these connection patterns may 'bind' perceptual features in subnetworks of layer V pyramidal cells which are different to those subnetworks which form between layer II and III pyramidal cells <sup>97</sup>.

As in layer IV, the output of layer II and III pyramidal neurons is shaped by many interneurons, particularly in layer II where ~17% of cells are interneurons, whereas interneurons make up only ~9% in layer III and ~8-9% in layer IV <sup>98</sup>. All major histological classes of interneurons are represented in layers II and III <sup>99</sup> but approximately half are 5-HT<sub>3A</sub>R<sup>+</sup>, meaning they can be driven by serotonergic neurons <sup>83</sup>. Layer II and III interneurons are mainly driven by layer IV excitatory cells <sup>100</sup>, causing feedforward inhibition, but layer II and III pyramidal neurons also activate feedforward inhibition circuits by synapsing with some FS (possible BC) layer II and III interneurons <sup>91,101</sup>. A wide variety of interneurons, each with unique intrinsic properties and functions, are likely to exist in layer II and III, including BCs, Martinotti cells (MCs), chandelier cells (ChCs), neurogliaform cells (NGFCs), double bouquet cells (DBC), bitufted cells (BTCs), and bipolar cells (BPCs) <sup>70,72,102,103</sup> (see Table 1 for basic descriptions of these cells and their identifying characteristics). ChCs target axon initial segments of layer II and III pyramidal neurons (where they can be uniquely excitatory <sup>104</sup>), while BCs, DBCs, and some NGFCs synapse onto basal dendrites of local pyramidal neurons; BPCs target proximal apical dendrites; and MCs and BTCs synapse on apical tufts

and the middle portion of the apical dendrites. On average, most of these interneurons will synapse onto three to six pyramidal neurons in layer II and III and make similar kinds and numbers of connections with layer V pyramidal neurons. These interneuronal connections onto layer II and III pyramidal cells, in combination with the intricate excitatory connection patterns from layer IV and thalamus, allows cells to be finely tuned to complex, higher-order features of sensory input.

In addition to these local interactions, there are also some interesting BC-involving microcircuits in which BCs are innervated by long-range vibrassal motor cortex (vM1) axons which synapse onto BCs' apical dendrite extensions in layer I of barrel cortex. These BCs cause a strong disinhibition of SOM<sup>+</sup> interneurons in layer II and III, and thus activity from vM1 projections can increase the excitability of layer II, III, and V pyramidal neurons, as seen during whisking behaviour *in vivo* <sup>105,106</sup>.

Highly peculiar layer II and III inhibitory microcircuits involving PV<sup>+</sup> and calretinin-positive (CR<sup>+</sup>) interneurons have also been observed <sup>107,108</sup>. These PV<sup>+</sup> cells are called multipolar bursting cells (MPBCs) as they show burst rather than FS firing when depolarised and project densely within layer II, with some collaterals to layer V. The CR<sup>+</sup> cells are BPCs and multipolar cells (MPCs) – BPCs project narrowly down to layer V and, like MPBCs, have a high-frequency burst upon initial depolarisation, whereas MPCs' axons project laterally within layer II and III only. These peculiar circuits are driven and modulated by layer II and III pyramidal cells, with MPBCs receiving extra inputs from layer IV excitatory cells.

<b>Table 1.</b> Summary of interneuron sub-types mentioned in text (abbreviations same as text).		
<i>Name</i>	<i>Basic description</i>	<i>Identifying characteristics</i> <sup>48,70,73,109</sup>
Spiny stellate cell (SSC)	Filters and relays thalamic excitation from layer IV to layer II/III <sup>65</sup> .	Spiny morphology.
Large basket cell (LBC)	Most common basket cell found in cortex <sup>70</sup> . Inhibits many pyramidal cells across barrels at or near the soma <sup>110</sup> .	FS, non-accommodating (N-Ac), non-adapting (N-Ad). PV (+++), CB (++), NPY (+), CR (+), VIP (+), SOM (-), CCK (+).
Small basket cell (SBC)	Least common basket cell found in cortex <sup>70</sup> . Inhibits few pyramidal cells, usually within a single layer and column, at or near the soma <sup>110</sup> .	FS, N-Ac, N-Ad. PV (-), CB (++), NPY (+), CR (-), VIP (+++), SOM (++), CCK (+).

Nest basket cell (NBC)	Second-most common basket cell found in cortex <sup>70</sup> . Inhibits few pyramidal cells within a barrel at or near the soma <sup>110</sup> .	FS, N-Ac, N-Ad. PV (+++), CB (++), NPY (+), CR (++), VIP (+), SOM (-), CCK (+).
Chandelier cell (ChC)	Inhibits the initial segment of pyramidal neurons and found in layers II to VI <sup>70,111-114</sup> to control excessive excitation <sup>115</sup> , although some connections could themselves be excitatory <sup>104</sup> .	FS or late spiking (LS), N-Ad. PV (+) and/or CB (+), GABA transporter 1 (GAT-1) (+), SOM (-).
Neurogliaform cell (NGFC)	Inhibits dendrites of pyramidal neurons <sup>70</sup> , especially in instances of persistent excitation <sup>116,117</sup> .	LS. PV (-), CB (-), NPY (+), reelin (+), COUP transcription factor 2 (+).
Double bouquet cell (DBoC)	Inhibits basal dendrites and somas of pyramidal neurons <sup>70</sup> , typically extending its dendrites vertically, across multiple layers <sup>118-120</sup> .	Irregular spiking (IS) or regular non-pyramidal (RSNP) firing (adapting). PV (-), CB (-), NPY (-), CR (++), VIP (+++), SOM (++)
Bitufted cell (BTC)	Inhibits distal dendrites of pyramidal neurons <sup>70</sup> , often spanning its dendrites across the entire cortical column <sup>121-123</sup> .	RSNP and BSNP, adapting. PV (-), CB (++), NPY (+), CR (++), VIP (+), SOM (++)
Bipolar cell (BPC)	Extends narrow bipolar or bitufted dendrites vertically within the column. Inhibits the basal dendrites of relatively few pyramidal neurons <sup>70</sup> .	IS, LS, or RSNP (adapting). PV (-), CB (-), NPY (-), CR (++), VIP (+++), SOM (++)
Multipolar bursting cell (MPBC)	Extends densely within layer II, with some collaterals to layer V. Inhibits the basal dendrites of local pyramidal neurons <sup>107,108</sup> .	Burst firing. CR (+).
Martinotti cell (MC)	Inhibit distal dendrites of pyramidal neurons <sup>70</sup> , especially the apical tuft regions in layer I (of deeper pyramidal neurons).	RSNP or burst-spiking non-pyramidal (BSNP). PV (-), CB (++), NPY (++), CR (-), VIP (-), SOM (+++).

Single bouquet cell (SBoC)	Inhibits interneurons in supragranular layers, indirectly disinhibiting layer V pyramidal neurons <sup>102,103,124</sup> .	Varied spiking patterns. Typically VIP (+).
Elongated neurogliaform cell (ENGFC)	Inhibits distal dendrites present in layer I, typically the apical tufts, of layer II, III, and V pyramidal neurons <sup>102,103,124</sup> .	LS and varied spiking patterns. Typically NPY (+) and reelin (+).
Cajal-Retzius cell	Important for establishing intracortical and cortico-thalamic connections during development <sup>125-129</sup> , although some may survive into adulthood <sup>125,128</sup> .	Glutamergic. Typically reelin (+).

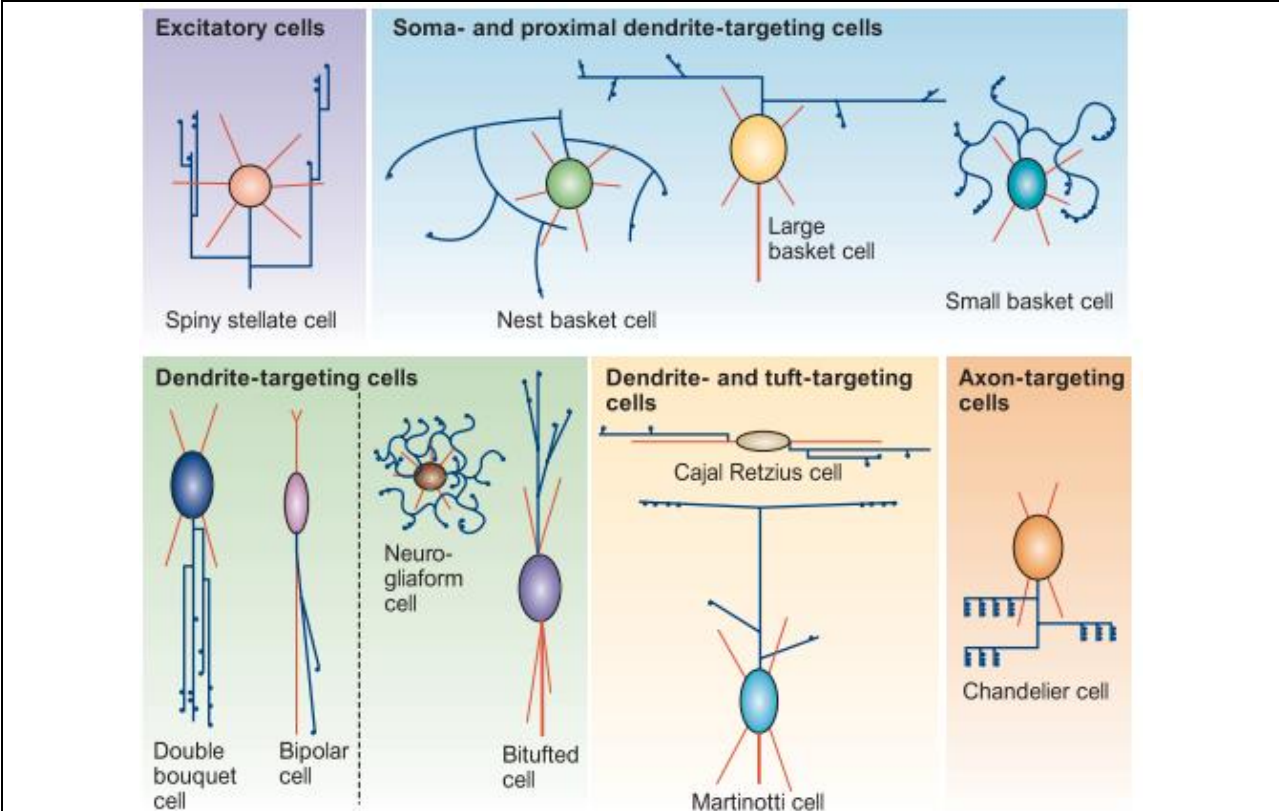


**Figure 3.** Simplified drawings of some cortical interneuron subtypes reviewed (from Markram et al. <sup>70</sup>).

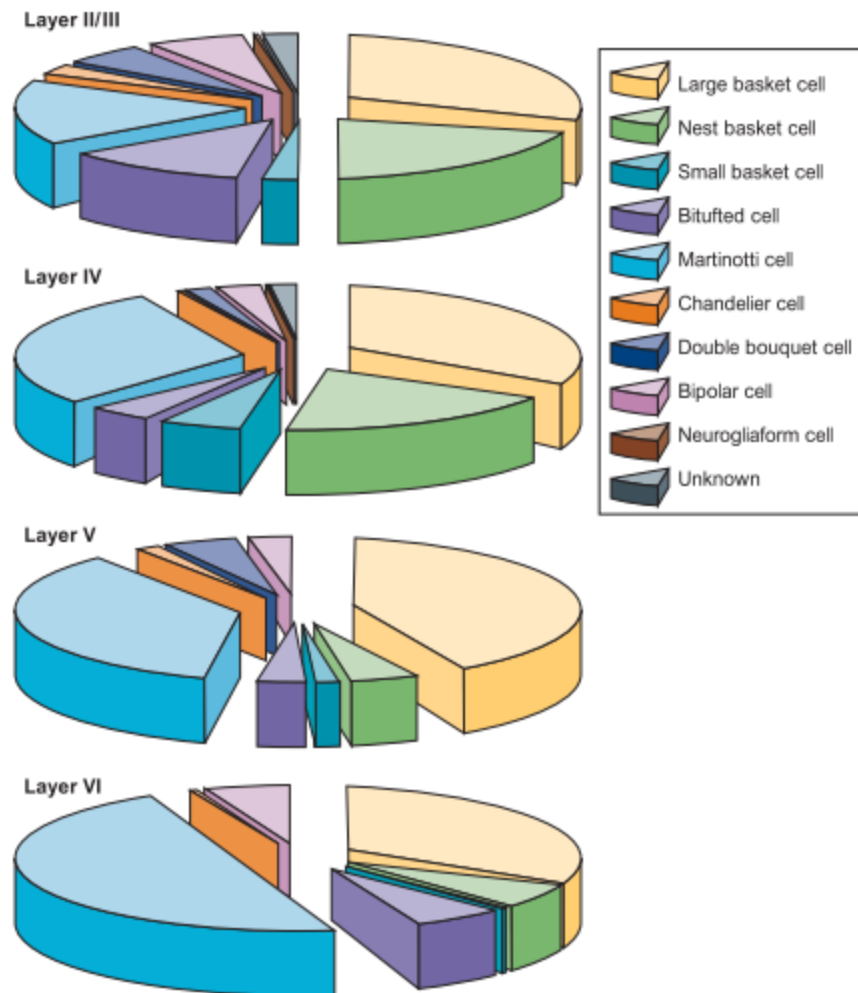


**Figure 4.** Relative proportions of cortical interneuron subtypes present across cortical layers (from Markram et al. <sup>70</sup>).

### Layer V

Layer V receives excitation and inhibition from all overlying layers and, combined with excitatory input from VPM and POm, likely integrates the processing of the column as a whole before sending its processed output to downstream areas. Layer V pyramidal neurons receive innervation from supragranular and granular excitatory cells, as well as other layer V pyramidal neurons. Of these supragranular and granular cells, three morphologies are distinguishable: slender-tufted (found mostly in upper layer V), thick-tufted (found mostly in lower layer V), and untufted (found throughout layer V, though in relatively low numbers) <sup>88,89</sup>. Slender-tufted pyramidal neurons receive thalamic input from

POm and project dense axons extensively within supragranular layers across the entire ipsilateral barrel cortex, ipsilateral vM1, and to contralateral barrel cortex, making them the primary output cells in layer V<sup>130,131</sup>. Thick-tufted pyramidal neurons receive thalamic input mostly from VPM and make most of their synapses to other layer V pyramidal neurons and subcortical areas, thus providing local and subcortical feedback<sup>130,132</sup>. Untufted pyramidal neurons receive a mix of VPM and POm thalamic input depending on their depth within layer V and project extensively to layer III and to the contralateral barrel cortex, making them important for intracolumnar feedback and inter-hemispheric coordination of sensory outputs<sup>89,133</sup>.

As in other layers of cortex, the activity of pyramidal neurons in layer V receives inhibitory modulation – from other layers, especially layer II and III interneurons as discussed above, as well as local layer V inhibition. Local Inhibition comes from PV<sup>+</sup>, FS and SOM<sup>+</sup> cells driven by VPM<sup>134</sup>, FS cells driven by upper layer VI pyramidal cells<sup>56</sup>, and local MCs<sup>82,135</sup>. Local PV<sup>+</sup>, FS and MCs generally behave as in other cortical layers but SOM<sup>+</sup> cells synapse onto dendrites of layer IV spiny stellate cells instead of apical dendrites of local pyramidal cells as in other layers<sup>134</sup>. Because of this, their delayed facilitation response effectively adds a late-onset inhibitory input to layer IV excitation during long periods of ongoing thalamocortical input and so could be important for excitation-inhibition balance at longer-time scales.

## Layer I

Layer I, also known as the molecular layer, contains few neuron cell bodies and many glia. It receives input from thalamic matrix cells and acts as a medium through which feedback and transmission from ipsilateral and contralateral cortical areas can communicate<sup>102,103,136,137</sup>. Except for Cajal-Retzius cells, which are important during neurodevelopment<sup>126,127</sup>, the mature layer I almost exclusively contains GABAergic inhibitory neurons expressing 5-HT<sub>3A</sub>R<sup>+</sup> and SOM<sup>+</sup><sup>83,106</sup>, which are predominately driven by layer II/III pyramidal cells from the same column<sup>137</sup>. These layer I interneurons have some functional spiking differences<sup>137</sup> and have recently been described as possessing two distinct morphologies, each being involved in two distinct microcircuits<sup>102,103,124</sup>: (1) single bouquet cells (SBoCs) establish local, unidirectional inhibition to layer I interneurons and most inhibitory and pyramidal cells in layer II and III; and (2) elongated neurogliaform cells (ENGFCs) establish broad, reciprocal inhibition (directly and via gap junctions) to layer II and III MCs, NGFCs, and BTCs, as well direct inhibition to layer II, III, and V pyramidal neurons. Therefore, SBoCs exert an indirect, disinhibitory effect on layer V pyramidal cells whereas ENGFCs exert direct and indirect inhibition on layer V pyramidal cells (thus stipulated as a yin and yang system of inhibitory control for layer V<sup>124</sup>).

## Layer VI

Relative to other cortical layers, much less is known about layer VI<sup>138</sup>. Its involvement in thalamocortical feedback is well-established<sup>139–142</sup> but it also makes some unique and varied projections to other layers and acts as a supplementary output layer<sup>60,141,143–145</sup>. In upper layer VI, pyramidal cells receive input from VPM and POm, and typically project either back into the thalamus, providing corticothalamic feedback, or project intracortically. Intracortical projections are made to other layers of the same cortical column, within layer VI itself, or to long-range cortical areas outside of barrel cortex. Pyramidal cells in lower layer VI are much more heterogeneous and typically synapse within layer VI, however longer-range connections to layer I, layer II, and the thalamus are also present<sup>146–148</sup>. Interneurons in layer VI are significantly understudied, but are likely driven by thalamic nuclei and local pyramidal cells and appear to be involved in local and translaminar inhibition<sup>55,140,142,149</sup>. Functionally, this makes layer VI highly important for thalamic-cortex interaction, supplementary corticocortical output, and specialised inhibition within a barrel.

Throughout this discussion of barrel cortex microcircuits, some dendritic processing effects have been implied via mention of where presynaptic neurons synapse on postsynaptic cells (soma, perisoma, basal or distal dendrites, etc.). It is important to explicitly note that dendroarchitecture plays an important role in synapse (and, thus, postsynaptic cell) function<sup>8,30,61,150–154</sup>. For example, GABA<sub>B</sub> receptors work by different biochemical mechanisms in the soma than in dendrites; mostly this means that they have the same resulting effect on postsynaptic firing<sup>155</sup> however exceptions can and do arise due to these differences<sup>152</sup>. Complete exploration of such exceptions is beyond the scope of this review but underscores a caveat of dual intracellular somatic recordings (a technique which some studies discussed so far have used): if one is attempting to establish connection probability from presynaptic neurons to a postsynaptic cell, distal dendritic synapses may be so attenuated or filtered that they fail to register at the soma (where the experimenter is often recording from in such studies). However, despite their distal locations, there may be strategies such presynaptic neurons use to boost their signal *in vivo* (such as synchronous firing with other presynaptic neurons). Thus, in the absence of observing such strategies, studies may significantly underestimate the probability of these presynaptic connections<sup>48</sup>.

Nevertheless, much is known about barrel cortex and its microcircuits. The sum of interactions between cortical microcircuits across and within layers ultimately leads to corticocortical output<sup>87</sup>, which transmits essential sensory information upstream to higher sensory, motor, and associative cortical areas.

### 1.3 Encoding of whisker movement

What we have discussed up until this point – whisker-sensing pathways to barrel cortex, and the barrel cortex's somatotopy and microcircuitry – ultimately serves to generate the neural encoding of whisker movements in the brain. Such encoding relies not on individual neurons alone, but rather on populations on neurons spread across the cortical column. While populations within the same barrel tend to do have redundancy<sup>156,157</sup>, there exist different populations within each barrel, each of which encode complementary features of whisker movements in concert with one another to represent a wide diversity and complexity sensory information<sup>158,159</sup>. For example, different populations can encode whisker deflection velocity, amplitude, or angle of deflection. Such populations can also place different emphases on certain quantitative metrics of their coding system, e.g. neurons encoding stimulus location appear to place an emphasis on the timing of individual spikes, especially of the first spike after stimulus onset<sup>157</sup>.

Within populations, nearby neurons can fire in pairs during both spontaneous and evoked activity<sup>160</sup>. This redundancy allows sampling pairs across the population to provide greater accuracy for determining stimulus onset times<sup>160</sup>, which as mentioned is a vital and sensitive metric for encoding stimulus location<sup>157</sup> and many other complex stimulus features of whisker movement<sup>158,159</sup>. However, such representations can and do change over time due to adaptation and sensory experience<sup>159,160</sup>.

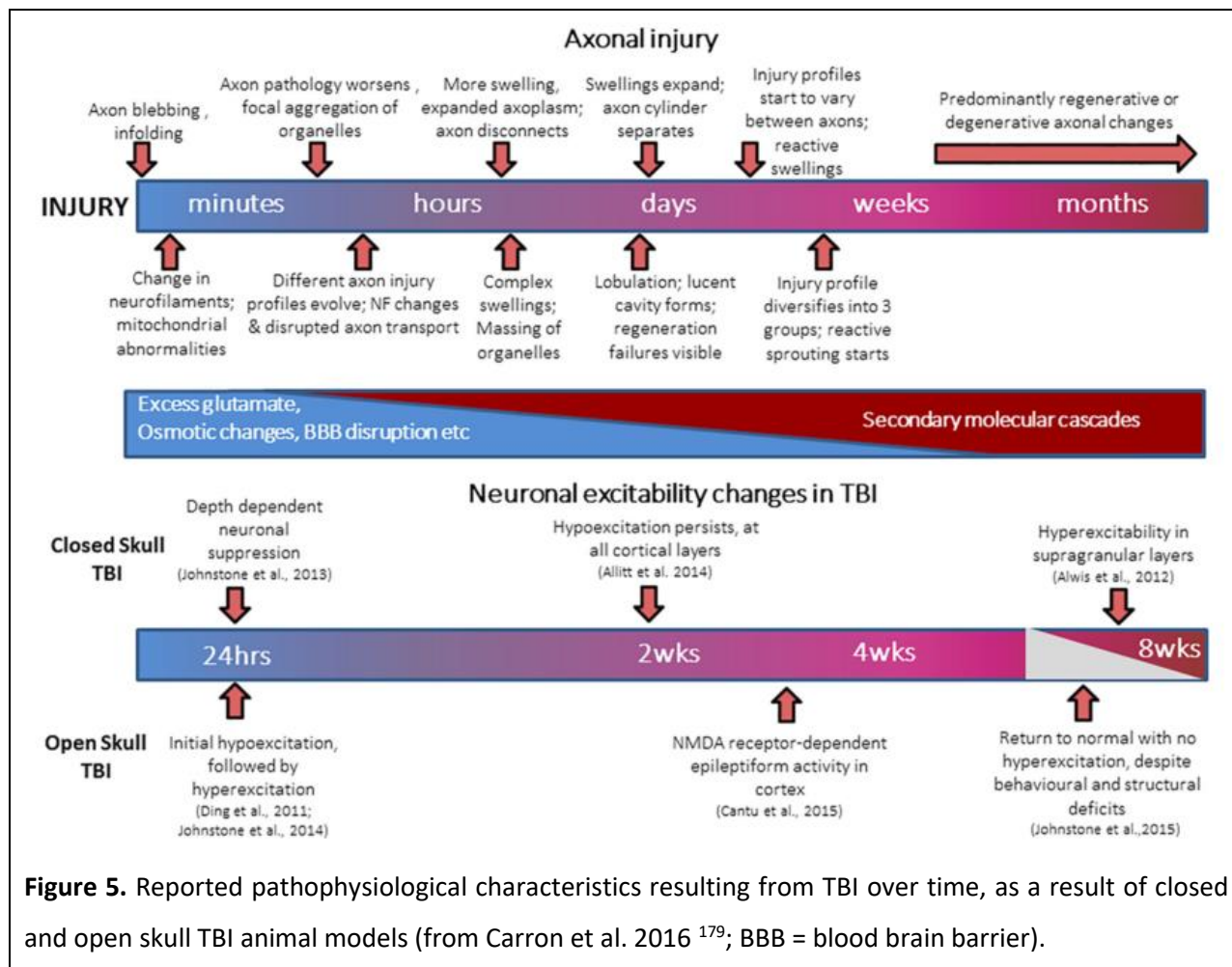
These encoding mechanisms are important for the healthy function not only of barrel cortex but also of the upstream areas which barrel cortex projects to, such as those responsible for functions such as cognition and motor coordination. As discussed next, perturbations of the barrel cortex affect sensory processing and encoding of sensory information in specific ways across different timescales, which are also associated with cognitive and motor impairments.

### 1.4 Animal models of brain injury and their effects on cortical inhibition

In 2006, an estimated 5.3 million people in the United States of America<sup>161</sup> were living with medical disabilities resulting from TBI. Such injuries are frequently acquired from common sporting and recreational activities<sup>162,163</sup>, as well as motor vehicle and other physical accidents<sup>161</sup>. They are associated with increased risks of depression<sup>164</sup> and epilepsy<sup>165,166</sup>, likely caused by damage to and/or reorganization of inhibitory microcircuits<sup>167–172</sup>. Accordingly, animal models of TBI and similar brain injury have been developed to study their pathophysiology and possible avenues of medical intervention<sup>5,173</sup>.

Two major animal models of TBI involving rodents are closed and open skull TBI, where an object (usually a weight) makes a controlled impact with the intact head or opened skull (i.e. directly onto the

brain), respectively. These two models produce different severities of TBI and thus the primary and subsequent secondary damage is different in severity and kind<sup>5,167,171,174</sup>. These models produce different combinations of diffuse and focal traumatic brain injury; closed skull TBI is more likely to produce only diffuse injury whereas open skull TBI produces a mixture of diffuse and focal injury<sup>175</sup>. Focal injury refers to injury which is more localized to a particular brain area and is generally the result of severe mechanical forces impacting with that area. As such, focal injury is generally noticeable using current clinical imaging techniques due to bleeding, bruising, and other gross tissue damage. In comparison, diffuse injury is less localized and usually undetectable via clinical imaging techniques because damage is on a cellular scale and not grossly visible via normal clinical imaging techniques since there is an absence of noticeable bleeding and bruising. Diffuse TBI damage can be caused by hypoxia, meningitis, edema, or rapid fluid movement in the brain, like those caused by rapid acceleration/deceleration or rotational forces in vehicular accidents<sup>176,177</sup>. It is important to remain cognizant of these differences when studying or using data from different TBI animal models, since both types of injury – focal and diffuse – are acquired to different extents in different clinical cases and may be clinically detected or treated in different ways<sup>161,164,167,169,176,178</sup>.



The immediate and primary damage in both focal and diffuse TBI is axonal injury and primary axotomy, i.e. the tearing of axons, swelling, enfolding and, in severe instances, total disconnection of the axon from the soma or cell death, which can also accumulate to cause secondary axotomy<sup>180-184</sup> (see Figure 5). This damage further compounds with glutamergic excitotoxicity, hypoxia-ischemia, general inflammation, oxidative stress, and possible microcircuit diaschisis<sup>167,171,185,186</sup>. The specific loss and damage of axons and cells will differ between individuals and progress at different rates. However, animals that survive the mechanical impacts employed in these models of TBI show a series of changes in excitation and inhibition in the long- and short-term. Typically, in open skull TBI, at 24 hours post-injury, there is a brief, initial presence of hypoexcitation followed by continuing and prominent hyperexcitation<sup>13,178</sup> and epileptiform activity is present at around four weeks post-injury<sup>173</sup>. By six to eight weeks post-injury, most layers return to regular levels of excitation, however animals demonstrate cognitive deficiencies, as indicated by behavioural changes<sup>13,173,178</sup>. In cases of closed skull TBI, hypoexcitation

across cortical layers persists for several weeks (more so in supragranular layers) but by eight weeks post-injury, the supragranular layers show hyperexcitation<sup>12,187,188</sup>. This so-called 'spontaneous recovery' (or natural recovery) is slow and generally leaves permanent disability, despite multifaceted and interacting regenerative processes being triggered post-injury<sup>189</sup>. Such adaptive neuroplastic processes appear to be strongly linked with behavioural experience<sup>190</sup>, initiating axonal and collateral sprouting of neurons and – ultimately – cortical remapping.

This has led to the hypothesis<sup>5,12,174,187</sup> that maladaptations of the recovering cortex, like potential synaptic changes between particular cell types due to specific cell type(s) death and circuit remapping, cause disruption to microcircuit function in such ways that cause these excitability changes. Further supporting this hypothesis are the observations that TBI has a range of complex effects on the homeostasis of GABA, glutamate, and dopamine<sup>191,192</sup>, neurotransmitters vital in maintaining balance of excitation and inhibition in cortex. These effects include evidence<sup>191,192</sup> of short-, medium-, and long-term effects on receptor composition on postsynaptic cells, impaired reuptake or removal of neurotransmitter at synapses, and specific cell population deaths along excitatory pathways.

Two additional sets of observations are noteworthy with respect to TBI. First, females tend to fare better than males in TBI and other neurotrauma<sup>193</sup>. While there have been reported sex differences in gross neocortex size<sup>194</sup>, it seems more likely that these differences arise because of hormonal<sup>193,195</sup> or other related differences, though results differ for hormonal therapy post-injury<sup>196–199</sup>. However, it might also be possible that steroid-independent sex differences in cortical inhibition<sup>200,201</sup> or intrinsic differences in serotonergic pathways related to female sex steroids<sup>202–204</sup> are obtained during development (which could be important for inhibitory interneurons expressing 5-HT<sub>3A</sub>R). The second interesting set of observations are the effects of prolonged environmental enrichment (EE) in healthy barrel cortex (i.e., enhancing social and physical stimulation in rodents' housing). EE causes significant potentiation of evoked sensory responses in supragranular and granular layers, and additionally for some stimuli in infragranular layers<sup>205</sup>, yet after closed skull TBI, EE *attenuates* cortical hyperexcitability, especially in layers II and III<sup>206</sup>. This is somewhat perplexing, however could hold an important key to how and why particular changes in inhibition evolve post-TBI.

Diffuse TBI appears to cause significant and long-lasting changes in inhibitory microcircuit function in barrel cortex<sup>5</sup>. Additionally, these changes depend on the sex of the animal and whether or not it experiences EE. So, what causes or mediates these changes in inhibition? As the changes appear to evolve over time and are more prominent in different layers or cell types<sup>5,173,179</sup>, it seems likely that intrinsic properties of inhibitory neurons or their networks in different cortical layers somehow facilitate these

different changes. For this reason, a general pathological feature of post-TBI, e.g. waves of slow-moving cortical spreading depression (CSD) (which spread throughout the whole cortex immediately following brain injury and which is a characteristic brain response following major brain perturbation<sup>207</sup>), is unlikely to be the proximate cause of such changes. However, we cannot discount that general pathological features, like CSD, are not involved, e.g. the possibility that CSD affects inhibitory interneuron function in the long-term, and this effect changes according to intrinsic differences between interneuron subtypes. This logic (that intrinsic interneuron differences are partially responsible for post-TBI changes in inhibition) is supported by the wide variety of interneurons being differently affected post-injury<sup>179,208–214</sup> in combination with the apparent systematic loss of dendritic but not somatic inhibition (since different interneurons preferentially target somatic or dendritic sites on post-synaptic neurons)<sup>179,209</sup>. In cortex it also appears that CR expression from interneurons changes significantly post-TBI (it is reduced in supragranular layers and increased in infragranular layers), while other common markers does not<sup>5</sup>, which gives us some clues as to which types of interneurons are potentially responsible for these changes (per CR expression differences in Table 1 and interneurons appearing in different proportions depending on cortical layer per Figure 4).

## 1.5 Computational methods

As will be further discussed in section 3.3, the current work uses a number of computational methods, notably temporal component analysis and graph-theory methods. For completeness of this review, a brief introduction to each is included here.

Temporal component analysis applied to neural data involves identification (or even segmentation) of temporally distinct components within neural activity. Two of the most common methods to achieve this are: (i) to directly measure and compare neural activities in terms such as mean amplitude over time, response onset delay, or the delay to maximum response<sup>160,188</sup>; or, since neural data is often rich and complex, (ii) to reduce the dimensionality of the data using techniques such as principal components analysis (PCA)<sup>215,216</sup> or manifold learning<sup>217</sup> to then measure and compare neural activities in those terms. Section 3.3 and Appendix I describes how we applied and compared these methods in the current thesis.

Graph theory is an area of mathematics which deals with the object of graphs, networks of vertices connected by edges. Graphs are generally described independent of a coordinate system and are instead described in terms of how the vertices and edges are connected to each other, i.e. instead of saying vertices *A* and *B* are distance *C* apart, we may say that they share a common connection to vertex

$X$  and are therefore  $W$  vertices apart from one another. This is a very useful type of abstraction, since it lets us represent connectivity and spatial relationships explicitly while maintaining abstraction – and therefore generalisation – for the purposes of analysis. Note, however, that distance can still be incorporated implicitly via edge weightings. This set of features has made graph theory methods popular for analysing neural connectivity graphs created from neuroanatomical investigations to identify connectivity or the flow of activity in biological networks<sup>218,219</sup>. However, and as discussed in section 3.3, to the best of our knowledge such methods have not previously been employed in the analysis of neural data to identify temporal components in the way we describe.

## 2. Project summary

In this project, I performed advanced analyses on an electrophysiological database of barrel cortex experiments in healthy and perturbed states. I compared responses to a simple and a complex, naturalistic stimulus. These electrophysiological data have been previously collected at Monash University, Department of Physiology by various experimenters in the Rajan Lab from rats which have sustained TBI<sup>5,12,13,179,187,188,196,206,220–223</sup>, and make up the database used in this project. In these recordings, online sorting was conducted to differentiate between individual neuronal waveforms, using parameters of the spike sorting algorithms within the Cambridge Electronic Design Spike2 software which had been well tested in the laboratory<sup>12,188,206</sup>. The sorting was monitored continuously online to ensure that the individual waveforms were sufficiently different to have confidence that each was from a different neuron. Thus, 'unit' in this context refers to an individual neuron from which data were obtained.

The aims of the project are to analyse the functional database on a unit-by-unit basis. While such analysis has been done for different purposes and in different ways for some data in this database, e.g. at the 24h post-injury time-point, it has not been done across multiple post-injury time-points in the systematic way this project does (see 3.2.1). The analyses presented here allow us to identify and quantify individual units' temporal activity patterns in response to the simple and the complex stimulus – both in healthy and perturbed states. Such analyses allow us to observe how temporal activity patterns transform between cortical layers IV and II (the layers of interest, see below) and, when analysed with knowledge of the neuroanatomy, may give us indications as to how different layers process sensory information in barrel cortex in healthy and perturbed states. These processing roles and the transformation of unit temporal activity patterns between layers IV and II are particularly interesting to analyse in the context of TBI, since recent studies suggest that functional changes occur throughout the cortical column, especially the function of inhibitory microcircuits. As well as presenting a good opportunity to procure novel results in terms of barrel cortex function and the effects of TBI, this work helps to further describe the electrophysiological database and will be an important resource for future analysis or modelling studies.

For three reasons, the general focus of this project is on layers II and IV of neocortex rather than other layers: (1) layer II has a high proportion of well-described interneurons<sup>70</sup>; (2) layers II and IV are the first and major input and processing layers in the cortical column, respectively; and (3) data from TBI-affected rats consistently show that more superficial layers have medium- and long-term changes in their excitability<sup>188,223</sup>. Once layers II and IV have been analysed using the methods in this project, it will remain

possible for others to extend the analysis across other layers of cortex. Although it is also possible to relate particular results from this project back to histological or behavioural data (which has also been collected from many animals in the electrophysiological database), the current project focusses purely on the electrophysiological changes and especially on how individual units express different temporal activity patterns. However, another possible extension of the project could be to relate these histological or behavioural data with what we find in the present analyses.

These analyses allow precise comparisons of how individual neurons respond to simple and complex stimuli in healthy and perturbed barrel cortex. Such comparisons may help to establish the importance of specific interneuron subtypes, microcircuits, and their biologically-plausible maladaptations relevant to TBI pathophysiology. Done in a systematic way, such information may help to identify the ultimate causer(s) of inhibitory imbalance associated with TBI and therefore help to identify potential therapeutic targets for future medical interventions. Whether or not the project has this indirect consequence for public health, it will also have the benefit of helping to elucidate the basic science of sensory processing in layers II and IV of barrel cortex. It also presents a novel analytical method for studying temporal activity patterns of neurons, which could be employed in other electrophysiological datasets.

### 3. Temporal neuronal activity patterns in layers II and IV of rat barrel cortex in response to simple and complex stimuli and the effects of traumatic brain injury

#### 3.1 Aims and hypotheses

**Aim 1:** To identify and quantify significantly different unit temporal activity patterns (defined as times at which the unit firing rate is markedly higher than the apparent baseline) in layers II and IV of barrel cortex in response to different stimuli in healthy rats, including how temporal activity patterns transform between these layers.

Hypotheses:

- a. There are significantly different distributions of unit temporal activity patterns in layers II and IV of barrel cortex for the same stimuli.
- b. There is less diversity in temporal activity patterns in layers IV than in layer II.
- c. Layer IV has proportionally fewer complex temporal activity patterns (temporal activity patterns with more than one major activity component) than simple temporal activity patterns (temporal activity patterns with only one major activity component) compared with layer II.
- d. The timing of components within temporal activity patterns is regular and consistent within individual layers, i.e. the time it takes between components regular between different units within the same layers.
- e. Peak response times for the same stimuli will occur later in layer II than in layer IV.

**Aim 2:** To identify and quantify how unit temporal activity patterns in layers II and IV of barrel cortex are altered by traumatic brain injury when compared with healthy units.

Hypotheses:

- a. There are fewer temporal activity patterns in layer II in the TBI conditions compared with the sham condition.
- b. Among the TBI conditions, the least diverse distribution of temporal activity patterns is found in TBI animals four days following perturbation, and the most diverse distribution of temporal

activity patterns are found in animals who received perturbation after eight-to-twelve weeks of recovery.

- c. Complex temporal activity patterns (temporal activity patterns with more than one major activity component) account for fewer temporal activity patterns in TBI conditions, proportionally, than units with simple temporal activity patterns (temporal activity patterns with only one major activity component).
- d. The timing of components of within temporal activity patterns is distorted in TBI conditions compared to sham.

## 3.2 Methods

### 3.2.1 Electrophysiological database

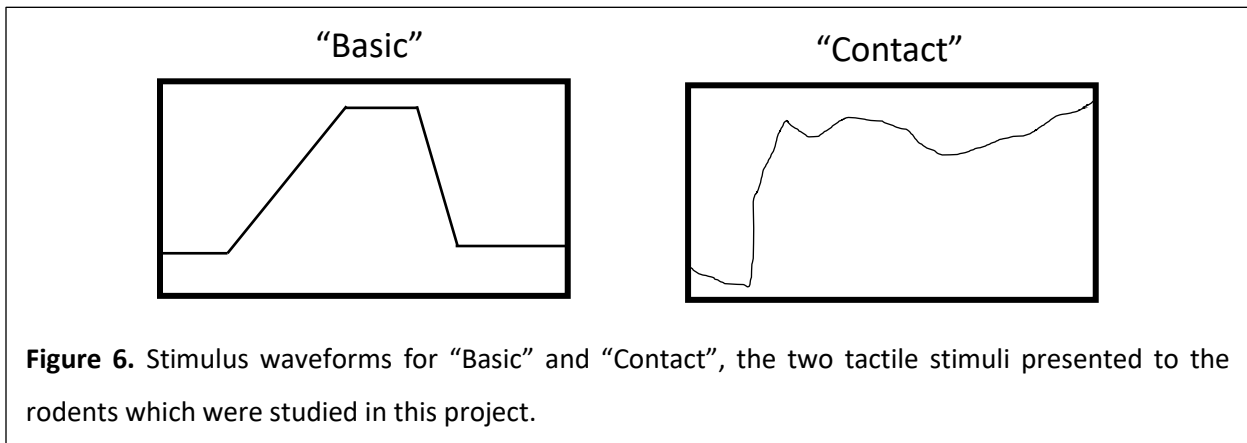
This project relies on the meticulous and long-term work carried out by numerous experimentalists in the Rajan lab over the course of 2013 and 2014<sup>5,12,13,179,187,188,196,206,220–223</sup>. The electrophysiological database is composed of data from 36 animals, across three time-points after traumatic brain injury (TBI) or sham surgery: four days (sham=4, TBI=6), two weeks (sham=4, TBI=9), and eight weeks (sham=5, TBI=8). The TBI was caused by a modified version of the weight-drop impact acceleration method<sup>224,225</sup>, which aims to make the primary injury a diffuse TBI. An impact velocity of 6.15 m/s was used to model a severe injury<sup>226</sup>. All animals were male, housed regularly, and received no forms of treatment or environmental enrichment (as has been used in some experiments). Animals which responded poorly to anaesthesia or surgery have been excluded. (Further details of this injury model method can be found here:<sup>188</sup>).

All animals had electrophysiological recordings made with a tungsten, single tip, extracellular microelectrode (2–4M $\Omega$ ; FHC) across the cortical column in barrel cortex, at depths ranging from 150um to 1400um. A principal whisker (PW) was identified for each penetration by observing neural activity while manually deflecting whiskers with a fine probe. Where no PW could be identified or where there was strong multi-whisker drive, the electrode was protracted and a new penetration at a different site in barrel cortex was made. Once identified, the PW was threaded through a motorised lever arm which stimulated the whisker in precise stimuli patterns<sup>227</sup>. The two stimuli for which evoked electrophysiological data is analysed in this project (also depicted visually in Figure 6) were:

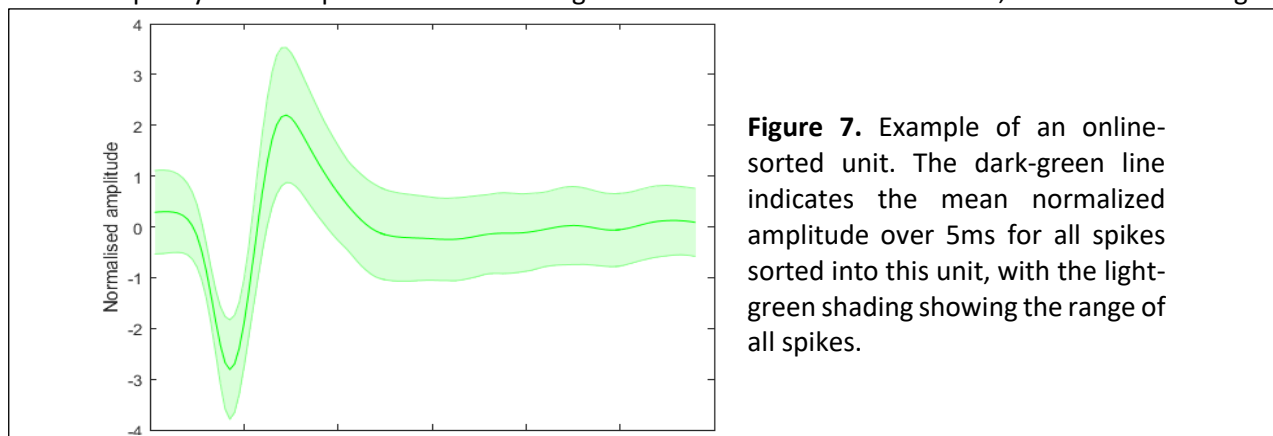
- a) “Basic”: A trapezoid stimulus had an on-ramp of varying velocity (30, 60, 150, 250, or 400mm/sec) to a distance of 3.6mm from the rest whisker position, a hold period of 20ms, and an off-ramp over 40ms back to rest<sup>12,188</sup>; and

- b) “Contact”: A naturalistic object contact stimulus which lasted a total of 100ms and included an initial deflection followed by complex movement, reconstructed from high-speed video-tracking of awake behaving rats’ whiskers contacting an object and then brushing past it <sup>228</sup>.

The Contact stimulus was varied by maximum amplitude with the amplitudes of all other components of the stimulus being altered proportionally. Ten maximum amplitudes for the Contact stimulus were tested at 0.2mm, then 0.4mm to 3.6mm in steps of 0.4mm.



All analyses from this database used online-sorted units, sorted separately during each stimulus trial at each recording depth. For example, while the extracellular electrode was at a depth of 200µm from pia, the basic stimulus was presented and evoked activity recorded. These spikes were sorted into separate units. The contact stimulus was presented and new units were sorted for those responses only. This online-sorting was performed by highly-experienced electrophysiologists using the Cambridge Electronic Design Spike2 software. The relative amplitudes of spikes were visualised and shape-based criteria (including rise time of the upstroke, the width of the action potential waveform, the size of the overshoot, etc.) were used to accept and reject units, ensuring units analysed were highly reliable and of excellent quality. An example unit is shown in Figure 7. This amounted to a total of 1,210 units. Recordings



obtained between 150–300µm deep from pia were classified as layer II units and recordings obtained between 750–1000µm deep from pia were classified as layer IV units. Unit activity profiles were then quantified for each unit by counting spikes in 1ms windows between 5-50ms post-stimulus onset, as has been used in a previous study<sup>188</sup> to encompass the responses of these stimuli (see<sup>12,188</sup> for further information).

### *3.2.2 Response components analysed*

In past studies<sup>5,12,13,179,187,188,196,206,220–223</sup>, the primary response features analysed of these units have been peak firing rate (including as a ratio of sham to TBI, and the temporal latency to this peak after stimulus onset) and normalised firing rates across time (including how this changed temporally and the area under the generated curve). This project represents the first effort to systematically analyse individual unit activity in layers II and IV, focussing on the major components of their activity (defined as times at which the unit firing rate is markedly higher than the apparent baseline). We analyse the number, timing, distribution, and qualities of such components in this database, and conduct several types of novel analyses thereafter.

Before conducting our analyses, unit activity profiles were produced by calculating the peristimulus time histograms (PSTHs) for each unit at each velocity (for Basic) or amplitude (for Contact) across all the repetitions of that stimulus at that depth for that recording. Following the convention of recent studies<sup>206–209</sup> and to allow for easier comparison to such studies, spikes were counted in 1ms bins up until 50ms post-stimulus onset. We then manually examined unit activity profiles in form seen in Figures 8 and 9 and found that a diversity of response patterns existed (see Figure 9). Most notably, some units appear to be non-responsive whereas other units contain one or more response components, i.e. one or more times at which the unit firing rate is markedly higher than the apparent baseline. Further, some of these components appeared to be relatively stationary in time whereas others are non-stationary and appear to occur earlier or later depending on the stimulus velocity (for Basic) or amplitude (for Contact). A PCA analysis based on the raw unit activities was also conducted (Appendix I) but the results were unsatisfactory due to the PCs being difficult to relate back to basic and interpretable unit features or components (such as those we had manually observed). The PCA analysis also showed an insufficient ability to, for example, reliably separate unit activity profiles of sham and TBI units (distinguishing between these units was vital to addressing aim two, see above).

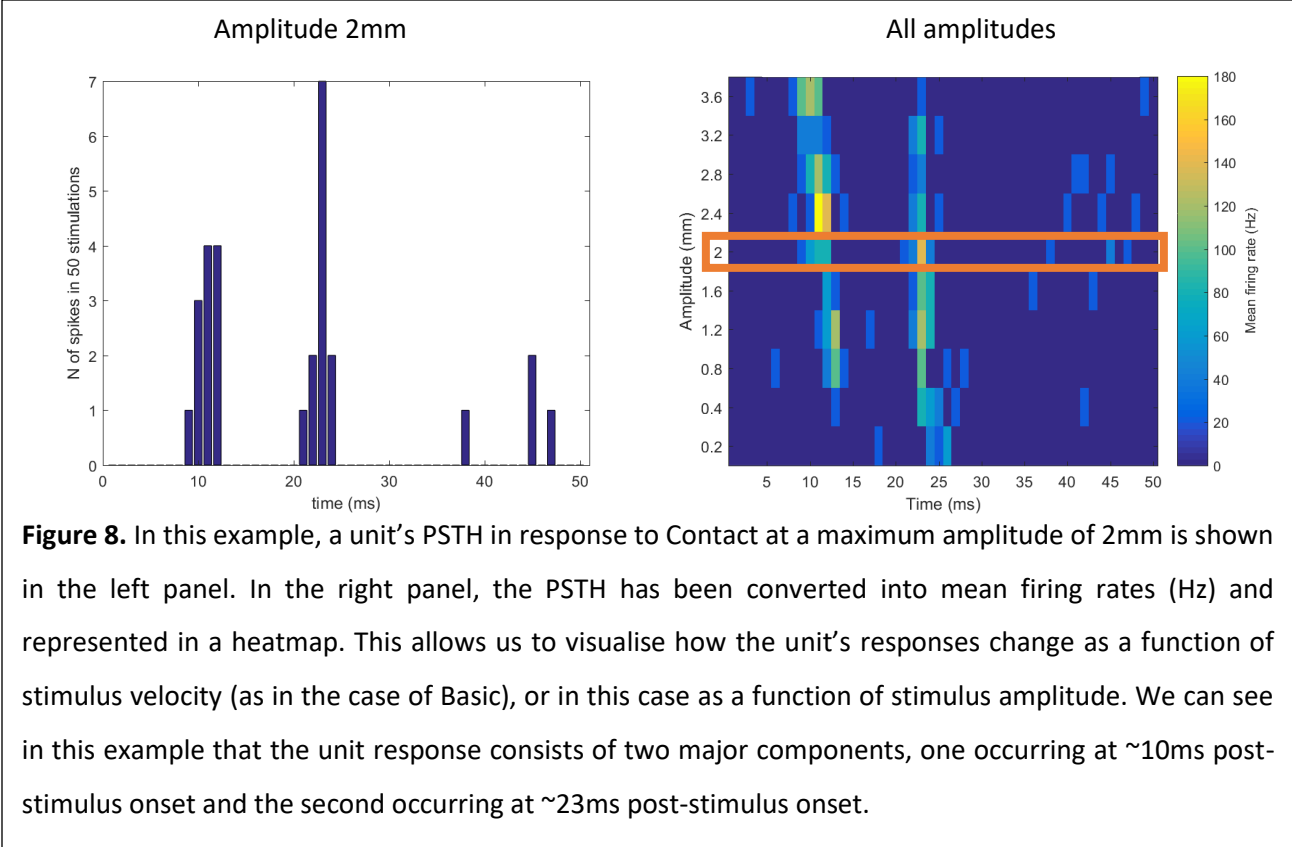


**Figure 8.** In this example, a unit's PSTH in response to Contact at a maximum amplitude of 2mm is shown in the left panel. In the right panel, the PSTH has been converted into mean firing rates (Hz) and represented in a heatmap. This allows us to visualise how the unit's responses change as a function of stimulus velocity (as in the case of Basic), or in this case as a function of stimulus amplitude. We can see in this example that the unit response consists of two major components, one occurring at ~10ms post-stimulus onset and the second occurring at ~23ms post-stimulus onset.

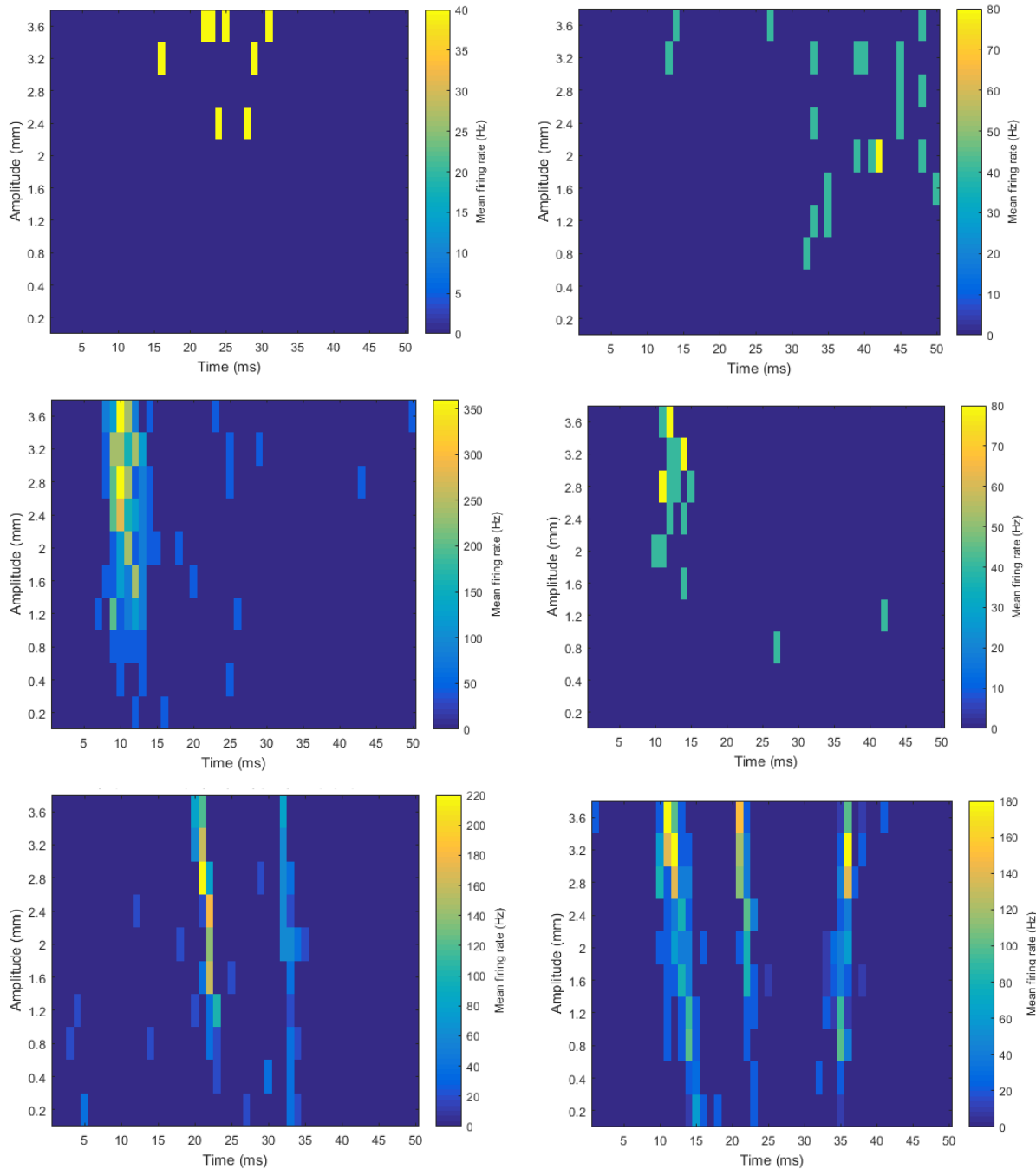


**Figure 9.** Example units responding to the Contact stimulus identified as having 0 (top row), 1 (middle row), or  $\geq 2$  components (bottom row) by the independent neural response components analysis (extended local maxima algorithm). Units with 0 components are classed as non-responders and although they may show some tendencies to spike in general periods, e.g. offset periods, these responses are not as reliable as those in units with  $\geq 1$  components. Units with  $\geq 2$  exhibit a wide diversity of component strengths and timings.

### 3.3 Data Analyses and Results

The following results relied on the aforementioned electrophysiological database (described in 3.2.1) and consisted of 1,210 online-sorted units. The number of units for each layer and condition is given in Table 2.

<b>Table 2.</b> Number of online-sorted units for each condition and layer for Basic and Contact stimuli.			
<i>Condition</i>	<i>Layer II</i>	<i>Layer IV</i>	<i>Total</i>
<b>Basic stimulus</b>			
Sham	88	142	230
TBI four-days post-injury (4d TBI)	26	42	68
TBI two-weeks post-injury (2w TBI)	39	65	104
TBI 8-12-weeks post-injury (8-12w TBI)	55	88	143
<b>Contact stimulus</b>			
Sham	103	142	245
TBI four-days post-injury (4d TBI)	39	66	105
TBI two-weeks post-injury (2w TBI)	71	94	165
TBI 8-12-weeks post-injury (8-12w TBI)	63	87	150

#### 3.3.1 Independent neural response components analysis

To objectively identify and quantify response components, an independent neural response components analysis was developed by extending the traditional local maxima algorithm. This analysis was done on a unit-by-unit basis and involved first identifying the local maxima in each PSTH for a given unit and noting the times at which these local maxima occurred. Local maxima were discarded if the mean firing rate for that 1ms bin was < 25% of max firing rate and the neighbouring 1ms bins had no spikes (or 0% of max firing rate). Local maxima occurring within 5ms of each other were combined and the median 1ms time bin between these bins was taken as a single local maxima. These combinations were performed iteratively, starting with the two local maxima nearest each other. This left an approximation of the times where mean firing rates in the PSTH were highest and at least > 25% of max firing rate. This analysis was conducted across all stimulus velocities (for Basic) or amplitudes (for Contact). We then used the same combination method to take the median times at which local maxima occurred and combine them across amplitudes to approximate, for the whole unit, when the major components of activity occurred. This

resulted in units being identified as having either none or one or more neural response components, where we considered the components to be temporally independent.

Following on from this analysis, for layers II and IV separately, histograms were plotted for when and how many unit components occurred at each 1ms step post-stimulus onset for both Basic and Contact. Kolmogorov–Smirnov (KS) tests (which tests if the one-dimensional probability distributions of two populations are equal), were conducted using MATLAB to determine if the component timing distributions were significantly different between the groups. We also aligned the times at which these components occurred post-stimulus onset to estimate what stimulus features components at certain times were likely representing (see Figure 11).

For units with multiple components, linear regressions were conducted to determine if the times at which independent components occurred within the same unit were related, and whether this relationship changed after TBI. All of these analyses were done independently for the healthy (sham) and TBI animals at each post-injury time-point. We then plotted circle charts (Figures 12 and 13) showing the relative proportions, for each layer and animal condition (and again independently for both Basic and Contact), of units which were non-responders (having no response components) and for units which had one or more components. These relative proportions were then compared between layers and animal conditions using KS tests.

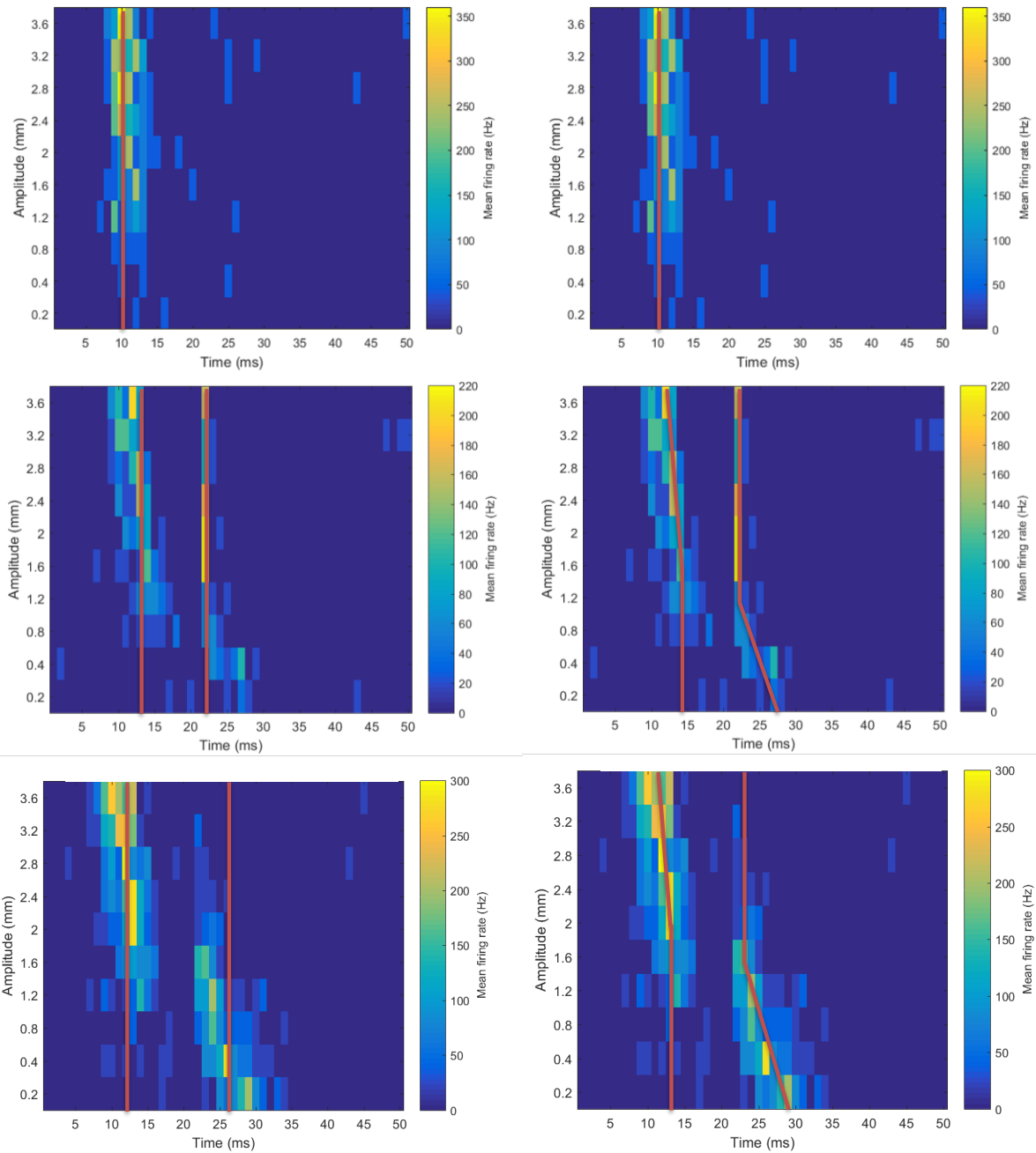


**Figure 10.** Example unit activity profiles with, in the left column, red lines showing the component time(s) approximated by the independent neural response components analysis. The right column shows the same unit activity profiles as the left, but the red lines have for illustration purposes been edited to track the true component activity with more precision.

### *3.3.2 Component timings using the independent response components analysis*

Units were identified by the independent neural response components analysis as having either no components (in which case it was classed a 'non-responder') or having up to three components. The times at which these components occurred for Basic and Contact in layers II and IV in the sham condition are shown in Figure 11. For both stimuli and layers there is a tendency for components to occur earlier rather than later. This is especially true for layer IV, whereas layer II (for both stimuli) appears to have a more lognormal distribution. The most common times for components to occur in layer II was typically a few ms after the most common times for components to occur in layer IV, however this difference was less pronounced for the Basic stimulus than for the Contact stimulus.

By overlaying the stimulus waveforms on to the histograms of Figure 11, it is possible to identify discrete modes or groups of components occurring together which may be representative of particular features. For instance, the component times in layer IV for Contact appear to have three separate modes: 9ms-18ms representing the initial whisker deflection; 22ms-31ms representing a second 'bump' in the stimulus; and 39ms-44ms representing where the stimulus dips to its lowest point since the original whisker deflection. Further, the vast majority of the components in the second mode and all of the components in the third mode belong to units with two or three components, meaning that many units which respond to these later features of the stimulus also respond to earlier features. In comparison to layer IV, the component timings for Contact in layer II do not appear as well separated into distinct modes. Component timings in response to the Basic stimulus are more difficult to interpret, perhaps due to amplitude differences between the on-ramp velocity conditions at particular time-points. However, in the case of layer IV, all components occurring after 26ms come from units which have previously responded to earlier stimulus features. Such components could therefore be signaling velocity or amplitude accumulation over slower on-ramps, or the beginning or continuation of the holding period. Components which occur after 35ms could also be associated with the beginning of the off-ramp for the 400mm/s on-ramp velocity condition.

Component timings for TBI conditions for both stimuli are provided in Appendix II. These timing distributions are very similar to the sham component timings, with the exception of there being fewer components which can be associated with the initial whisker deflection caused by the stimulus (especially for the 4d TBI condition).

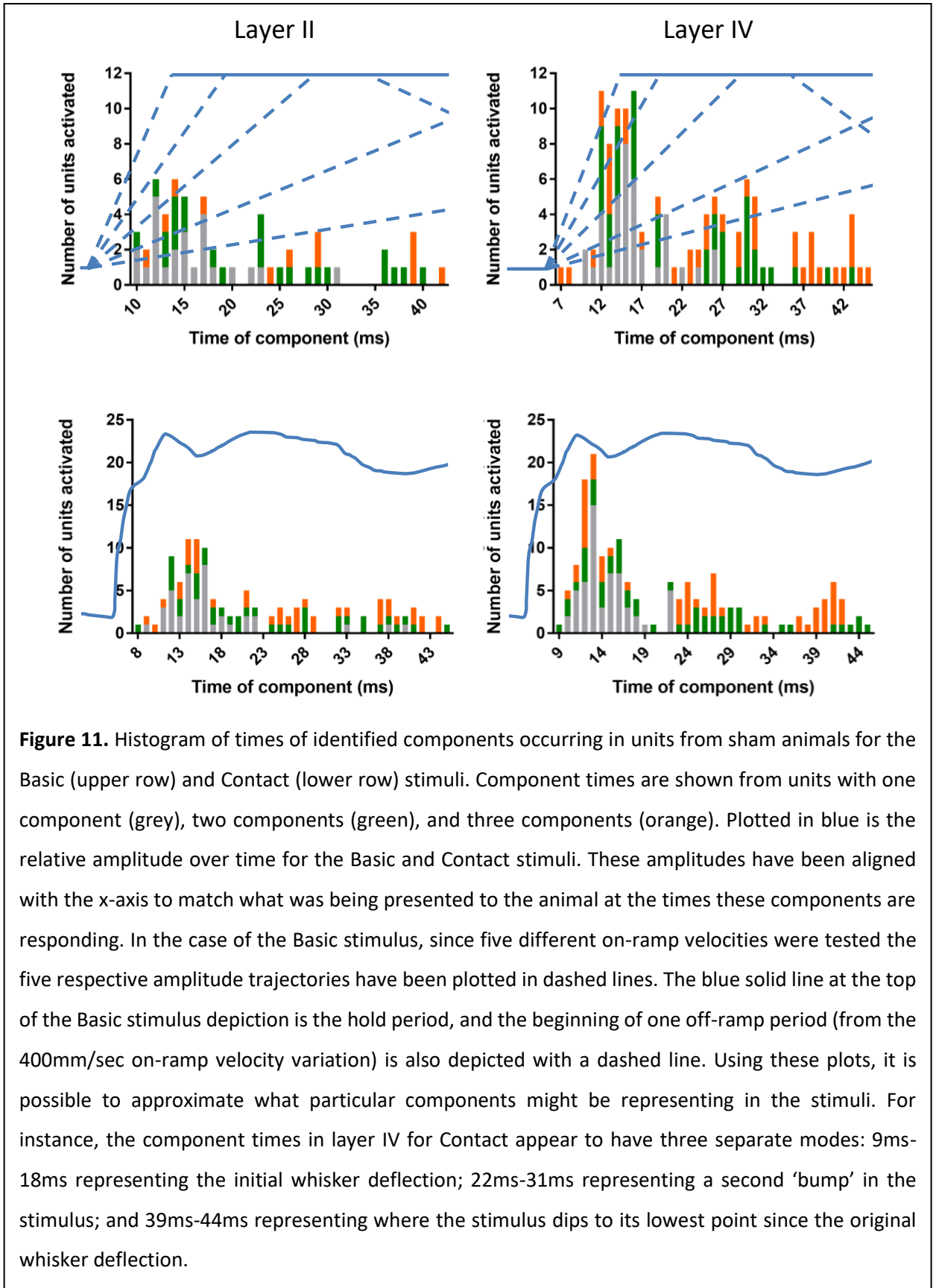
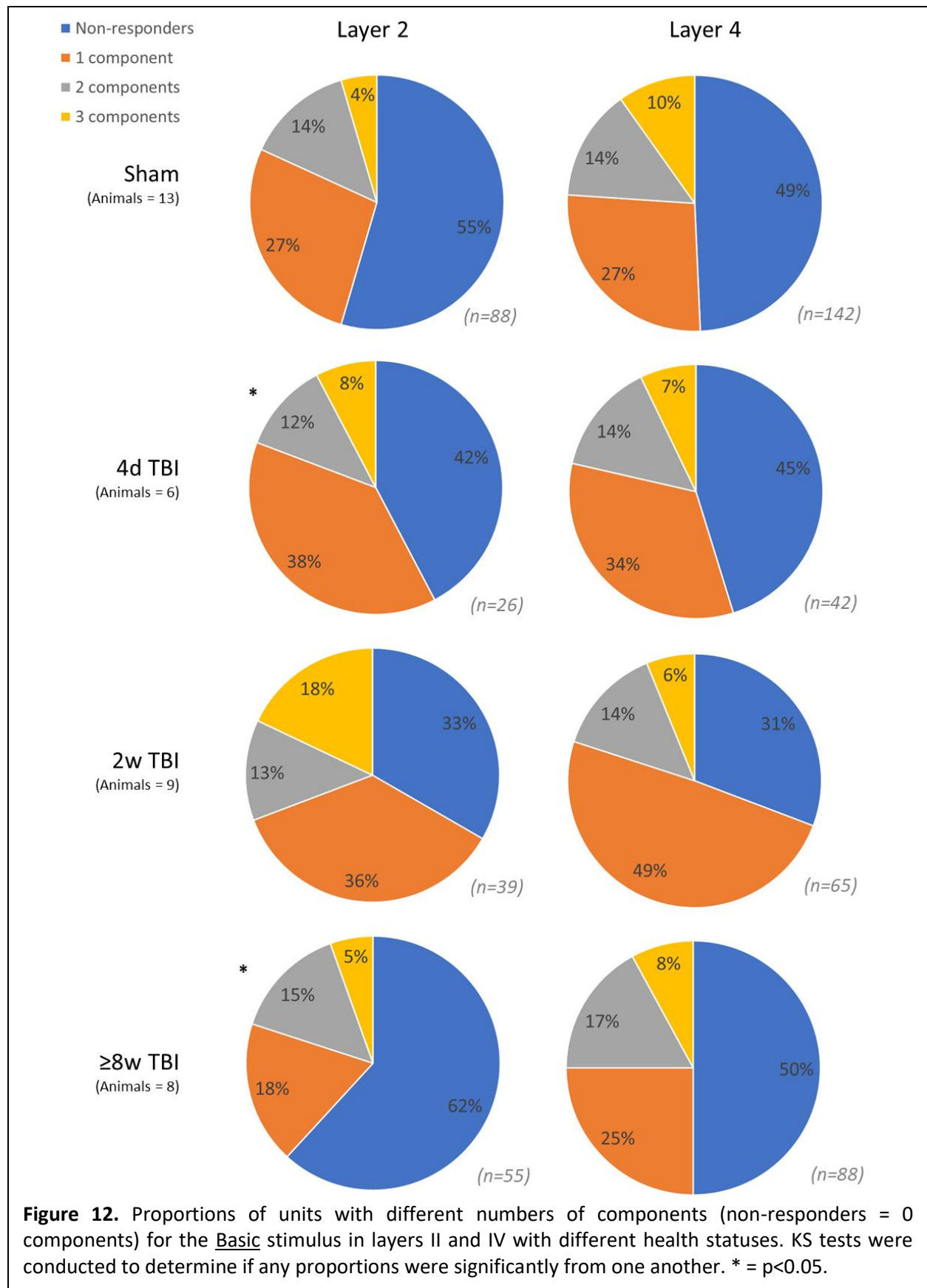


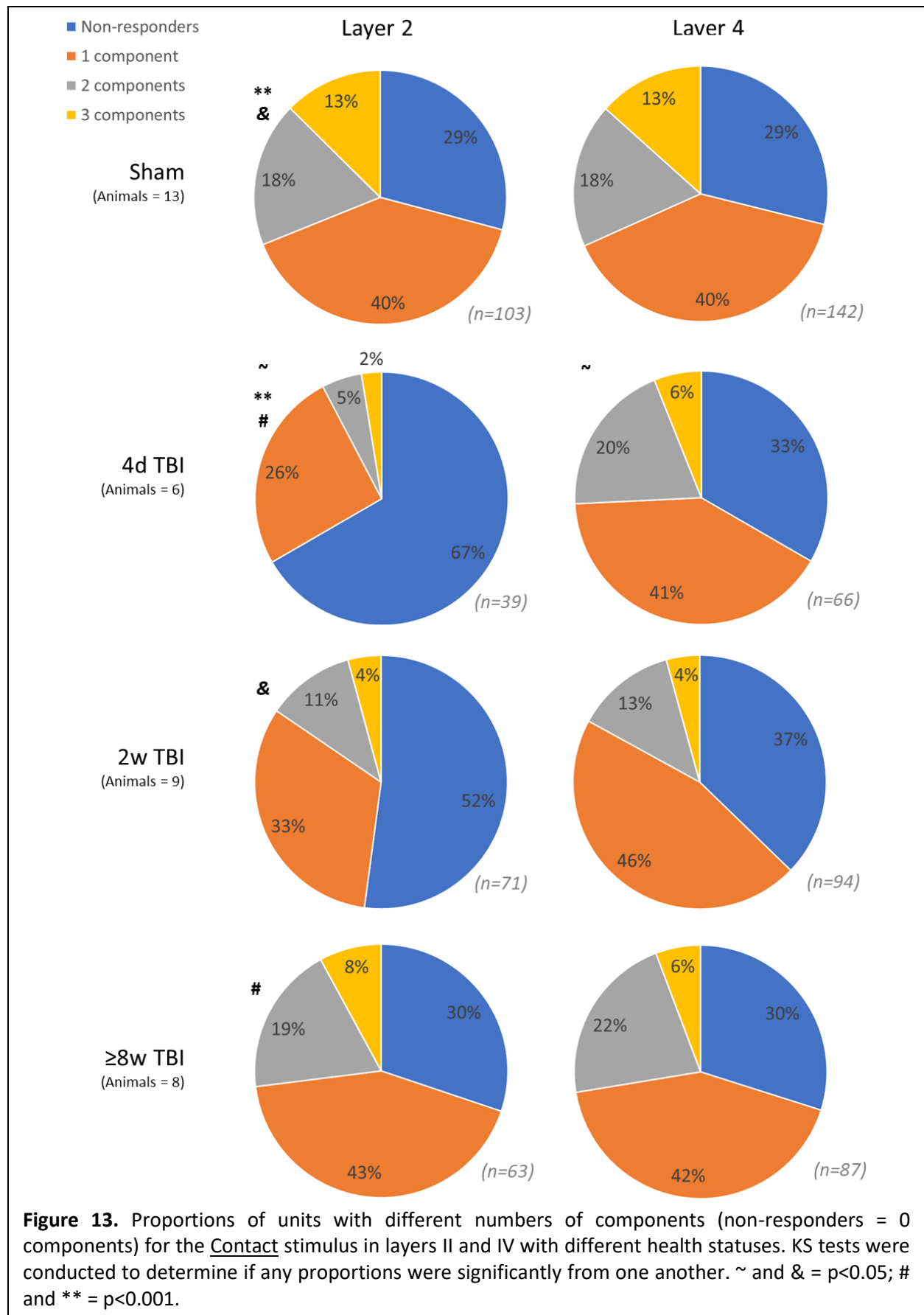
**Figure 11.** Histogram of times of identified components occurring in units from sham animals for the Basic (upper row) and Contact (lower row) stimuli. Component times are shown from units with one component (grey), two components (green), and three components (orange). Plotted in blue is the relative amplitude over time for the Basic and Contact stimuli. These amplitudes have been aligned with the x-axis to match what was being presented to the animal at the times these components are responding. In the case of the Basic stimulus, since five different on-ramp velocities were tested the five respective amplitude trajectories have been plotted in dashed lines. The blue solid line at the top of the Basic stimulus depiction is the hold period, and the beginning of one off-ramp period (from the 400mm/sec on-ramp velocity variation) is also depicted with a dashed line. Using these plots, it is possible to approximate what particular components might be representing in the stimuli. For instance, the component times in layer IV for Contact appear to have three separate modes: 9ms-18ms representing the initial whisker deflection; 22ms-31ms representing a second ‘bump’ in the stimulus; and 39ms-44ms representing where the stimulus dips to its lowest point since the original whisker deflection.

### *3.3.3 Proportions of units with different numbers of components and effect of brain injury*

Figures 12 and 13 show the proportions of units with different numbers of components (including with no components, which we term 'non-responders') in layers II and IV across the different animal conditions. Figure 12 shows the proportions for responses to the Basic stimulus indicates that in sham animals about half of all units are non-responders for both layers. A further 27% have a single component, and then the remainder have two or three components, although they together are outnumbered by units with single components. In the 4d TBI condition we notice that compared to sham, there is not much difference in the proportions of unit types – the only small difference is an increase in the proportion of units with single components and reduction in the proportion of non-responders, however this change was insignificant. In the 2w TBI condition for layer IV there is continuation of this trend, with proportionally fewer non-responders and more units with a single component, but this change is still insignificant. In layer II, there are also proportionally fewer non-responders, but instead of there being more single component units there are now proportionally more multi-component units than in sham or the 4d TBI condition (especially units which had three components). Nevertheless, this change is again insignificant as tested by KS tests. In the 8-12w TBI condition for layer IV the proportions return to very similar values as are seen in the sham animals. In layer II, however, the previously increasing proportion of single-component units has now shrunk to 18% of total units and the proportion of non-responders has increased. The proportions of units here are significantly different ( $p < 0.05$ ) to the proportions found in layer II for the 4d TBI condition, which has a similar proportion of multi-component units but the proportions of non-responders and single-component units is much more even than in the 8-12w TBI condition. This was the only significant difference found with KS tests between layers (for the same condition) or conditions (for the same layer) for the Basic stimulus.



In contrast to the results from the Basic stimulus, the results from the Contact stimulus had more significantly different distributions (see Figure 13). Across all conditions, the proportions of unit types in layer IV do not change much or in any significant way, with approximately one third of units being non-responsive, ~40-45% having single components, and the remainder being multi-component units. One small difference among the multi-component units, however, is a reduction in the number of units with three components in the TBI conditions compared to sham. Unlike in layer IV, unit type proportions in layer II for every condition were significantly different with to one or more other conditions, and in the case of the 4d TBI condition the layer II distribution was also significantly different to the layer IV distribution of the same condition. Overall, the sham and 8-12w TBI condition distributions are very similar, and both have extremely similar distributions to the distributions found in layer IV across all conditions. The major differences seen in the layer II distributions are for the 4d TBI and 2d TBI conditions, which are both have a much higher proportion of non-responders compared to sham and the 8-12w TBI condition. This makes the 4d TBI distribution significantly different to both the sham and 8-12w TBI distributions, and makes the 2w TBI distribution significantly different to the sham distribution. A general difference in layer II is also, like in layer IV, the proportional reduction in units with three components in the TBI conditions compared to sham.



### 3.3.4 Peakiness and significance of components

A concern about the definition of components using the independent neural response components analysis described above, was that some components, while being ‘local maxima’, may or may not be statistically significant. Therefore, we used two methods to analyse how statistically valid the components we identified were: (i) a ‘peakiness’ detection algorithm<sup>229–231</sup>; and (ii) a t-test (which tests if the means of two populations are equal) conducted in MATLAB comparing the components’ firing rates with the surrounding, non-component firing rates. Both methods were used individual components on a component-by-component basis for all units which had been identified as having at least one component. To calculate the peakiness or conduct the t-test, we took the mean firing rates (averaged across all velocities, for Basic, or amplitudes, for Contact) at the 5, 1ms time bins occurring immediately before the identified component time, as well at the 5, 1ms time bins occurring immediately after the identified component time. Together with the identified component time bin, this represented an 11ms segment of mean firing rates for that unit, where the 6<sup>th</sup> ms bin represented the component time.

In the case of the peakiness detection algorithm, we took mean firing rate (as a proportion of the mean firing rate at the identified component time) at the local minima within the segment and called this  $g_k$ . Then,  $peakiness = \frac{g_{i+1}}{g_{k+1}}$ , where  $g_i$  is the mean firing rate of the 6<sup>th</sup> ms bin, i.e. the identified component time. This provides us with a single number, ‘peakiness’, which described every component. This number varied on a scale of 0 to 2, where 0 represented that the identified component time had infinitely less firing than the local minima within  $\pm 5$ ms from the component time, where 2 represented it having infinitely more, and where 1 represented it being equal. In practice, this meant that a peakiness value of 1.25 indicates that the mean firing rate at the identified component time was > 25% than the surrounding mean firing rate minima within  $\pm 5$ ms from the component time; a value of 1.5 would indicate >50%, and so on.

For conducting the t-tests, we took the 5<sup>th</sup>, 6<sup>th</sup>, and 7<sup>th</sup> ms bin mean firing rates and called this group the ‘component’ group. We then performed a one-tailed two-sample t-test, comparing the mean firing rates of the ‘component’ group with the remaining 8, 1ms bin mean firing rates of the original 11ms-long segment. By conducting this test, we assumed an equal variance of the mean firing rate across the 11ms segment. Also, we conceded that due to the small sample sizes, the ability to detect highly significant differences would be diminished and we would only detect differences if the group means were very different. Using this method, we calculated p-values representing how significantly or insignificantly different each component’s mean firing rates were from the surrounding mean firing rates.

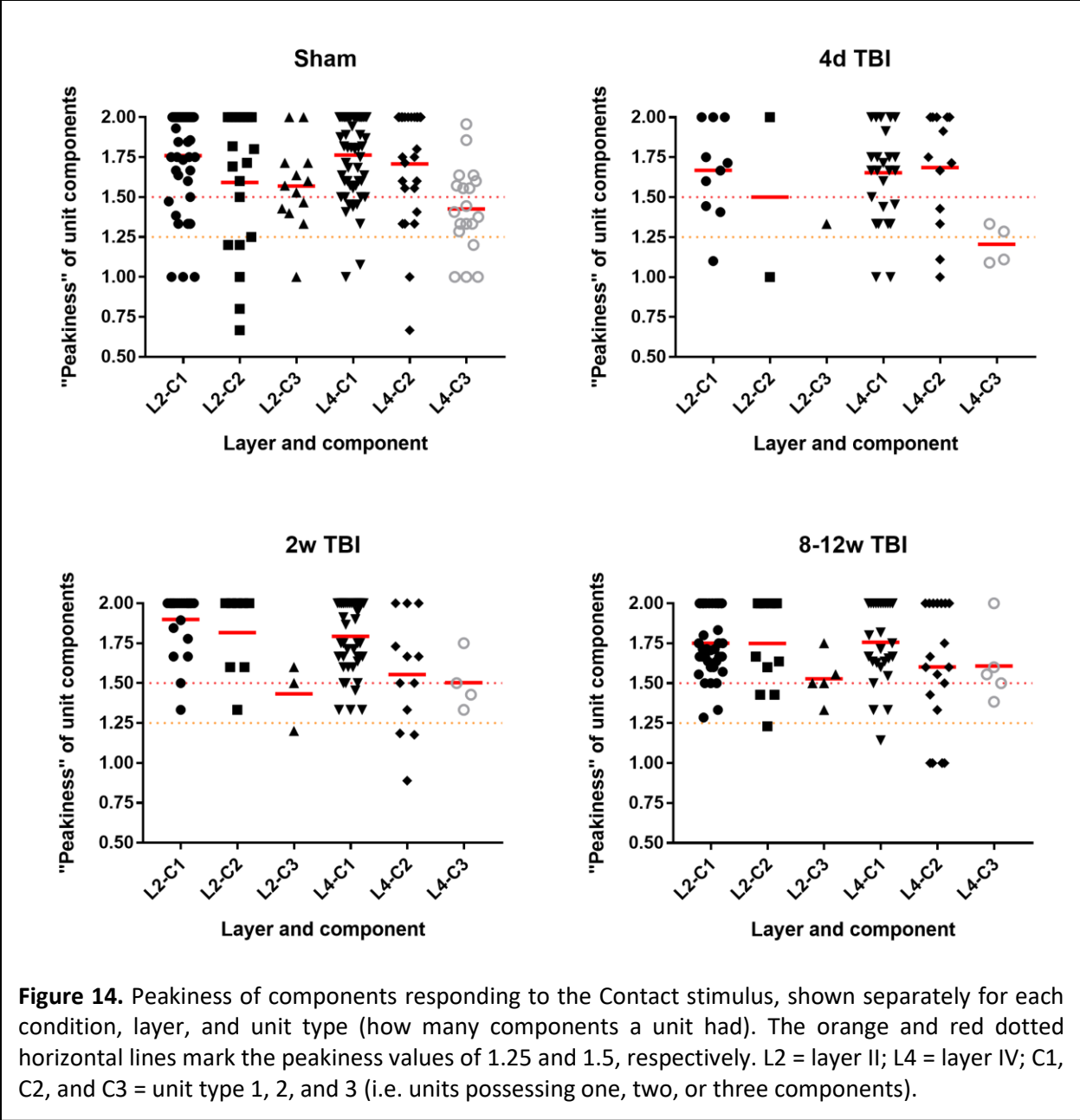


**Figure 14.** Peakiness of components responding to the Contact stimulus, shown separately for each condition, layer, and unit type (how many components a unit had). The orange and red dotted horizontal lines mark the peakiness values of 1.25 and 1.5, respectively. L2 = layer II; L4 = layer IV; C1, C2, and C3 = unit type 1, 2, and 3 (i.e. units possessing one, two, or three components).

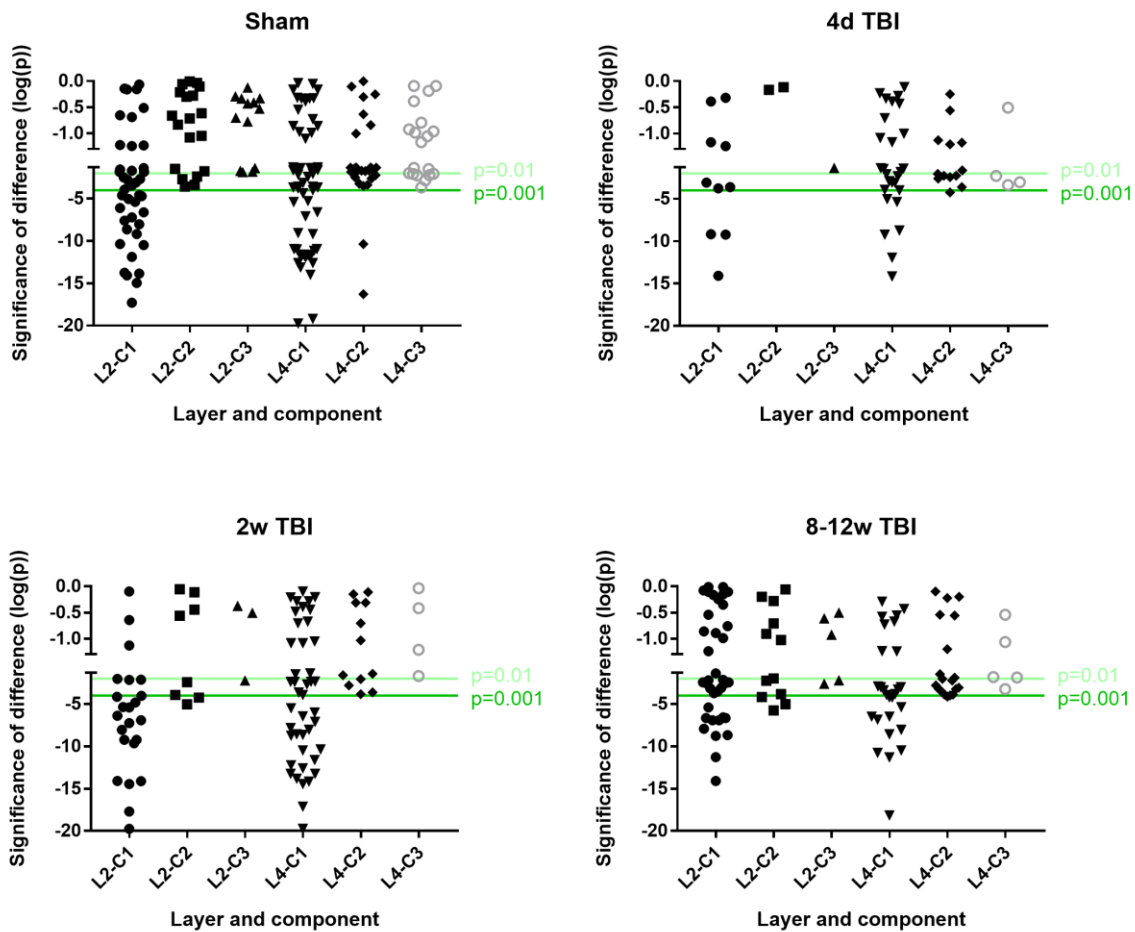


**Figure 15.** Significance of components' mean firing rates compared to mean firing rates within  $\pm 5$ ms. All components are responding to the Contact stimulus and shown separately for each condition, layer, and unit type (how many components a unit had). The break in the y-axis is where  $p=0.05$ . The light and dark green horizontal lines mark the p-values of 0.01 and 0.001, respectively. L2 = layer II; L4 = layer IV; C1, C2, and C3 = unit type 1, 2, and 3 (i.e. units possessing one, two, or three components).

After calculating the aforementioned 'peakiness' and p-values for all components of all units, we repeated the earlier pie charts and KS tests, however this time we excluded units containing components which did not meet certain levels of statistical criteria. We created four separate levels based on the aforementioned 'peakiness' and p-values – two stringent conditions and two less stringent conditions. These conditions were: (a)  $p < 0.05$ ; (b)  $p < 0.01$ ; (c) peakiness  $\geq 1.25$ ; and (d) peakiness  $\geq 1.5$ . We then examined and report the outcomes for each of those four criteria since there is no *a priori* way of knowing which criteria the brain uses to distinguish between significant and insignificant peaks in firing rate (or 'components') during a stimulus. This gives the advantage of a broader and non-prejudiced approach to the data, and allows us to discuss how the information available about the stimulus might change depending on how stringently the brain filters peaks in unit activity.

Almost all components had a peakiness of  $\geq 1.25$  (94% of Basic and 92% of Contact components), indicating that averaged across all velocities or amplitudes, the mean firing rate was  $\geq 25\%$  higher at the identified component time than at the local minima within  $\pm 5\text{ms}$  of the component. A large majority of components (76% of Basic and 79% of Contact components) also had a peakiness of  $\geq 1.5$ . Figure 16 shows the peakiness of components for Contact for each condition, separated by layer and whether the unit came had one, two, or three components. From looking at this figure it seems that units with two and, more especially, with three components generally have lower peakiness values than units with just one component, indicating that multi-component unit responses are normally 'weaker' than single component unit responses. This difference becomes more pronounced at higher thresholds, e.g. for the Contact stimulus, 97% of units with one component and 87% of units with two or three components had  $\geq 1.25$  peakiness, whereas these numbers fell to 87% and 68%, respectively, at peakiness values  $\geq 1.5$ .

These differences were more pronounced when looking at the t-tests performed using the mean firing rates on the components and the surrounding  $\pm 5\text{ms}$ . While a vast majority of components had significantly higher mean firing rates than the surrounding  $\pm 5\text{ms}$  at  $\alpha=0.05$  (91% of Basic and 87% of Contact components), far fewer reached significance at  $\alpha=0.01$  (46% of Basic and 52% of Contact components). Figure 17 shows the significance of components' mean firing rates compared to mean firing rates within  $\pm 5\text{ms}$  for the Contact stimulus, for each condition, separated by layer and whether the unit came had one, two, or three components. It is clear that the most significant differences are found for units with a single component, whereas few units with two or three components reach similar levels of significance; at  $\alpha=0.01$  for Contact, 63% of single component units, 39% two component units, and 27% of three component units reached significance. Granted, 86% of multi-component units reached significance at  $\alpha=0.05$  (compared with 90% for single-component units).

### 3.3.5 Temporal regularity of components occurring within the same unit

For both Basic and Contact stimuli, a number of significant relationships were found between the timings of first and second components in multi-component units. These relationships were particularly significant in the sham condition ( $p < 0.001$  for both stimuli in both layers II and IV). Relationships in the 8-12w TBI condition were also highly significant, especially in layer IV ( $p < 0.0001$  for Basic and  $p = 0.0014$  for Contact). However, there were irregular and insignificant timing relationships for both stimuli at the 4d TBI and 2w TBI conditions (see Figures 16 and 17), however in the case of the 4d TBI condition this may have been due to the relatively low numbers of units being analysed. The 2w TBI condition, however, analysed a comparable number of units as the 8-12w TBI condition (which found highly significant relationships) but failed to reach significance for three of four regressions.

To see how the relationships between these timings might reflect changes in the intracortical information flow after TBI, we calculated the y-intercepts shown in Table 3. We notice that in both layers and for both stimuli there is a general increase in the SEs of the y-intercepts, reflective of the higher scatter seen in Figures 18 and 19 for these relationships. Interestingly, considering the y-intercepts from just the sham and 8-12w TBI conditions shows that where the intercepts in one layer increase, in the other it decreases – and the relationships are opposite in the two stimuli. This may suggest some temporal changes in thalamic input to cortex via layer IV which is then being compensated for in layer II.

<i>Condition</i>	<i>Layer II</i>	<i>Layer IV</i>
<b>Basic stimulus</b>		
Sham	9.459 ± 4.103	16.26 ± 3.393
TBI four-days post-injury (4d TBI)	# 13.28 ± 5.899	10.37 ± 3.678
TBI two-weeks post-injury (2w TBI)	9.06 ± 5.682	# 22.49 ± 9.354
TBI 8-12-weeks post-injury (8-12w TBI)	7.271 ± 7.403	4.711 ± 2.052
<b>Contact stimulus</b>		
Sham	12.97 ± 2.618	8.248 ± 3.507
TBI four-days post-injury (4d TBI)	# -11.63 ± 8.814	21.05 ± 2.887
TBI two-weeks post-injury (2w TBI)	# 37.63 ± 13.38	# 15.47 ± 9.723
TBI 8-12-weeks post-injury (8-12w TBI)	7.877 ± 8.245	12.15 ± 5.265

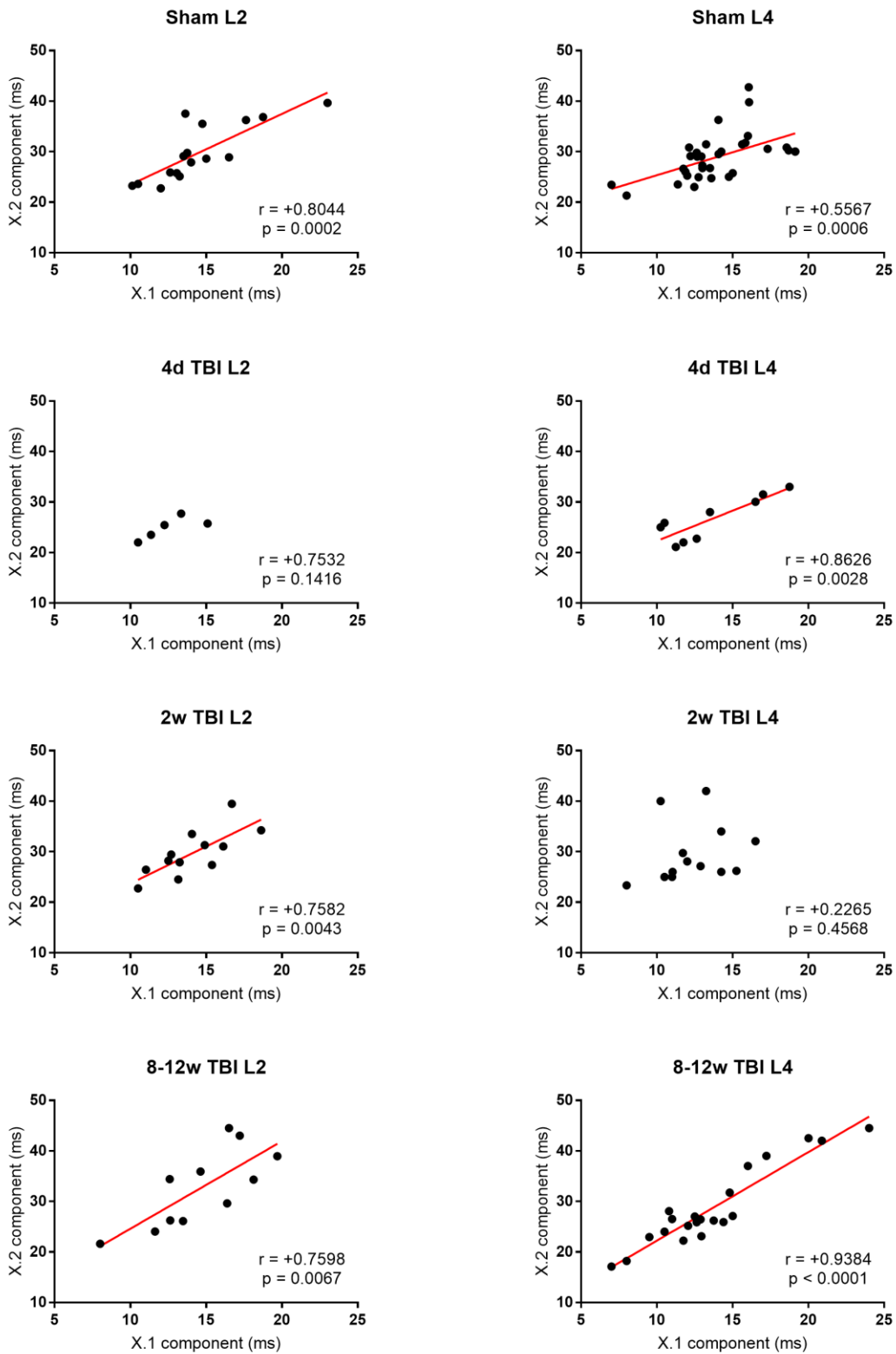


**Figure 16.** Linear regressions between the timings of first and second components of multi-component units responding to the Basic stimulus, separated by layer and condition. Red lines show line of best fit where the relationship is significantly correlated. L2 and L4 = layers II and IV; X.1 and X.2 = first and second components.

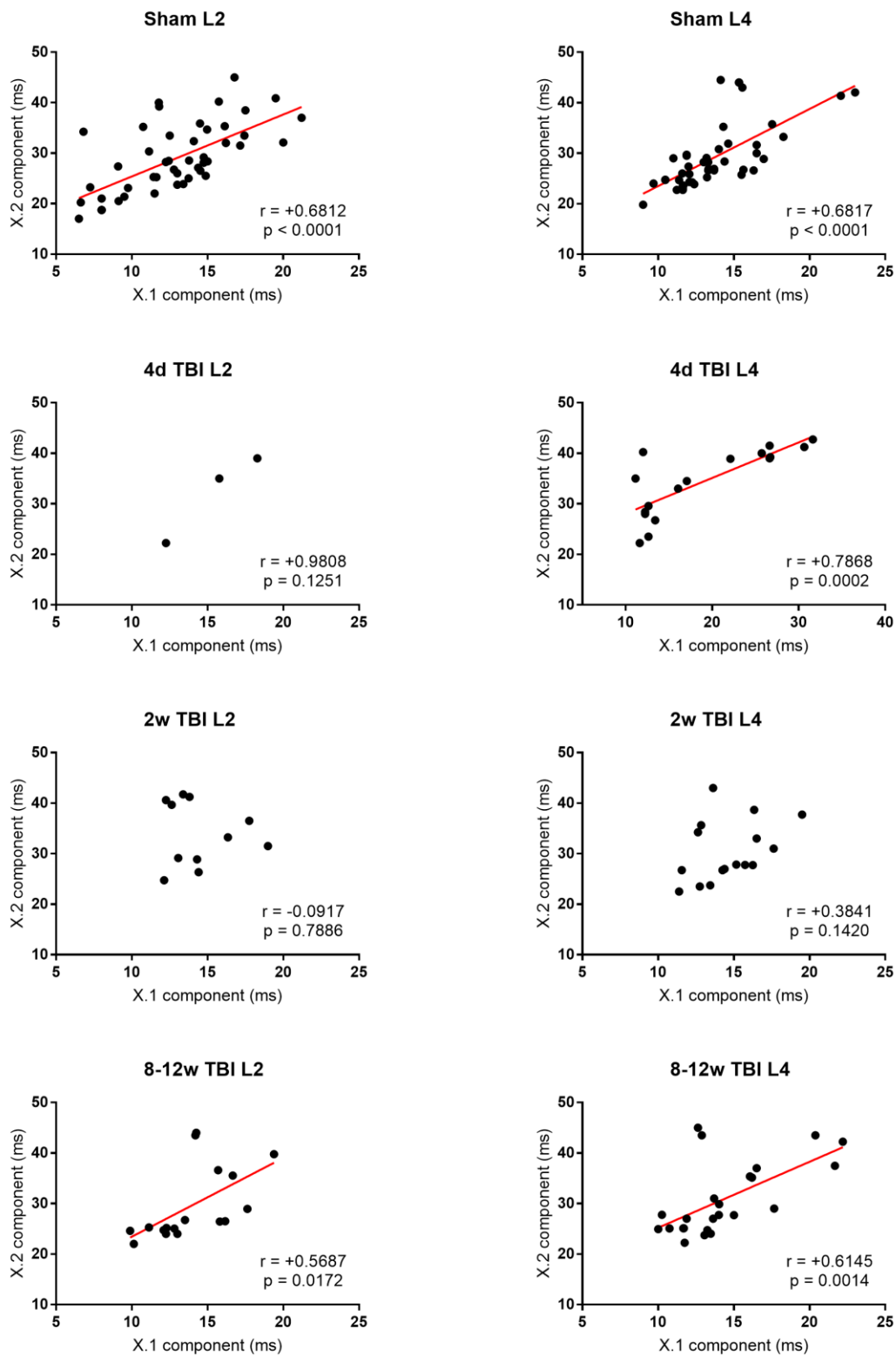


**Figure 17.** Linear regressions between the timings of first and second components of multi-component units responding to the Basic stimulus, separated by layer and condition. Red lines show line of best fit where the relationship is significantly correlated. L2 and L4 = layers II and IV; X.1 and X.2 = first and second components.

### 3.3.6 Graph-theoretic analysis

The independent neural response components analysis which forms the basis of the analyses up until this point was shown to be good at identifying single, temporally stationary components. However, as previously mentioned, some components noticeably shifted in time as a function of velocity (for Basic) or amplitude (for Contact). The previous analysis therefore was unable to capture information about how stationary or non-stationary these components were (see Figure 10 for examples), and indeed the reported peakiness (Figure 14) or significance of peaks (Figure 15) would be negatively affected by non-stationary components. We thought the non-stationarity of components could be an important feature to measure since, for units which had more than one component, some components appeared to interact, e.g. while ascending in amplitude one component might increase its activity while the other simultaneously and proportionally decreases (see Figure 10, bottom row for one such example). Such interactions, if sufficiently separated in time, could be evidence of feedforward inhibition or disinhibition, known to be present, for example, in layer IV of barrel cortex<sup>78-80</sup>. However, to accurately identify such interactions we cannot use the mean firing rates given by the independent neural response components analysis, as this represents essentially the median time at which the components occur across all velocities or amplitudes; in order to accurately identify such interactions, we need greater precision in the identification of the components across all velocities or amplitudes. For this we turn to a novel graph-theoretic analysis.

Although a wide variety of graph theoretic analyses have been employed in neuroscience datasets, such datasets have mostly been limited to neural network connectivity graphs created from neuroanatomical investigations to identify connectivity or the flow of activity in biological networks<sup>218,219</sup>. This is due to the usefulness of graphs in representing spatial relationships between mathematical objects and data. Here, we use such methods to identify components of a unit's activity. We do this by converting a unit's firing rates across all times and all velocities or amplitudes – as mapped in the velocity-time or amplitude-time space via PSTHs (see Figures 8 and 9) – into a directed graphical representation. Vertices represent the neural activity at different velocities/amplitudes and times and are connected to neighbouring vertices via weighted, directed edges. Vertices receive weighted, directed edges from other vertices representing the neural activity at velocities/amplitudes of  $z \pm 1$  and at times of  $t \pm 1$  (including at combinations  $z \pm 1, t \pm 1$ ), where  $z$  is the receiving vertex's velocity/amplitude and  $t$  is its time. These edges are made for all vertices that exist, i.e. because our analysis window ends at 50ms there can be no incoming edge from a 51ms vertex to a vertex representing 50ms since no such 51ms vertex exists. The

edges are weighted according to the mean firing rate of the vertex they are directed towards so that edges leading to vertices with relatively high mean firing rates have lower weights than edges leading to vertices with relatively low mean firing rates, like so:  $\frac{\text{unit max firing rate}}{\text{vertex mean firing rate}}$ . In the case of unit activity profiles for the Basic stimulus, this gives us a graph with 250 vertices in a grid spanning five velocities and 50ms; conversely, for the Contact stimulus, this gives us a graph with 500 vertices in a grid spanning 10 amplitudes and 50ms (see Figure 18 for visual representations).

By weighting the incoming, directed edges to all vertices by that respective vertex's firing rate, and adding a starting vertex (e.g. connected to all 0.2mm amplitude vertices) and goal vertex (e.g. connected to all 3.6mm amplitude vertices), one can then attempt to calculate the shortest path through the graph using Dijkstra's shortest path algorithm<sup>232</sup>, i.e. the route beginning at the starting vertex and ending at the goal vertex which travels through the graph along edges with the least accumulative weight. Such a path will preferentially travel through the vertices representing the highest mean firing rates (since edges leading to them had the least weight) but will ensure such vertices are as contiguous as possible according to the graph's structure (which, as mentioned, is constructed in a way that vertices representing neighbouring velocities/amplitudes and times are closely connected). This therefore gives us the ability of identifying a component which is freely-determined by the data, i.e. the path to move through velocity-time or amplitude-time space, as identified according to which velocity-time or amplitude-time bins possess the highest mean firing rates.

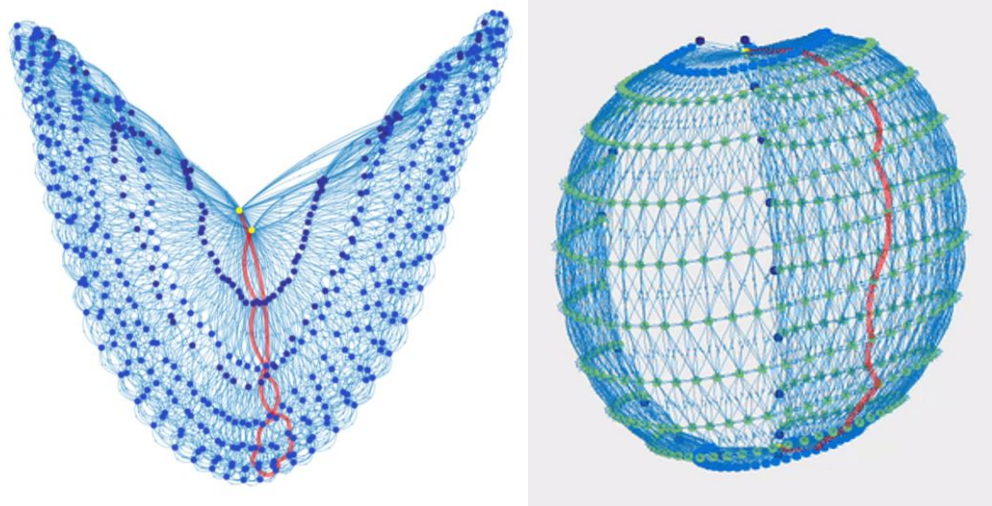
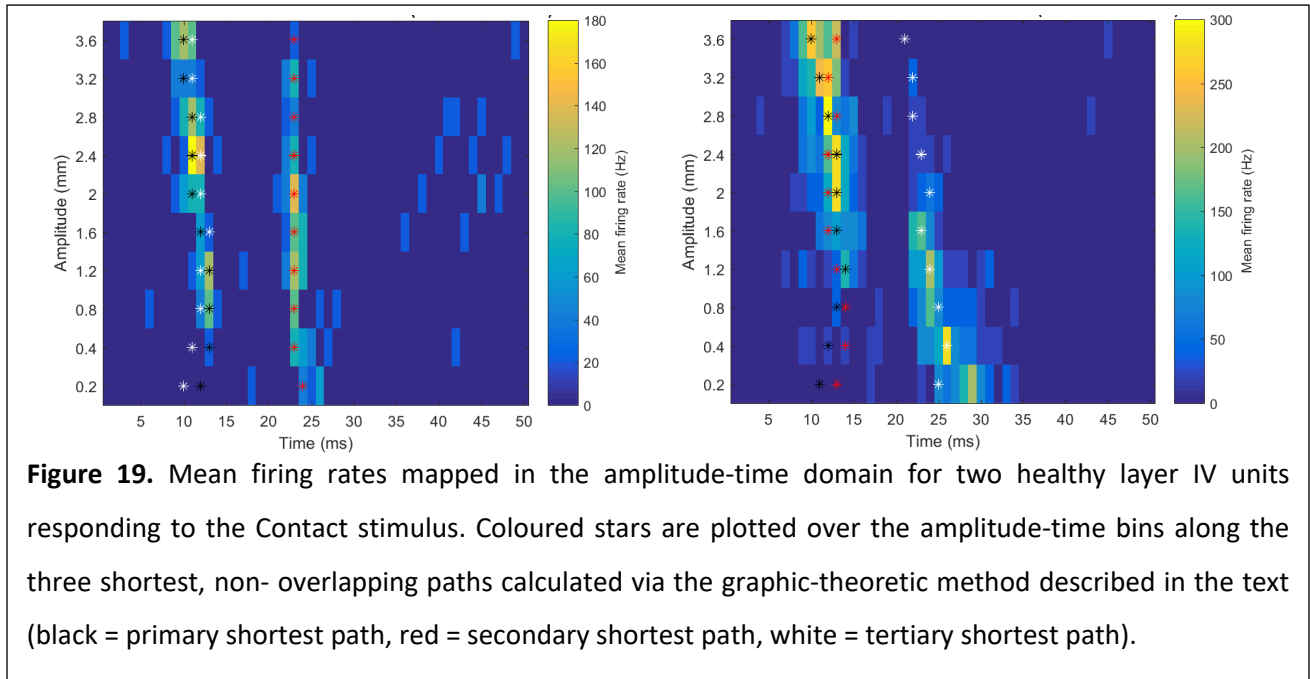


**Figure 18.** Visual representations of the 50ms x 10 amplitude vertex grid of mean firing rates for a unit activity profile with the Contact stimulus. (Left) 2D projection, (right) 3D projection of the same graph. Each vertex is equivalent to one ms bin at one amplitude. There are 50, 1ms bins arranged in 10 layers of increasing amplitude, each connected to their neighbours (both in the time and intensity domains) via edges. Edges arriving at a vertex are weighted according to the firing rate at that vertex. A vertex with a high firing rate has a low edge weight and a vertex with no firing at all will have a much higher weight. Using Dijkstra's shortest path algorithm <sup>232</sup>, the shortest possible path (travelling along edges which accumulate the lowest score, as determined by the sum of their weights) is searched for. Once found, this is plotted in red, along the edges and connecting the nodes with high firing rates (see Figure 19 for these paths plotted atop an example intensity-time heatmap). The colours of the nodes in both graphs in this figure are representative of the number of indegrees, or incoming edges arriving at that node, e.g. the green nodes are connected to by 8 other nodes. The yellow nodes at the top and bottom of the 3d projection (or the top centre of the 2d projection) are the start and goal nodes, as required by Dijkstra's algorithm, and are connected to the top and bottom layers of intensity-amplitude array, respectively.

Once the shortest path is calculated, we can re-weight the edges leading to vertices in that shortest path with an arbitrarily large weight and re-run the shortest path algorithm to find the secondary shortest path, which does not re-visit any vertices from the primary shortest path. This process can be repeated as many times as desired. A copy of algorithm implemented in MATLAB is provided in Appendix II. However, for our purposes, since the independent neural response components analysis revealed units in our database had no more than three components within the analysis window, we chose to calculate only up

to the tertiary shortest path. Figure 19 shows an example of the three shortest, non-overlapping paths through two units' firing activity profiles, as mapped in the amplitude-time space for the Contact stimulus.



Once identified, the following features of these components were calculated: the median time bin which the path vertices represent; the mean firing rates at each path step (and how these change as a function of mean firing rates at the equivalent steps of other components' within the same unit); and how stationary or non-stationary the path is in time. These measures were calculated for all components across all units.

To provide a common point of reference, we compared the median path times of the primary shortest paths (strongest components) with the component times given by the independent neural response components analysis. However, we did this only for units identified by the independent neural response components analysis as having a single component. This was because of a limitation of the graph-theoretic analysis in identifying multiple components; notice in the examples in Figure 19 that multiple paths can trace the activity of a single component. This is because the path widths are only 1ms and the re-weighting method is designed to reweight only this 1ms path before iterating to find the next shortest path. Therefore, in cases where a single component spreads across more than 1ms time bins in multiple velocities or amplitudes, there can be secondary or tertiary shortest paths which trace what is actually the same component as traced by the primary shortest path. It can also theoretically lead to cases

where if one component is at least 3ms wide across most velocities and amplitudes and has much higher mean firing rates than a second or third component, the shortest paths may all trace this large, single component. Returning to the comparison being made between the graph-theoretic analysis and the independent neural response components analysis, by comparing the median path times of the primary shortest path with the component times for units identified as having only one component, we ensure that the primary path times can only represent one component. If they could represent more than one component, we could not be confident of which component it was representing (the first or the second) and therefore we could not reliably compare the median path times with the component times given by the independent neural response components analysis. To compare the median path times and component times for single-component units we performed linear regressions for all such units, and also for units from animals of different health statuses or layers.

For all components of all units, we quantified how non-stationary each component was as  $\max(\text{vertex time}) - \min(\text{vertex time})$  to estimate how far the component shifted in time across velocities or amplitudes. We then plotted and compared the proportions of components which shifted (and to what degree, in ms) across all health conditions and for each layer using KS tests. We also plotted the median times for each component in groups depending on how non-stationary the component was to see if non-stationary components were more common at particular stimulus time-points.

Finally, using the mean firing rates at each path step and comparing these rates between paths from the same units we performed linear regressions, calculating the Pearson correlation coefficients and associated p-values for regressions between the mean firing rates from the primary shortest paths and secondary (or tertiary) shortest paths. For paths which were highly positively correlated, this gave us an indication that these paths may well trace strong, single components that spread over at least 2ms at most velocities or amplitudes. Conversely, these positive correlations could indicate that two components had similar firing rates across most velocities or amplitudes. For paths which were negatively correlated, this gave us an indication that the paths had inversely proportional firing rates across velocities/amplitudes, which could be indicative of inhibitory mechanisms known to present in barrel cortex.

### *3.3.7 Relationship between graph-theoretic and independent neural response components analyses*

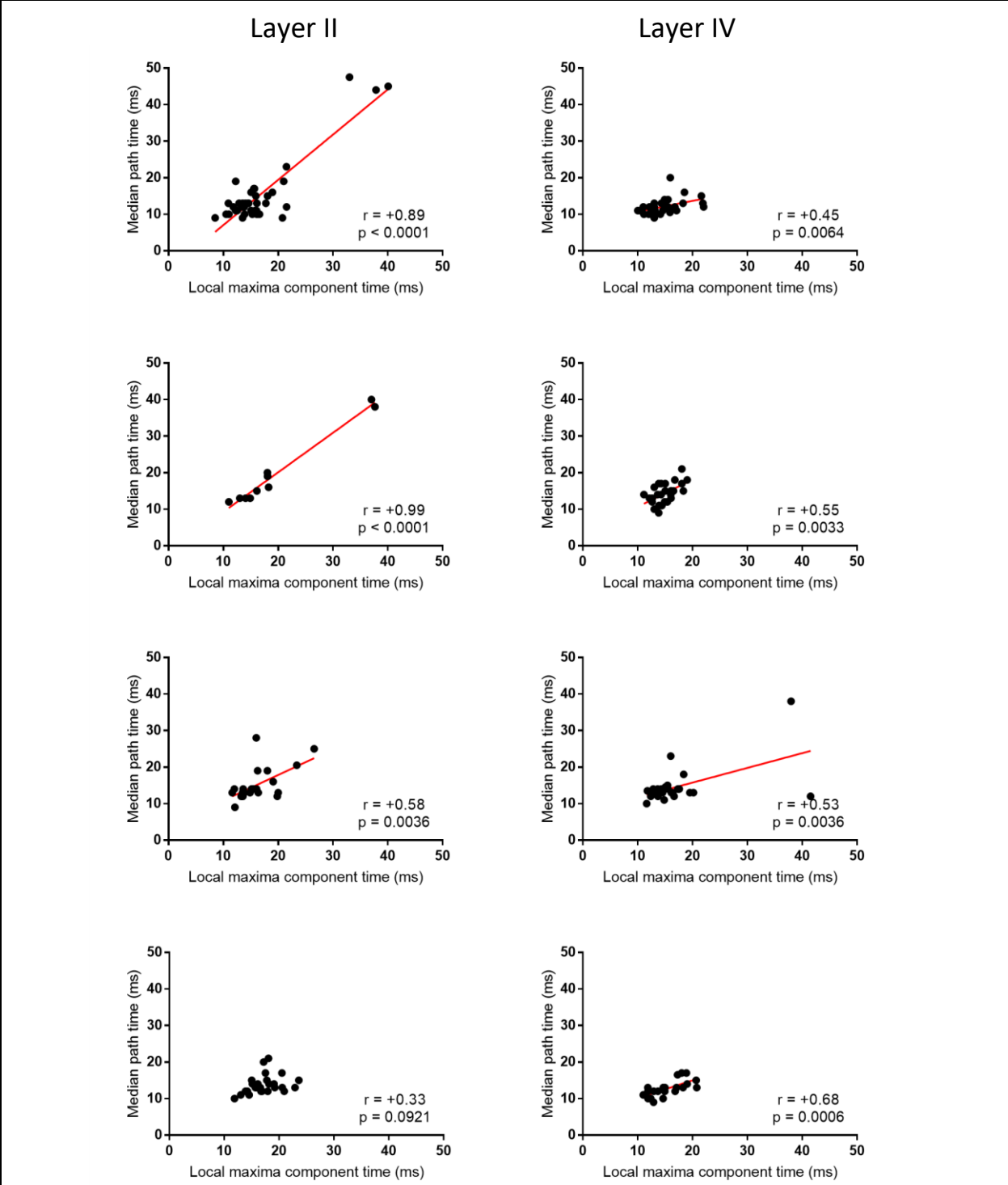
Figure 20 shows the relationships between the median path times calculated from the graph-theoretic analysis and the component times calculated from the independent neural response components analysis

for units responding to the Contact stimulus. Note that these mappings were only possible for units with one component (see 3.2.2 b). These relationships, where significant, are all positive. Similar relationships were seen for the Basic stimulus also, where all but the layer II, 8-12w TBI group were significantly correlated. These relationships serve as a point of reference to relate the results obtained from the two analyses. We can see from Figure 20 that these mappings are different between layers and conditions. In the case of layer II, for the sham and 4d TBI conditions the mapping is close to 1:1 between the times obtained for the same components from the two analyses. However, at the 2w and 8-12w TBI conditions this 1:1 mapping breaks down. In the case of layer IV, there is a weak positive correlation between the times obtained from the two methods, but this remains significant and relatively constant across animal conditions. Overall, the median path times tend to occur earlier than the local maxima component times calculated for the same unit components. While this comparison does not provide direct physiological insight, it serves as an important verification and comparison between these methods, and the physiological insights they provide.

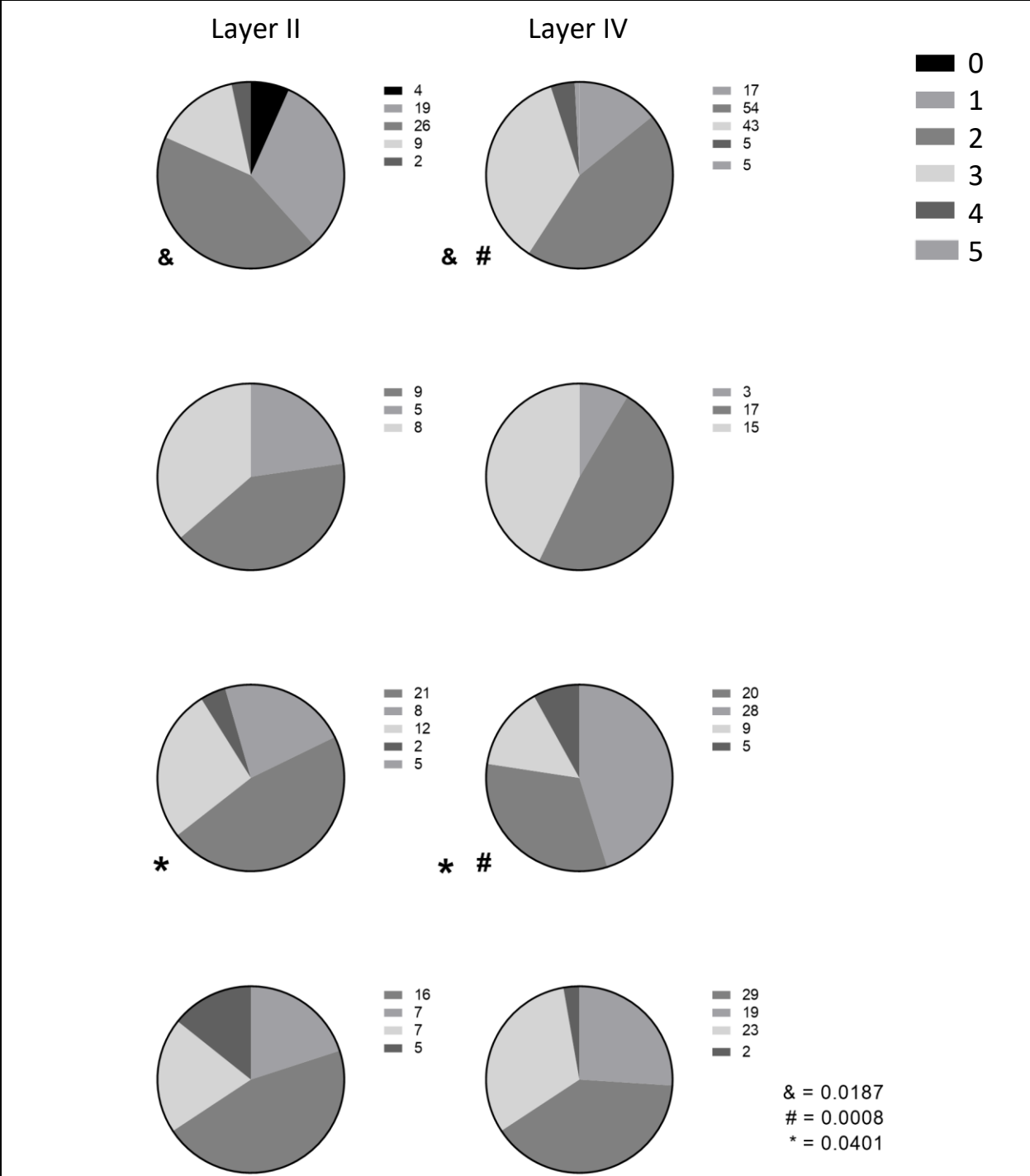
### *3.3.8 Non-stationarity of components*

Figure 21 shows the non-stationarity of components (how much components 'shifted' in time across different stimuli variations) for the Contact stimulus, separated by layer and condition. We can see that very few components are stationary, with most components moving across one or more ms as the stimulus varies in amplitude, the most common degree being 2ms and 3ms. This indicates that the function of microcircuitry controlling these temporal features are amplitude-dependent.

Across the layer II conditions, most components move 2-3ms, with a few being stationary in the sham condition and a minority across all conditions moving >3ms. However, this minority of less stationary components seems to proportionally increase in TBI conditions compared to sham, although this trend is insignificant. What is significant are the differences between layer II and IV for the sham and 2w TBI conditions. In the case of sham, layer IV components are much less stationary than layer II components, e.g. only 9 components had a movement of 3ms in layer II, whereas in layer IV there were 43 components. Conversely, for the 2w TBI condition, the significant difference between layers II and IV is due to a proportional increase in more stationary components – in layer II there were 8 components with a movement of 2ms, whereas in layer IV there were 28 components. This shift towards more stationary components also made the layer IV 2w TBI condition distribution significantly different to the layer IV sham condition, which proportionally had more non-stationary components. These results suggest that the amplitude-dependent microcircuit properties controlling these temporal features causes



**Figure 20.** Linear regressions between the median path times calculated from the graph-theoretic analysis and the component times calculated from the independent neural response components analysis (local maxima component times) for single-component units responding the Contact stimulus. Red lines indicate lines of best fit. First (top) row = sham; second row = 4d TBI; third row = 2w TBI; fourth (bottom) row = 8-12w TBI.



**Figure 21.** Proportions of units with different amounts of non-stationarity (0-5ms, indicated by the key top-right). Significantly different proportion pairs are marked with symbols and p-values given. First (top) row = sham; second row = 4d TBI; third row = 2w TBI; fourth (bottom) row = 8-12w TBI.

these changes in layers II and IV. Mechanistically, that components are more 'mobile' in layer IV than layer II could be due to a layer IV having more direct thalamocortical inputs than layer II or layer II having more interneurons which serve to lessen these amplitude-dependent effects. Most likely, it is some combination of these mechanisms.

### *3.3.9 Relationships between components' mean firing rates*

Figures 22 and 23 show the correlation (Pearson's  $r$  and associated  $p$ -values) for multi-component units' mean firing rates along their first and second (Figure 22) or first and third (Figure 23) shortest paths. We can see in both figures, across all layers and conditions, that there are many significant, positive correlations between the mean firing rates along these paths. Many of these paths are likely tracing segments of the same components (as discussed in 3.2.2 b), however it is also possible that these paths trace separate components which are affected by stimulus variations in a similar manner, e.g. see Figure 9, bottom-right panel. Unfortunately, we do not find any significant (at  $\alpha=0.05$ ), negative correlations, as we might expect from a unit like that shown in Figure 12, right panel. However, it should be noted that the majority of paths were not significantly correlated, positively or negatively, and this may be due to the low statistical power resulting in a higher likelihood of type II errors. Where we do see weak negative correlations, we notice that the sham condition generally contains more units with such relationships than do the TBI conditions (especially for the 4d TBI and 2w TBI conditions). By the 8-12w TBI condition, however, these weak negative correlations appear in more frequently and are more comparable to the sham condition than either of the other TBI conditions in this respect. This suggests that, if such results are indicative of cells with components which have oppositely-weighted amplitude-dependence (e.g. Figure 12, right panel), then such cells are less frequent in the early-to-mid recovery stages of TBI. This may indicate that such cells are more fragile or susceptible to TBI. In neither Figure 22 nor 23 does there appear to be any noticeable differences between layers II and IV, and any subtle (insignificant) differences between the conditions are similar across both layers.

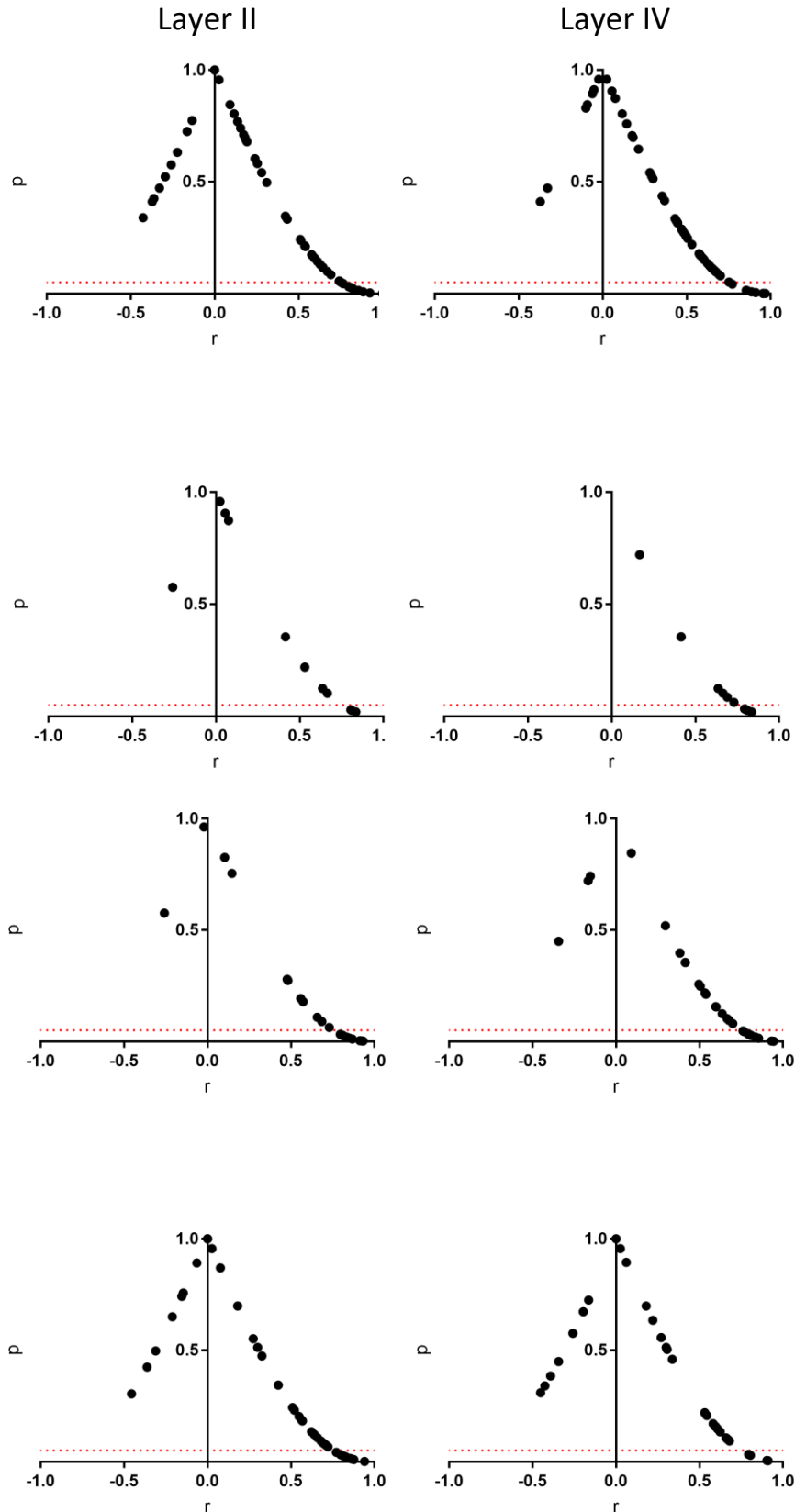


**Figure 22.** Linear correlation statistics (Pearson's  $r$  and associated  $p$ -value) for multi-component units' mean firing rates along their first and second shortest paths. The horizontal dotted red line marks where  $p=0.05$ . First (top) row = sham; second row = 4d TBI; third row = 2w TBI; fourth (bottom) row = 8-12w TBI.

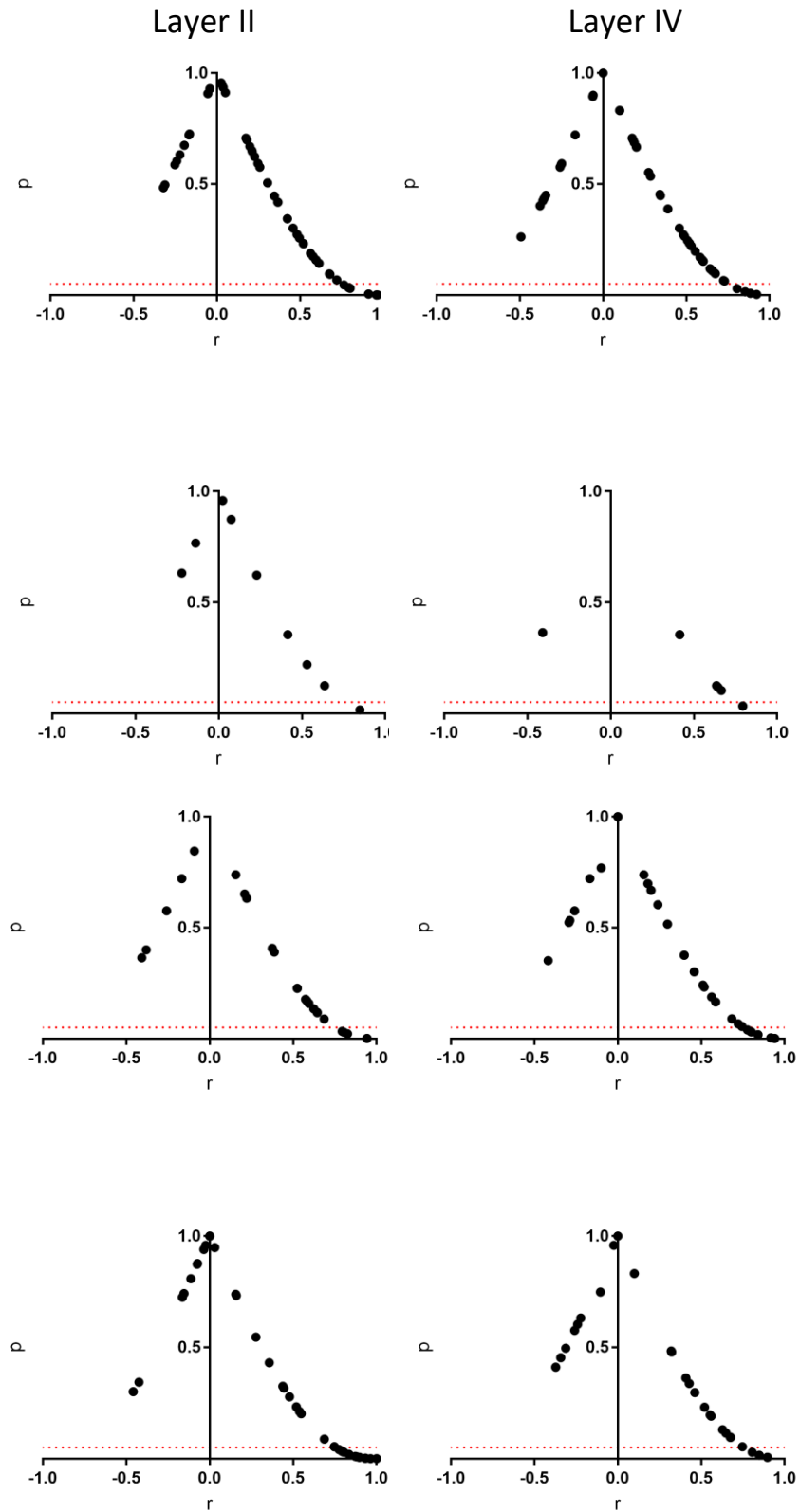


**Figure 23.** Linear correlation statistics (Pearson's  $r$  and associated  $p$ -value) for multi-component units' mean firing rates along their first and third shortest paths. The horizontal dotted red line marks where  $p=0.05$ . First (top) row = sham; second row = 4d TBI; third row = 2w TBI; fourth (bottom) row = 8-12w TBI.

## 3.4 Discussion

This project developed and applied novel analytical methods on a large electrophysiological database of barrel cortex experiments in healthy and perturbed states to demonstrate a number of significant differences between the temporal activity patterns of individual units and the distributions thereof in these states. We found further differences in the degrees of difference for responses to different stimuli, comparing data in layers II and IV.

### 3.4.1 Temporal activity patterns in healthy units

Our first aim was to identify and quantify significantly different unit temporal activity patterns in layers II and IV of barrel cortex in response to different stimuli in healthy rats, including how temporal activity patterns transform between these layers. In relation to this aim, we hypothesised that there are significantly different unit activity pattern distributions in layers II and IV of barrel cortex for the same stimuli. This hypothesis was not supported by our results, which showed no significant differences between the activity pattern distributions of layers II and IV for Basic or Contact.

We further hypothesised that there is less diversity in temporal activity patterns in layers IV than in layer II and that layer IV has proportionally fewer complex temporal activity patterns (temporal activity patterns with more than one major activity component) than simple temporal activity patterns (temporal activity patterns with only one major activity component) compared with layer II. This hypothesis must also be rejected based on our data, since no significant differences were observed for either Basic or Contact. However, although not statistically significant, we did observe a trend towards differences between layers II and IV for the Basic stimulus in the proportions of tri-component units – layer II had 4% whereas layer IV had 10%.

These results suggest that, under healthy conditions for stimuli similar to those we tested, layer II units largely reflect the same sorts of temporal activity patterns as are seen in layer IV and in almost the same proportions. However, this does not mean that no transformation or filtering of the VPM input is occurring via layer IV, since we did observe significant timing differences (see 3.4.2). What this does suggest, however, is for any other differences discussed in the following sections, such differences do not significantly change the overall activity structure (whether a unit contains one, two, or three components, or if it is a non-responder). At first this seems like a counter-intuitive result given that layer II neurons typically encode higher-level features of stimulus activity in barrel cortex than layer IV neurons do, and so it seems strange that there would be no significant change. However, that would assume the brain

ultimately cares about and interprets the overall activity structure or pattern and not also the timing or temporal relationships between such activity components. Further, even if we assumed that the brain ultimately cares more about the overall structure of temporal activity patterns than it cares about the timing of individual components within these patterns, we do not know that the brain interprets such temporal activity patterns in layers II and IV in the same way(s); it could be the case that despite having a similar structure, the rules for interpreting that structure are different for the afferent connections of layer IV and layer II. Indeed, this seems likely given that the main layer IV excitatory output is to layers II and III whereas the main layer II excitatory output is laterally to other parts of layer II (typically over several barrel columns), as well as to other cells in layers III and V, and to secondary somatosensory and motor cortices <sup>87,88</sup>. It also makes some intuitive sense that, mechanistically, it could be easier for layer II to transform the input in terms of timing than to completely abate major activity arriving via layer IV afferents, or to split such activity components into multiple components.

Finally, it should also be noted that while we assume most of our extracellular electrophysiological recordings are detecting voltage changes caused by the activity of pyramidal neurons (since they are typically much larger than inhibitory cells), there is the possibility that some of the voltage changes detected are measuring the activity of inhibitory cells. The chances of this happening are small, however are slightly smaller again in the case of layer IV compared to layer II, since layer IV has far fewer inhibitory neurons. So, although by virtue of analysing a large electrophysiological database we might be able to assume these chances are evenly distributed across layers, the intrinsic differences between layers in terms of their inhibitory makeups (see Figure 4) and their ratios of inhibitory to excitatory cells mean that in layer II the chance is higher.

### 3.4.2 Timing of components in healthy units

Also in relation to aim one, we hypothesised that the timing of components within temporal activity patterns is regular and consistent within individual layers. This hypothesis was supported by our results, where we found that for both the Basic and Contact stimuli there were highly significant ( $p < 0.001$ ) relationships between the times of components within individual layers. However, we noted that for both stimuli the y-intercepts of the slope of the regression line between component timings for each layer were dissimilar, and that the direction of difference between the layers was opposite between the stimuli (see Table 3). In the case of the Basic stimulus, the y-intercept for layer IV units was 16.260ms (with a SE of  $\pm 3.393$ ms) whereas for layer II it was 9.459ms (with a SE of  $\pm 4.103$ ms). In the case of the Contact stimulus,

the y-intercept for layer IV units was 8.248ms (with a SE of  $\pm 3.507$ ms) whereas for layer II it was 12.97ms (with a SE of  $\pm 2.618$ ms). This suggests that the way(s) layer II transforms temporal activity patterns from layer IV is stimuli-dependent. In both cases, the layer II y-intercept moves in the direction closer to  $\sim 10$ ms relative to the layer IV y-intercept. This might reflect an optimal inter-component timing for layer II for processing of higher features, whereas layer IV, not needing to perform such processing and primarily acting to amplify the thalamic signal and distribute it to other cortical layers<sup>49,57,58</sup>, is capable of producing a wider variety of inter-component timings (perhaps courtesy of its computationally simpler task). As to why the inter-component timings are so different for the two stimuli, we must refer back to the stimuli themselves and their features (see Figure 13). In doing so, we can see that the stimuli were varied in different aspects and also had other intrinsic differences. For instance, Basic was varied in on-ramp velocity while Contact was varied in peak amplitude. And once Basic reached its peak amplitude, it stayed constant whereas in Contact the peak amplitude was not constant and had other 'bumps' or features. However, to further complicate things, we should also note that by varying stimulus amplitude we also vary velocity (but not stimulus timing) and by varying stimulus velocity we also vary timing (but not ultimate amplitudes, except when compared at identical times). Considering these differences, it is not surprising that the inter-component timing was so different for the two stimuli, since the components almost certainly signal different features occurring at different times.

We also observed (as shown in Figure 13) that the component timings for the Contact stimulus were more neatly organised than were the timings for Basic, particularly in layer IV. In layer IV for the Contact stimulus, we noticed three apparent modes in which components occurred – the first corresponding with the initial whisker deflection, the second corresponding with a second 'bump' in the stimulus, and the third corresponding to the lowest amplitude since the initial deflection. Notably, however, a large majority of the components occurred during the initial stimulus onset period, which appears to be a common response characteristic in other sensory systems<sup>233</sup>.

Related to the same aim, we further hypothesised that peak response times will occur later for the same stimuli in layer II than in layer IV. This hypothesis was supported by our results from the Contact stimulus but not as well supported by our results from the Basic stimulus (see Figure 13). In the case of the Contact stimulus, the peak response time was around 12-13ms in layer IV and 14-15ms in layer II, whereas for the Basic stimulus, the earliest peak response times for both layers was  $\sim 12$ ms. The peak in layer IV ranges from  $\sim 12$ -15ms and the peak in layer II ranges from  $\sim 12$ -17ms, and the earliest components in layer IV occur at 7ms whereas the earliest components in layer II occur at 10ms. In this context it does

seem that components generally occur slightly later in layer II than in layer IV, however the fact remains that the earliest peak response time for both layers occurred in the same millisecond time bin. This could be due to errors relating to the method (see 3.2.2 a), since the components in Basic were observed to shift in their timing across stimulus velocity changes more than components in Contact shifted due to stimulus peak amplitude changes. However, this result might also indicate a difference in P<sub>Om</sub> input to layer II<sup>48,86</sup>, i.e. perhaps P<sub>Om</sub> is more sensitive than VPM to changes in velocity than amplitude, and thus driving proportionally more thalamic input to layer II at an earlier time-point, before VPM input can arrive via layer IV amplification and relay. If so, this could also help explain why we see early components in layer II (e.g. at 8ms) for the Contact stimulus (since, as discussed, by virtue of increasing the amplitude we indirectly increase velocity, especially in that early part of the stimulus where there is a large amplitude change).

### 3.4.3 Temporal activity patterns in TBI units

Our second aim was to identify and quantify how unit temporal activity patterns in layers II and IV of barrel cortex are altered by TBI when compared with healthy/sham units. These processing roles and the transformation of unit temporal activity patterns between layers IV and II are particularly interesting to analyse in the context of TBI, since recent studies suggest that functional changes occur throughout the cortical column, especially the function of inhibitory microcircuits<sup>5,173,179</sup>, which are known to be substantially different in layers II and IV of barrel cortex<sup>70</sup>. We therefore hypothesised that there are fewer temporal activity patterns in layer II (given the large diversity and number of inhibitory cells) in the TBI conditions compared with the sham condition. This hypothesis was supported by our results from the Contact stimulus, which showed two significant differences between such pattern distributions in layer II for the TBI conditions compared to sham; both the 4d and 2w TBI layer II unit activity pattern distributions were significantly different ( $p < 0.001$  and  $p < 0.05$ , respectively) compared to the layer II sham distribution. This was caused by a large increase in the proportion of non-responding cells in the 4d and 2w TBI condition compared to sham. These differences were also caused by a proportional decrease in the number of multi-component units in the TBI conditions, which confirmed another of our hypotheses, that complex temporal activity patterns (temporal activity patterns with more than one major activity component) account for fewer temporal activity patterns in TBI conditions, proportionally, than units with simple temporal activity patterns (temporal activity patterns with only one major activity component). In contrast, there were no significant differences for the Basic stimulus between the layer II activity pattern

distributions from sham and TBI conditions. This suggests that healthy inhibitory cell function in layer II might be more vital for accurate processing of the Contact stimulus compared to the Basic stimulus. We can be reasonably certain that the problem is in layer II more so than layer IV since there are no significant differences between any of the layer IV activity pattern distributions for either stimulus, suggesting the temporal activity patterns are relatively consistent in TBI and sham conditions. However, there is a significant difference ( $p < 0.05$ ) between the 4d TBI layer II and layer IV distributions for the Contact stimulus. That this difference is found for the Contact stimulus and not the Basic stimulus further reiterates the possible importance layer II inhibitory cells in the processing of complex, naturalistic stimuli such as Contact as opposed to simpler stimuli such as Basic.

We also hypothesised that among the TBI conditions, the least diverse distribution of temporal activity patterns is found in TBI animals four days following perturbation, and the most diverse distribution of temporal activity patterns is found in animals who received perturbation after eight-to-twelve weeks of recovery. This hypothesis was confirmed by our results, which showed for both the Basic and Contact stimuli that there were significant differences between the layer II activity pattern distributions at the 4d and 8-12w TBI conditions ( $p < 0.05$  for Basic and  $p < 0.001$  for Contact), where the 4d TBI condition has proportionally fewer responding units and also fewer multi-component units than the 8-12w TBI condition. This suggests that there is a gradual change between the 4d and 8-12w TBI condition time-points. That there is also no significant difference found between the sham and 8-12w TBI conditions for either layer or stimulus suggests that this gradual change represents, in effect, a recovery to sham-like activity pattern distributions. Before the 8-12w TBI time-point, past studies using segments of this data have shown<sup>12,187,188</sup> there is general hypoexcitation (particularly in supragranular layers), so our results showing a gradual increase in responsive units observed in this project across the 4d and 2w TBI conditions in layer II comports with these results. However, the same studies<sup>12,187,188</sup> have also shown that the supragranular layers show hyperexcitation at the 8-12w TBI time-point, whereas we found that there are no significant differences between the activity pattern distributions of sham and 8-12w TBI conditions (although we do find there to be a general reduction in multi-component units and a proportional increase in single component units). So, it is possible that the previously-observed hyperexcitation arises mostly from the reduction in these multi-component units, or that despite cells being more responsive at this time-point, they constrain their responses to activity profiles which are proportionally sham-like. This is also an interesting finding given that at the 8-12w TBI time-point animals demonstrate cognitive deficiencies as indicated by behavioural changes<sup>13,173,178</sup>, since our results show that not just is the cortex less responsive (especially in layer II, a supragranular layer), but that there are fewer units which we can

classify as responsive – and of those which are responsive, fewer of them contain multiple components. This suggests that the cognitive deficiencies generated by TBI at the 8-12w TBI time-point may be partially due not only to hypoexcitation but also to a lack of responsive cells and multi-component, complex responsive cells.

#### 3.4.4 Timing of components in TBI units

Also in relation to the second aim, we hypothesised that the timing of components within temporal activity patterns is distorted in TBI conditions compared to sham. This was supported by multiple analyses which show disruption in and significant differences between the timing of components for units from the sham and TBI conditions. In the case of the regressions between the component times for the multi-component units, we found that for both layers and stimuli, the times between the first and second component were significantly positively correlated in the sham and 8-12w TBI conditions. However, in the 4d and 2w TBI conditions these times were not always significantly correlated, especially in the 2w TBI condition. The y-intercepts (for those relationships which were significant), also gradually lowered (see Table 3) across the TBI conditions, e.g. Basic layer IV sham's y-intercept was  $16.26\text{ms} \pm 3.393\text{ms}$  and reduced to  $10.37\text{ms} \pm 3.678\text{ms}$  in the 4d TBI condition, then  $4.711\text{ms} \pm 2.052\text{ms}$  in the 8-12w TBI condition. However, there was one exception to this general reduction – Contact layer IV y-intercept was  $8.248\text{ms} \pm 3.507\text{ms}$  for sham but increased to  $12.15 \pm 5.265$  for 8-12w TBI. What makes this particularly unusual is that in layer II the y-intercept decreased. This suggests that there are some stimuli-dependent changes occurring in the timing between components, which agrees with the previously-discussed sham timing data (see 3.4.2). Supporting this, we can also notice that while in the case of the Basic stimulus the inter-component timing y-intercept is longer for layer IV than layer II for the sham condition, the opposite is true for the Contact stimulus. And the ultimate changes (increases or decreases) caused by TBI, as observed in the 8-12w TBI condition, show that these relationships swap, so that layer II's y-intercept is higher than layer IV's for Basic, and vice-versa for Contact. This suggests either some considerable changes in the timing of thalamic efferent activity arriving in layer IV (via VPM) and layer II (via POm), or that there is a combination of thalamic change (e.g. predominately a change in VPM input) and that subsequent compensatory mechanisms in cortex lead to the ultimate timing disparities we have observed. Given that the primary input to layer II is via layer IV and therefore VPM, however, it seems reasonable to expect that if this was purely a cortical compensatory effect, the y-intercept change should be immediate for layer IV at the 4d TBI condition for both stimuli and would remain constant, whereas the layer II y-

intercepts would slowly change, indicating compensation. However, in the case of Basic we find that while there is a change at this time-point, it is a gradual increase towards the values found for the 8-12w TBI condition. In the case of Contact there is a very large overshoot at the 4d TBI condition, before returning to a less extreme increase by the 8-12w TBI time-point. In both cases, however, the y-intercept is not constant across the TBI conditions, suggesting there are changes in the timing of VPM thalamic input to layer IV, and possibly additional changes happening in P<sub>Om</sub> input and cortex to effect compensation of these timing changes.

In addition to these changes we see in the timings between components in TBI conditions, we also see significant changes in the non-stationarity of these components. Per Figure 21, units responding to the Contact stimulus in layer IV of the 2w TBI condition distribution had significantly ( $p=0.008$ ) fewer non-stationary components compared to the sham condition. A similar, but less significant ( $p=0.035$ ) relationship was also found for the Basic stimulus. This further suggests that there is a change in VPM input to layer IV as a result of TBI, but that we find this only for the 2w TBI time-point suggests that this change is not permanent. And while we do not find significant differences among the layer II non-stationarity distributions for either stimulus, we do find significant differences for the Contact stimulus between layers II and IV for both the sham and 8-12w TBI conditions. In the case of sham, layer IV components, they were much less stationary than layer II components, e.g. only 9 components had a movement of 3ms in layer II, whereas in layer IV there were 43 components. Conversely, for the 2w TBI condition, the significant difference between layers II and IV is due to a proportional increase in more stationary components – in layer II there were 8 components with a movement of 2ms, whereas in layer IV there were 28 components. This mis-match between the direction of change for component timings agrees with our earlier results regarding multi-component unit timings and their regressions' y-intercepts. It also supports the idea that P<sub>Om</sub> input in layer II, cortical compensatory mechanisms, or some combination thereof, is attempting to work 'against' changes in layer IV activity, as driven by VPM. However, it is also possible that what we have been referring to as 'compensatory' mechanisms (whether in cortex or via P<sub>Om</sub> input) are actually the malfunctioning of inhibitory microcircuits in layer II and that such malfunctioning is the driver of these mis-matches. If so, taken together with our results regarding the activity component distributions (see 3.4.3), it seems likely that the major impact of inhibitory malfunction in TBI relates to disrupting the timing of components and not the overall number of such components.

### 3.4.5 Future directions

As well as presenting a good opportunity to procure novel results in terms of barrel cortex function and the effects of TBI, this work helps to further describe the electrophysiological database and will be an important resource for future analysis or modelling studies based on it. Having analysed layers II and IV using the methods in this project, it remains possible for others to extend the analysis across other layers of cortex, or to apply the novel analytical methods devised here to other datasets. It is also possible to relate particular results from this project back to histological or behavioural data (which has also been collected from many animals in the electrophysiological database). Another possible use of this work could be in developing computational models of barrel cortex, TBI, and TBI recovery; combined with knowledge of cortical neuroanatomy and the physiological changes post-TBI, results from this study allow specific predictions and constraints which can be placed on a model, e.g. in how unit-to-unit activity profiles transform between layers II and IV.

### 3.4.6 Conclusions

We have found evidence that microcircuits in layers II and IV functionally maladapt and/or reorganize in barrel cortex after diffuse TBI and that such maladaptation or reorganization is layer dependent. This layer dependency could be partially due to differences in the type and number of interneurons in the layers studied. Looking over the different time-points, we notice that in both layers II and IV of the 4d TBI condition many units were unresponsive, although those which did respond responded with more than one component had regular and consistent timing relationships between their components. For the 2w TBI condition in layer II, many units were still non-responsive and multi-component units which were responsive had timing disruptions, dissimilar to sham and 4d TBI conditions. The components were also less stationary than in layer IV for this condition. Layer IV had fewer non-responders than layer II, with a sham-like distribution. And multi-component responsive units had timing disruptions (but were less severe than those in layer II). For the 8-12w TBI condition in layer II, there was a return to sham-like unit activity pattern distributions, but far fewer tri-component/complex responsive units. These multi-component responsive units had regular and consistent timing relationships. In layer IV there was also a return to sham-like unit activity pattern distributions, but far fewer tri-component/complex responsive units. Like in layer II, these multi-component responsive units had regular and consistent timing relationships.

Collectively, along with the various stimulus-dependent and layer-dependent effects mentioned, these analyses suggest that TBI negatively effects the function of individual units in barrel cortex. Along

with the previously-established general reduction in inhibition after TBI<sup>5</sup>, this emphasises the importance of fine-tuned inhibition on temporal qualities of sensory signals in layers II and IV. Simultaneously, it demonstrates that some units appear functionally unchanged despite global excitatory-inhibitory imbalance and microcircuit changes. Commutatively, however, these effects lead to an increase in non-responsive units, changes in distributions of temporal activity patterns, and misalignment of the different components in multi-component temporal response patterns. While some of these changes appear transient, others appear to persist long after TBI. It is possible that some of these changes are partially responsible for the short- and long-term behavioural and cognitive changes which occur due to TBI.

## 4. Bibliography

1. WHO Programme for the Prevention of Deafness and Hearing Impairment. Report of the informal consultation on the economic analysis of sensory disabilities, WHO, Geneva 28-29 November 2000. 2001:23 p. [http://whqlibdoc.who.int/hq/2001/WHO\\_PBD\\_01.1.pdf](http://whqlibdoc.who.int/hq/2001/WHO_PBD_01.1.pdf).
2. WHO Programme for the Prevention of Deafness and Hearing Impairment. Global Data on Visual Impairments 2010. 2010:1-14. <http://www.who.int/topics/blindness/en/>. Accessed October 17, 2016.
3. Blakemore C, Clark JM, Nevalainen T, Oberdorfer M, Sussman A. Implementing the 3Rs in Neuroscience Research: A Reasoned Approach. *Neuron*. 2012;75(6):948-950. doi:10.1016/j.neuron.2012.09.001.
4. Semple BD, Blomgren K, Gimlin K, Ferriero DM, Noble-Haeusslein LJ. Brain development in rodents and humans: Identifying benchmarks of maturation and vulnerability to injury across species. *Prog Neurobiol*. 2012;100(2):130-134. doi:10.1016/j.pestbp.2011.02.012.
5. Carron SF, Alwis DS, Rajan R. Traumatic Brain Injury and Neuronal Functionality Changes in Sensory Cortex. *Front Syst Neurosci*. 2016;10(June):47. doi:10.3389/fnsys.2016.00047.
6. Reid RC, Koch C. Observatories of the mind. *Nature*. 2012;483(7390):397-398. doi:10.1038/483397a.
7. White EL, Rock MP. A comparison of thalamocortical and other synaptic inputs to dendrites of two non-spiny neurons in a single barrel of mouse Sml cortex. *J Comp Neurol*. 1981;195(2):265-277. doi:10.1002/cne.901950207.
8. Lavzin M, Rapoport S, Polsky A, Garion L, Schiller J. Nonlinear dendritic processing determines angular tuning of barrel cortex neurons in vivo. *Nature*. 2012;490(7420):397-401. doi:10.1038/nature11451.
9. Phoka E, Wildie M, Schultz SR, Barahona M. Sensory experience modifies spontaneous state dynamics in a large-scale barrel cortical model. *J Comput Neurosci*. 2012;33(2):323-339. doi:10.1007/s10827-012-0388-6.
10. Jensen KF, Killackey HP. Terminal arbors of axons projecting to the somatosensory cortex of the adult rat. I. The normal morphology of specific thalamocortical afferents. *J Neurosci*. 1987;7(11):3529-3543. <http://www.ncbi.nlm.nih.gov/pubmed/3316526><http://www.ncbi.nlm.nih.gov/pubmed/3316525>.
11. Feldmeyer D, Egger V, Lübke J, Sakmann B. Reliable synaptic connections between pairs of excitatory layer 4 neurones within a single 'barrel' of developing rat somatosensory cortex. *J Physiol*. 1999;521(1):169-190. doi:10.1111/j.1469-7793.1999.00169.x.
12. Alwis DS, Yan EB, Morganti-Kossmann M-C, Rajan R. Sensory Cortex Underpinnings of Traumatic Brain Injury Deficits. *PLoS One*. 2012;7(12). doi:10.1371/journal.pone.0052169.
13. Johnstone VPA, Shultz SR, Yan EB, O'Brien TJ, Rajan R. The acute phase of mild traumatic brain injury is characterized by a distance-dependent neuronal hypoactivity. *J Neurotrauma*. 2014;31(22). doi:10.1089/neu.2014.3343.
14. Rice FL, Mance A, Munger BL. A comparative light microscopic analysis of the sensory innervation of the mystacial pad. I. Innervation of vibrissal follicle-sinus complexes. *J Comp Neurol*. 1986;252(2):154-174. doi:10.1002/cne.902520203.
15. Stuttgen MC, Ruter J, Schwarz C. Two psychophysical channels of whisker deflection in rats align with two neuronal classes of primary afferents. *J Neurosci*. 2006;26(30):7933-7941. doi:10.1523/JNEUROSCI.1864-06.2006.

16. Marshall CD, Amin H, Kovacs KM, Lydersen C. Microstructure and innervation of the mystacial vibrissal follicle-sinus complex in bearded seals, *Erignathus barbatus* (Pinnipedia: Phocidae). *Anat Rec Part A, Discov Mol Cell Evol Biol.* 2006;288(1):13-25. doi:10.1002/ar.a.20273.
17. Dehnhardt G, Hyvärinen H, Palviainen A, Klauer G. Structure and innervation of the vibrissal follicle-sinus complex in the Australian water rat, *Hydromys chrysogaster*. *J Comp Neurol.* 1999;411(4):550-562. doi:10.1002/(SICI)1096-9861(19990906)411:4<550::AID-CNE2>3.0.CO;2-G.
18. Kim JN, Koh KS, Lee E, Park SC, Song WC. The morphology of the rat vibrissal follicle-sinus complex revealed by three-dimensional computer-aided reconstruction. *Cells Tissues Organs.* 2011;193(3):207-214. doi:10.1159/000319394.
19. Ebara S, Kumamoto K, Matsuura T, Mazurkiewicz JE, Rice FL. Similarities and differences in the innervation of mystacial vibrissal follicle-sinus complexes in the rat and cat: A confocal microscopic study. *J Comp Neurol.* 2002;449(2):103-119. doi:10.1002/cne.10277.
20. Lazarov NE. Comparative analysis of the chemical neuroanatomy of the mammalian trigeminal ganglion and mesencephalic trigeminal nucleus. *Prog Neurobiol.* 2002;66(1):19-59. doi:10.1016/S0301-0082(01)00021-1.
21. Morton D. The Trigeminal System. In: Iggo A, ed. *Handbook of Sensory Physiology, Somatosensory Systems.* Berlin: Springer-Verlag; 2013:271-314. [http://library.med.utah.edu/diganat/SOM/dental.neuro/05 Trigeminal system 2013.pdf](http://library.med.utah.edu/diganat/SOM/dental.neuro/05%20Trigeminal%20system%202013.pdf).
22. Castro-Alamancos M a. Properties of primary sensory (lemniscal) synapses in the ventrobasal thalamus and the relay of high-frequency sensory inputs. *J Neurophysiol.* 2002;87(2):946-953. doi:10.1013/jphysiol.2001.013283.
23. Miyata M, Imoto K. Different composition of glutamate receptors in corticothalamic and lemniscal synaptic responses and their roles in the firing responses of ventrobasal thalamic neurons in juvenile mice. *J Neurophysiol.* 2006;95(Pt 1):161-174. doi:10.1113/jphysiol.2006.114413.
24. Castro-Alamancos MA. The Whisker Thalamus. In: Krieger P, Groh A, eds. *Sensorimotor Integration in the Whisker System.* Heidelberg: Springer Science; 2015:31-58. doi:10.1007/978-1-4939-2975-7.
25. Land PW, Buffer SA, Yaskosky JD. Barreloids in adult rat thalamus: Three-dimensional architecture and relationship to somatosensory cortical barrels. *J Comp Neurol.* 1995;355(4):573-588. doi:10.1002/cne.903550407.
26. Saporta S, Kruger L. The organization of thalamocortical relay neurons in the rat ventrobasal complex studied by the retrograde transport of horseradish peroxidase. *J Comp Neurol.* 1977;174(2):187-208. doi:10.1002/cne.901740202.
27. Pierret T, Lavallée P, Deschênes M. Parallel streams for the relay of vibrissal information through thalamic barreloids. *J Neurosci.* 2000;20(19):7455-7462.
28. Landisman CE, Long MA, Beierlein M, Deans MR, Paul DL, Connors BW. Electrical synapses in the thalamic reticular nucleus. *J Neurosci.* 2002;22(3):1002-1009. doi:10.1523/JNEUROSCI.22-03-2002.2002 [pii].
29. Sohal VS, Huguenard JR. Inhibitory interconnections control burst pattern and emergent network synchrony in reticular thalamus. *J Neurosci.* 2003;23(26):8978-8988. doi:10.1523/JNEUROSCI.23-26-2003.2003 [pii].
30. Varga C, Sík A, Lavallée P, Deschênes M. Dendroarchitecture of relay cells in thalamic barreloids: a substrate for cross-whisker modulation. *J Neurosci.* 2002;22(14):6186-6194. doi:10.1523/JNEUROSCI.2002-06.2002.
31. Lavallée P, Deschênes M. Dendroarchitecture and lateral inhibition in thalamic barreloids. *J Neurosci.* 2004;24(27):6098-6105. doi:10.1523/JNEUROSCI.0973-04.2004.
32. Bokor H, Frère SGA, Eyre MD, et al. Selective GABAergic control of higher-order thalamic relays. *Neuron.* 2005;45(6):929-940. doi:10.1016/j.neuron.2005.01.048.
33. Trageser JC, Keller A. Reducing the Uncertainty: Gating of Peripheral Inputs by Zona Incerta. *J Neurosci.* 2004;24(40):8911-8915. doi:10.1523/JNEUROSCI.3218-04.2004.

34. Lavallée P, Urbain N, Dufresne C, Bokor H, Acsády L, Deschênes M. Feedforward inhibitory control of sensory information in higher-order thalamic nuclei. *J Neurosci*. 2005;25(33):7489-7498. doi:10.1523/JNEUROSCI.2301-05.2005.
35. Barthó P, Freund TF, Acsády L. Selective GABAergic innervation of thalamic nuclei from zona incerta. *Eur J Neurosci*. 2002;16(6):999-1014. doi:10.1046/j.1460-9568.2002.02157.x.
36. Bourassa J, Pinault D, Deschenes M. Corticothalamic projections from the cortical barrel field to the somatosensory thalamus in rats: A single-fibre study using biocytin as an anterograde tracer. *Eur J Neurosci*. 1995;7(1):19-30. doi:10.1111/j.1460-9568.1995.tb01016.x.
37. Deschênes M, Veinante P, Zhang ZW. The organization of corticothalamic projections: Reciprocity versus parity. *Brain Res Rev*. 1998;28(3):286-308. doi:10.1016/S0165-0173(98)00017-4.
38. Castro-Alamancos M a, Calcagnotto ME. Presynaptic long-term potentiation in corticothalamic synapses. *J Neurosci*. 1999;19(20):9090-9097. doi:10.1038/361031a0.
39. Castro-Alamancos MA. Dynamics of sensory thalamocortical synaptic networks during information processing states. *Prog Neurobiol*. 2004;74(4):213-247. doi:10.1016/j.pneurobio.2004.09.002.
40. McCormick DA, von Krosigk M. Corticothalamic activation modulates thalamic firing through glutamate “metabotropic” receptors. *Proc Natl Acad Sci U S A*. 1992;89(7):2774-2778. doi:10.1073/pnas.89.7.2774.
41. Sherman SM, Guillery RW. On the actions that one nerve cell can have on another: distinguishing “drivers” from “modulators”. *Proc Natl Acad Sci U S A*. 1998;95(12):7121-7126. doi:10.1073/pnas.95.12.7121.
42. Golshani P, Liu XB, Jones EG. Differences in quantal amplitude reflect GluR4- subunit number at corticothalamic synapses on two populations of thalamic neurons. *Proc Natl Acad Sci U S A*. 2001;98(7):4172-4177. doi:10.1073/pnas.061013698.
43. Hoogland P V, Wouterlood FG, Welker E, Van der Loos H. Ultrastructure of giant and small thalamic terminals of cortical origin: a study of the projections from the barrel cortex in mice using Phaseolus vulgaris leuco-agglutinin (PHA-L). *Exp Brain Res*. 1991;87(1):159-172. doi:10.1007/BF00228517.
44. Reichova I. Somatosensory Corticothalamic Projections: Distinguishing Drivers From Modulators. *J Neurophysiol*. 2004;92(4):2185-2197. doi:10.1152/jn.00322.2004.
45. Steriade M, Jones E, McCormick D. *Thalamus*. Oxford: Elsevier; 1997.
46. Lee L-J, Erzurumlu RS. Altered parcellation of neocortical somatosensory maps in N-methyl-D-aspartate receptor-deficient mice. *J Comp Neurol*. 2005;485(1):57-63. doi:10.1002/cne.20514.
47. Schubert D, Kötter R, Staiger JF. Mapping functional connectivity in barrel-related columns reveals layer- and cell type-specific microcircuits. *Brain Struct Funct*. 2007;212(2):107-119. doi:10.1007/s00429-007-0147-z.
48. Radnikow G, Qi G, Feldmeyer D. Synaptic Microcircuits in the Barrel Cortex. In: Krieger P, Groh A, eds. *Sensorimotor Integration in the Whisker System*. Heidelberg: Springer Science; 2015:59-108. doi:10.1007/978-1-4939-2975-7.
49. Feldmeyer D. Excitatory neuronal connectivity in the barrel cortex. *Front Neuroanat*. 2012;6(July):24. doi:10.3389/fnana.2012.00024.
50. Vitali I, Jabaudon D. Synaptic biology of barrel cortex circuit assembly. *Semin Cell Dev Biol*. 2014;35:156-164. doi:10.1016/j.semcdb.2014.07.009.
51. Narayanan RT, Egger R, Johnson AS, et al. Beyond columnar organization: Cell type- and target layer-specific principles of horizontal axon projection patterns in rat vibrissal cortex. *Cereb Cortex*. 2015;25(11):4450-4468. doi:10.1093/cercor/bhv053.
52. Bosman LWJ, Houweling AR, Owens CB, et al. Anatomical Pathways Involved in Generating and Sensing Rhythmic Whisker Movements. *Front Integr Neurosci*. 2011;5(October):53.

- doi:10.3389/fnint.2011.00053.
53. Meyer HS, Wimmer VC, Hemberger M, et al. Cell type-specific thalamic innervation in a column of rat vibrissal cortex. *Cereb Cortex*. 2010;20(10):2287-2303. doi:10.1093/cercor/bhq069.
  54. Suzuki N, Bekkers JM. Microcircuits Mediating Feedforward and Feedback Synaptic Inhibition in the Piriform Cortex. *J Neurosci*. 2012;32(3):919-931. doi:10.1523/JNEUROSCI.4112-11.2012.
  55. Cruikshank SJ, Urabe H, Nurmikko A V., Connors BW. Pathway-Specific Feedforward Circuits between Thalamus and Neocortex Revealed by Selective Optical Stimulation of Axons. *Neuron*. 2010;65(2):230-245. doi:10.1016/j.neuron.2009.12.025.
  56. Kim J, Matney CJ, Blankenship A, Hestrin S, Brown SP. Layer 6 corticothalamic neurons activate a cortical output layer, layer 5a. *J Neurosci*. 2014;34(29):9656-9664. doi:10.1523/JNEUROSCI.1325-14.2014.
  57. Staiger JF, Flaggmeyer I, Schubert D, Zilles K, Kötter R, Luhmann HJ. Functional diversity of layer IV spiny neurons in rat somatosensory cortex: Quantitative morphology of electrophysiologically characterized and biocytin labeled cells. *Cereb Cortex*. 2004;14(6):690-701. doi:10.1093/cercor/bhh029.
  58. Cowan AI, Stricker C. Functional connectivity in layer IV local excitatory circuits of rat somatosensory cortex. *J Neurophysiol*. 2004;92(4):2137-2150. doi:10.1152/jn.01262.2003.
  59. White EL, Rock MP. Distribution of thalamic input to different dendrites of a spiny stellate cell in mouse sensorimotor cortex. *Neurosci Lett*. 1979;15(2-3):115-119. doi:10.1016/0304-3940(79)96099-3.
  60. Lefort S, Tomm C, Floyd Sarria JC, Petersen CCH. The Excitatory Neuronal Network of the C2 Barrel Column in Mouse Primary Somatosensory Cortex. *Neuron*. 2009;61(2):301-316. doi:10.1016/j.neuron.2008.12.020.
  61. Jia H, Varga Z, Sakmann B, Konnerth A. Linear integration of spine Ca<sup>2+</sup> signals in layer 4 cortical neurons in vivo. *Proc Natl Acad Sci U S A*. 2014;111(25):9277-9282. doi:10.1073/pnas.1408525111.
  62. Brecht M, Sakmann B. Dynamic representation of whisker deflection by synaptic potentials in spiny stellate and pyramidal cells in the barrels and septa of layer 4 rat somatosensory cortex. *J Physiol*. 2002;543(1):49-70. doi:10.1113/jphysiol.2002.018465.
  63. Bruno RM, Sakmann B. Cortex is driven by weak but synchronously active thalamocortical synapses. *Science (80- )*. 2006;312(5780):1622-1627. doi:10.1126/science.1124593.
  64. Staiger JF, Bojak I, Miceli S, Schubert D. A gradual depth-dependent change in connectivity features of supragranular pyramidal cells in rat barrel cortex. *Brain Struct Funct*. 2014:1-21. doi:10.1007/s00429-014-0726-8.
  65. Schubert D, Kotter R, Zilles K, Luhmann HJ, Staiger JF. Cell Type-Specific Circuits of Cortical Layer IV Spiny Neurons. *J Neurosci*. 2003;23(7):2961-2970. <http://www.jneurosci.org/content/23/7/2961>.
  66. Lübke J, Egger V, Sakmann B, Feldmeyer D. Columnar organization of dendrites and axons of single and synaptically coupled excitatory spiny neurons in layer 4 of the rat barrel cortex. *J Neurosci*. 2000;20(14):5300-5311. doi:10.1523/JNEUROSCI.0184-00.2000 [pii].
  67. Jones EG. Varieties and distribution of non-pyramidal cells in the somatic sensory cortex of the squirrel monkey. *J Comp Neurol*. 1975;160(2):205-267. doi:10.1002/cne.901600204.
  68. Egger V, Nevian T, Bruno RM. Subcolumnar dendritic and axonal organization of spiny stellate and star pyramid neurons within a barrel in rat somatosensory cortex. *Cereb Cortex*. 2008;18(4):876-889. doi:10.1093/cercor/bhm126.
  69. Feldmeyer D, Lübke J, Silver RA, Sakmann B. Synaptic connections between layer 4 spiny neurone-layer 2/3 pyramidal cell pairs in juvenile rat barrel cortex: physiology and anatomy of interlaminar signalling within a cortical column. *J Physiol*. 2002;538(Pt 3):803-822.

- doi:10.1113/jphysiol.2001.012959.
70. Markram H, Toledo-Rodriguez M, Wang Y, Gupta A, Silberberg G, Wu C. Interneurons of the neocortical inhibitory system. *Nat Rev Neurosci*. 2004;5(10):793-807. doi:10.1038/nrn1519.
  71. Halabisky B. Electrophysiological Classification of Somatostatin-Positive Interneurons in Mouse Sensorimotor Cortex. *J Neurophysiol*. 2006;96(2):834-845. doi:10.1152/jn.01079.2005.
  72. DeFelipe J, López-Cruz PL, Benavides-Piccione R, et al. New insights into the classification and nomenclature of cortical GABAergic interneurons. *Nat Rev Neurosci*. 2013;14(3):202-216. doi:10.1038/nrn3444.
  73. Druckmann S, Hill S, Schürmann F, Markram H, Segev I. A hierarchical structure of cortical interneuron electrical diversity revealed by automated statistical analysis. *Cereb Cortex*. 2013;23(12):2994-3006. doi:10.1093/cercor/bhs290.
  74. Kubota Y, Karube F, Nomura M, Kawaguchi Y. The Diversity of Cortical Inhibitory Synapses. *Front Neural Circuits*. 2016;10(April):1-15. doi:10.3389/fncir.2016.00027.
  75. Porter JT, Johnson CK, Agmon A. Diverse types of interneurons generate thalamus-evoked feedforward inhibition in the mouse barrel cortex. *J Neurosci*. 2001;21(8):2699-2710. doi:10.1523/JNEUROSCI.1869-10.2010.
  76. Beierlein M, Gibson JR, Connors BW. Two dynamically distinct inhibitory networks in layer 4 of the neocortex. *J Neurophysiol*. 2003;90(5):2987-3000. doi:10.1152/jn.00283.2003.
  77. Lee S, Hjerling-Leffler J, Zaghera E, Fishell G, Rudy B. The largest group of superficial neocortical GABAergic interneurons expresses ionotropic serotonin receptors. *J Neurosci*. 2010;30(50):16796-16808. doi:10.1523/JNEUROSCI.1869-10.2010.
  78. Koelbl C, Helmstaedter M, Lübke J, Feldmeyer D. A barrel-related interneuron in layer 4 of rat somatosensory cortex with a high intrabarrel connectivity. *Cereb Cortex*. 2015;25(3):713-725. doi:10.1093/cercor/bht263.
  79. Chittajallu R, Pelkey KA, McBain CJ. Neurogliaform cells dynamically regulate somatosensory integration via synapse-specific modulation. *Nat Neurosci*. 2013;16(1):13-15. doi:10.1038/nn.3284.
  80. Xu H, Jeong H-Y, Tremblay R, Rudy B. Neocortical somatostatin-expressing GABAergic interneurons dis-inhibit the thalamorecipient layer 4. *Neuron*. 2013;77(1):155-167. doi:10.1016/j.neuron.2012.11.004.
  81. Ma Y, Hu H, Berrebi AS, Mathers PH, Agmon A. Distinct subtypes of somatostatin-containing neocortical interneurons revealed in transgenic mice. *J Neurosci*. 2006;26(19):5069-5082. doi:10.1523/JNEUROSCI.0661-06.2006.
  82. Silberberg G, Markram H. Disynaptic Inhibition between Neocortical Pyramidal Cells Mediated by Martinotti Cells. *Neuron*. 2007;53(5):735-746. doi:10.1016/j.neuron.2007.02.012.
  83. Rudy B, Fishell G, Lee S, Hjerling-Leffler J. Three groups of interneurons account for nearly 100% of neocortical GABAergic neurons. *Dev Neurobiol*. 2011;71(1):45-61. doi:10.1002/dneu.20853.
  84. Oberlaender M, De Kock CPJ, Bruno RM, et al. Cell type-specific three-dimensional structure of thalamocortical circuits in a column of rat vibrissa cortex. *Cereb Cortex*. 2012;22(10):2375-2391. doi:10.1093/cercor/bhr317.
  85. Arnold PB, Li CX, Waters RS. Thalamocortical arbors extend beyond single cortical barrels: an in vivo intracellular tracing study in rat. *Exp Brain Res*. 2001;136(2):152-168. doi:10.1007/s002210000570.
  86. Ohno S, Kuramoto E, Furuta T, et al. A morphological analysis of thalamocortical axon fibers of rat posterior thalamic nuclei: A single neuron tracing study with viral vectors. *Cereb Cortex*. 2012;22(12):2840-2857. doi:10.1093/cercor/bhr356.
  87. Aronoff R, Matyas F, Mateo C, Ciron C, Schneider B, Petersen CCH. Long-range connectivity of mouse primary somatosensory barrel cortex. *Eur J Neurosci*. 2010;31(12):2221-2233.

- doi:10.1111/j.1460-9568.2010.07264.x.
88. Feldmeyer D, Lübke J, Sakmann B. Efficacy and connectivity of intracolumnar pairs of layer 2/3 pyramidal cells in the barrel cortex of juvenile rats. *J Physiol.* 2006;575(Pt 2):583-602. doi:10.1113/jphysiol.2006.105106.
  89. Larsen DD, Callaway EM. Development of layer-specific axonal arborizations in mouse primary somatosensory cortex. *J Comp Neurol.* 2006;494(3):398-414. doi:10.1002/cne.20754.
  90. Bruno RM, Hahn TTG, Wallace DJ, de Kock CPJ, Sakmann B. Sensory experience alters specific branches of individual corticocortical axons during development. *J Neurosci.* 2009;29(10):3172-3181. doi:10.1523/JNEUROSCI.5911-08.2009.
  91. Holmgren C, Harkany T, Zilberter Y. Pyramidal cell communication within local networks in layer 2/3 of rat neocortex. *J Physiol.* 2003;551(1):139-153. <https://www.ncbi.nlm.nih.gov/pubmed/12813147>.
  92. Sarid L, Feldmeyer D, Gidon A, Sakmann B, Segev I. Contribution of intracolumnar layer 2/3-to-Layer 2/3 excitatory connections in shaping the response to whisker deflection in rat barrel cortex. *Cereb Cortex.* 2015;25(4):849-858. doi:10.1093/cercor/bht268.
  93. Cheetham CEJ, Hammond MSL, Edwards CEJ, Finnerty GT. Sensory experience alters cortical connectivity and synaptic function site specifically. *J Neurosci.* 2007;27(13):3456-3465. doi:10.1523/JNEUROSCI.5143-06.2007.
  94. Reyes a, Sakmann B. Developmental switch in the short-term modification of unitary EPSPs evoked in layer 2/3 and layer 5 pyramidal neurons of rat neocortex. *J Neurosci.* 1999;19(10):3827-3835.
  95. Schubert D, Kötter R, Luhmann HJ, Staiger JF. Morphology, electrophysiology and functional input connectivity of pyramidal neurons characterizes a genuine layer Va in the primary somatosensory cortex. *Cereb Cortex.* 2006;16(2):223-236. doi:10.1093/cercor/bhi100.
  96. Petreanu L, Mao T, Sternson SM, Svoboda K. The subcellular organization of neocortical excitatory connections. *Nature.* 2009;457(7233):1142-1145. doi:10.1038/nature07709.
  97. Kampa BM, Letzkus JJ, Stuart GJ. Cortical feed-forward networks for binding different streams of sensory information. *Nat Neurosci.* 2006;9(12):1472-1473. doi:10.1038/nn1798.
  98. Meyer HS, Schwarz D, Wimmer VC, et al. Inhibitory interneurons in a cortical column form hot zones of inhibition in layers 2 and 5A. *Proc Natl Acad Sci U S A.* 2011;108(40):16807-16812. doi:10.1073/pnas.1113648108.
  99. Gentet LJ. Functional diversity of supragranular GABAergic neurons in the barrel cortex. *Front Neural Circuits.* 2012;6(August):52. doi:10.3389/fncir.2012.00052.
  100. Helmstaedter M, Staiger JF, Sakmann B, Feldmeyer D. Efficient recruitment of layer 2/3 interneurons by layer 4 input in single columns of rat somatosensory cortex. *J Neurosci.* 2008;28(33):8273-8284. doi:10.1523/JNEUROSCI.5701-07.2008.
  101. Avermann M, Tomm C, Mateo C, Gerstner W, Petersen CCH. Microcircuits of excitatory and inhibitory neurons in layer 2/3 of mouse barrel cortex. *J Neurophysiol.* 2012;107(11):3116-3134. doi:10.1152/jn.00917.2011.
  102. Jiang X, Wang G, Lee AJ, Stornetta RL, Zhu JJ. The organization of two new cortical interneuronal circuits. *Nat Neurosci.* 2013;16(2):210-218. doi:10.1038/nn.3305.
  103. Lee AJ, Wang G, Jiang X, et al. Canonical Organization of Layer 1 Neuron-Led Cortical Inhibitory and Disinhibitory Interneuronal Circuits. *Cereb Cortex.* 2014;2(in mM):1-13. doi:10.1093/cercor/bhu020.
  104. Szabadics J, Varga C, Molnár G, Oláh S, Barzó P, Tamás G. Excitatory effect of GABAergic axo-axonic cells in cortical microcircuits. *Science (80- ).* 2006;311(5758):233-235. doi:10.1126/science.1121325.
  105. Lee S, Kruglikov I, Huang ZJ, Fishell G, Rudy B. A disinhibitory circuit mediates motor integration

- in the somatosensory cortex. *Nat Neurosci.* 2013;16(11):1662-1670. doi:10.1038/nn.3544.
106. Xu N, Harnett MT, Williams SR, et al. Nonlinear dendritic integration of sensory and motor input during an active sensing task. *Nature.* 2012;492(7428):247-251. doi:10.1038/nature11601.
  107. Blatow M, Rozov A, Katona I, et al. A novel network of multipolar bursting interneurons generates theta frequency oscillations in neocortex. *Neuron.* 2003;38(5):805-817. doi:10.1016/S0896-6273(03)00300-3.
  108. Caputi A, Rozov A, Blatow M, Monyer H. Two calretinin-positive gabaergic cell types in layer 2/3 of the mouse neocortex provide different forms of inhibition. *Cereb Cortex.* 2009;19(6):1345-1359. doi:10.1093/cercor/bhn175.
  109. Markram H, Muller E, Ramaswamy S, et al. Reconstruction and Simulation of Neocortical Microcircuitry. *Cell.* 2015;163(2):456-492. doi:10.1016/j.cell.2015.09.029.
  110. Wang Y. Anatomical, Physiological, Molecular and Circuit Properties of Nest Basket Cells in the Developing Somatosensory Cortex. *Cereb Cortex.* 2002;12(4):395-410. doi:10.1093/cercor/12.4.395.
  111. Taniguchi H, Lu J, Huang ZJ, et al. The spatial and temporal origin of chandelier cells in mouse neocortex. *Science (80- ).* 2013;339(6115):70-74. doi:10.1126/science.1227622.
  112. Hardwick C, French SJ, Southam E, Totterdell S. A comparison of possible markers for chandelier cartridges in rat medial prefrontal cortex and hippocampus. *Brain Res.* 2005;1031(2):238-244. doi:10.1016/j.brainres.2004.10.047.
  113. Borden LA. GABA transporter heterogeneity: pharmacology and cellular localization. *Neurochem Int.* 1996;29(4):335-356. doi:10.1016/0197-0186(95)00158-1.
  114. Woodruff A, Yuste R. Of mice and men, and chandeliers. *PLoS Biol.* 2008;6(9):1833-1836. doi:10.1371/journal.pbio.0060243.
  115. Zhu Y, Stornetta RL, Zhu JJ. Chandelier Cells Control Excessive Cortical Excitation : Characteristics of Whisker-Evoked Synaptic Responses of Layer 2 / 3 Nonpyramidal and Pyramidal Neurons. *New York.* 2004;24(22):5101-5108. doi:10.1523/JNEUROSCI.0544-04.2004.
  116. Suzuki N, Tang CS-M, Bekkers JM. Persistent barrage firing in cortical interneurons can be induced in vivo and may be important for the suppression of epileptiform activity. *Front Cell Neurosci.* 2014;8(March):76. doi:10.3389/fncel.2014.00076.
  117. Overstreet-Wadiche L, McBain CJ. Neurogliaform cells in cortical circuits. *Nat Rev Neurosci.* 2015;16(8):458-468. doi:10.1038/nrn3969.
  118. Kawaguchi Y, Kubota Y. Physiological and morphological identification of somatostatin- or vasoactive intestinal polypeptide-containing cells among GABAergic cell subtypes in rat frontal cortex. *J Neurosci.* 1996;16(8):2701-2715.
  119. Somogyi, P; Cowey A. Double Bouquet Cells. In: *Cerebral Cortex, Vol 1.* ; 1984:337-360.
  120. Krimer LS. Cluster Analysis-Based Physiological Classification and Morphological Properties of Inhibitory Neurons in Layers 2-3 of Monkey Dorsolateral Prefrontal Cortex. *J Neurophysiol.* 2005;94(5):3009-3022. doi:10.1152/jn.00156.2005.
  121. Peters a, Harriman KM. Enigmatic bipolar cell of rat visual cortex. *J Comp Neurol.* 1988;267(3):409-432. doi:10.1002/cne.902670310.
  122. Tamás G, Somogyi P, Buhl EH. Differentially interconnected networks of GABAergic interneurons in the visual cortex of the cat. *J Neurosci.* 1998;18(11):4255-4270. <http://www.ncbi.nlm.nih.gov/pubmed/9592103>. Accessed October 23, 2016.
  123. Kaiser KMM, Zilberter Y, Sakmann B. Back-propagating action potentials mediate calcium signalling in dendrites of bitufted interneurons in layer 2/3 of rat somatosensory cortex. *J Physiol.* 2001;535(1):17-31. doi:10.1111/j.1469-7793.2001.t01-1-00017.x.
  124. Larkum ME. The yin and yang of cortical layer 1. *Nat Neurosci.* 2013;16(2):114-115. doi:10.1038/nn.3317.

125. Soriano E, Del Río JA. The cells of cajal-retzius: Still a mystery one century after. *Neuron*. 2005;46(3):389-394. doi:10.1016/j.neuron.2005.04.019.
126. Hevner RF, Neogi T, Englund C, Daza RAM, Fink A. Cajal-Retzius cells in the mouse: Transcription factors, neurotransmitters, and birthdays suggest a pallial origin. *Dev Brain Res*. 2003;141(1-2):39-53. doi:10.1016/S0165-3806(02)00641-7.
127. Imamoto K, Karasawa N, Isomura G, Nagatsu I. Cajal-Retzius neurons identified by GABA immunohistochemistry in layer I of the rat cerebral cortex. *Neurosci Res*. 1994;20(1):101-105. doi:10.1016/0168-0102(94)90027-2.
128. Meyer G, Goffinet A, Fairén a, Namur B. What is a Cajal – Retzius Cell ? A Reassessment of a Classical Cell Type Based on Recent Observations in the Developing Neocortex. *Cereb Cortex*. 1999;9(8):765-775. doi:10.1093/cercor/9.8.765.
129. Del Río J a, Heimrich B, Borrell V, et al. A role for Cajal-Retzius cells and reelin in the development of hippocampal connections. *Nature*. 1997;385:70-74. doi:10.1038/385070a0.
130. Larsen DD, Wickersham IR, Callaway EM. Retrograde tracing with recombinant rabies virus reveals correlations between projection targets and dendritic architecture in layer 5 of mouse barrel cortex. *Front Neural Circuits*. 2007;1(March):5. doi:10.3389/neuro.04.005.2007.
131. Oberlaender M, Boudewijns ZSRM, Kleele T, Mansvelder HD, Sakmann B, de Kock CPJ. Three-dimensional axon morphologies of individual layer 5 neurons indicate cell type-specific intracortical pathways for whisker motion and touch. *Proc Natl Acad Sci U S A*. 2011;108(10):4188-4193. doi:10.1073/pnas.1100647108.
132. Veinante P, Lavallée P, Deschênes M. Corticothalamic projections from layer 5 of the vibrissal barrel cortex in the rat. *J Comp Neurol*. 2000;424(2):197-204. doi:10.1002/1096-9861(20000821)424:2<197::AID-CNE1>3.0.CO;2-6.
133. Le Bé JV, Silberberg G, Wang Y, Markram H. Morphological, electrophysiological, and synaptic properties of corticocallosal pyramidal cells in the neonatal rat neocortex. *Cereb Cortex*. 2007;17(9):2204-2213. doi:10.1093/cercor/bhl127.
134. Tan Z, Hu H, Huang ZJ, Agmon A. Robust but delayed thalamocortical activation of dendritic-targeting inhibitory interneurons. *Proc Natl Acad Sci U S A*. 2008;105(6):2187-2192. doi:10.1073/pnas.0710628105.
135. Berger TK, Silberberg G, Perin R, Markram H. Brief bursts self-inhibit and correlate the pyramidal network. *PLoS Biol*. 2010;8(9). doi:10.1371/journal.pbio.1000473.
136. Rubio-Garrido P, Pérez-De-Manzo F, Porrero C, Galazo MJ, Clascá F. Thalamic input to distal apical dendrites in neocortical layer 1 is massive and highly convergent. *Cereb Cortex*. 2009;19(10):2380-2395. doi:10.1093/cercor/bhn259.
137. Wozny C, Williams SR. Specificity of synaptic connectivity between layer 1 inhibitory interneurons and layer 2/3 pyramidal neurons in the rat neocortex. *Cereb Cortex*. 2011;21(8):1818-1826. doi:10.1093/cercor/bhq257.
138. Thomson AM. Neocortical layer 6, a review. *Front Neuroanat*. 2010;4(March):13. doi:10.3389/fnana.2010.00013.
139. Lam YW, Sherman SM. Functional organization of the somatosensory cortical layer 6 feedback to the thalamus. *Cereb Cortex*. 2010;20(1):13-24. doi:10.1093/cercor/bhp077.
140. Perrenoud Q, Rossier J, Geoffroy H, Vitalis T, Gallopin T. Diversity of gabaergic interneurons in layer VIa and VIb of mouse barrel cortex. *Cereb Cortex*. 2013;23(2):423-441. doi:10.1093/cercor/bhs032.
141. Mercer A, West DC, Morris OT, Kirchhecker S, Kerkhoff JE, Thomson AM. Excitatory connections made by presynaptic cortico-cortical pyramidal cells in layer 6 of the neocortex. *Cereb Cortex*. 2005;15(10):1485-1496. doi:10.1093/cercor/bhi027.
142. West DC, Mercer A, Kirchhecker S, Morris OT, Thomson AM. Layer 6 cortico-thalamic pyramidal

- cells preferentially innervate interneurons and generate facilitating EPSPs. *Cereb Cortex*. 2006;16(2):200-211. doi:10.1093/cercor/bhi098.
143. Zhang ZW, Deschênes M. Intracortical axonal projections of lamina VI cells of the primary somatosensory cortex in the rat: a single-cell labeling study. *J Neurosci*. 1997;17(16):6365-6379.
  144. Pichon F, Nikonenko I, Kraftsik R, Welker E. Intracortical connectivity of layer VI pyramidal neurons in the somatosensory cortex of normal and barrelless mice. *Eur J Neurosci*. 2012;35(6):855-869. doi:10.1111/j.1460-9568.2012.08011.x.
  145. Kumar P, Ohana O. Inter- and intralaminar subcircuits of excitatory and inhibitory neurons in layer 6a of the rat barrel cortex. *J Neurophysiol*. 2008;100(4):1909-1922. doi:10.1152/jn.90684.2008.
  146. Killackey HP, Sherman SM. Corticothalamic Projections from the Rat Primary Somatosensory Cortex. *J Neurosci*. 2003;23(19):7381-7384. <http://www.jneurosci.org/content/23/19/7381.abstract>.
  147. Marx M, Feldmeyer D. Morphology and physiology of excitatory neurons in layer 6b of the somatosensory rat barrel cortex. *Cereb Cortex*. 2013;23(12):2803-2817. doi:10.1093/cercor/bhs254.
  148. Clancy B, Caulier LJ. Widespread projections from subgriseal neurons (layer VII) to layer I in adult rat cortex. *J Comp Neurol*. 1999;407(2):275-286. doi:10.1002/(SICI)1096-9861(19990503)407:2<275::AID-CNE8>3.0.CO;2-0.
  149. Bortone DS, Olsen SR, Scanziani M. Translaminar inhibitory cells recruited by layer 6 corticothalamic neurons suppress visual cortex. *Neuron*. 2014;82(2):474-485. doi:10.1016/j.neuron.2014.02.021.
  150. Kurotani T, Yamada K, Yoshimura Y, Crair MC, Komatsu Y. State-Dependent Bidirectional Modification of Somatic Inhibition in Neocortical Pyramidal Cells. *Neuron*. 2008;57(6):905-916. doi:10.1016/j.neuron.2008.01.030.
  151. Schoonover CE, Tapia J-C, Schilling VC, et al. Comparative strength and dendritic organization of thalamocortical and corticocortical synapses onto excitatory layer 4 neurons. *J Neurosci*. 2014;34(20):6746-6758. doi:10.1523/JNEUROSCI.0305-14.2014.
  152. Stuart GJ. Dendritic Spikes Veto Inhibition. *Neuron*. 2012;75(5):744-746. doi:10.1016/j.neuron.2012.08.024.
  153. Bar-Ilan L, Gidon A, Segev I. The role of dendritic inhibition in shaping the plasticity of excitatory synapses. *Front Neural Circuits*. 2013;6(April):118. doi:10.3389/fncir.2012.00118.
  154. Araya R. Input transformation by dendritic spines of pyramidal neurons. *Front Neuroanat*. 2014;8(December):141. doi:10.3389/fnana.2014.00141.
  155. Breton JD, Stuart GJ. Somatic and dendritic GABA(B) receptors regulate neuronal excitability via different mechanisms. *J Neurophysiol*. 2012;108(10):2810-2818. doi:10.1152/jn.00524.2012.
  156. Panzeri S, Petroni F, Petersen RS, Diamond ME. Decoding neuronal population activity in rat somatosensory cortex: Role of columnar organization. 2003;13(1):45-52.
  157. Petersen RS, Panzeri S, Diamond ME. Population coding of stimulus location in rat somatosensory cortex. *Neuron*. 2001;32(3):503-514. doi:10.1016/S0896-6273(01)00481-0.
  158. Campagner D, Evans MH, Loft MSE, Petersen RS. What the whiskers tell the brain. *Neuroscience*. 2018;368:95-108. doi:10.1016/j.neuroscience.2017.08.005.
  159. Adibi M, McDonald JS, Clifford CWG, Arabzadeh E. Population Decoding in Rat Barrel Cortex: Optimizing the Linear Readout of Correlated Population Responses. *PLoS Comput Biol*. 2014;10(1). doi:10.1371/journal.pcbi.1003415.
  160. Maravall M, Petersen RS, Fairhall AL, Arabzadeh E, Diamond ME. Shifts in coding properties and maintenance of information transmission during adaptation in barrel cortex. *PLoS Biol*. 2007;5(2):0323-0334. doi:10.1371/journal.pbio.0050019.

161. Langlois JA, Rutland-Brown W, Wald MM. The Epidemiology and Impact of Traumatic Brain Injury A Brief Overview. *J Head Trauma Rehabil.* 2006;21(5):375-378. doi:00001199-200609000-00001 [pii].
162. Powell JW. Traumatic Brain Injury in High School Athletes. *J Am Med Assoc.* 1999;282(10):958. doi:10.1001/jama.282.10.958.
163. Di Virgilio TG, Hunter A, Wilson L, et al. Evidence for Acute Electrophysiological and Cognitive Changes Following Routine Soccer Heading. *EBioMedicine.* 2016. doi:10.1016/j.ebiom.2016.10.029.
164. Kreutzer JS, Seel RT, Gourley E, Jeffrey S, Kreutzer RTS. The prevalence and symptom rates of depression after traumatic brain injury: a comprehensive examination. *Brain Inj.* 2001;15(7):563-576. doi:10.1080/02699050010009108.
165. Liesemer K, Bratton SL, Zebrack CM, Brockmeyer D, Statler KD. Early post-traumatic seizures in moderate to severe pediatric traumatic brain injury: rates, risk factors, and clinical features. *J Neurotrauma.* 2011;28(1557-9042 (Electronic)):755-762.
166. Yeh C, Chen T, Hu C, et al. Risk of epilepsy after traumatic brain injury: a retrospective population-based cohort study. *J Neurol Neurosurg Psychiatry.* 2013;84(4):441-445. doi:10.1136/jnnp-2012-302547.
167. Werner C, Engelhard K. Pathophysiology of traumatic brain injury. *Br J Anaesth.* 2007;99(1):4-9. doi:10.1093/bja/aem131.
168. Reeves TM, Lyeth BG, Phillips LL, Hamm RJ, Povlishock JT. The effects of traumatic brain injury on inhibition in the hippocampus and dentate gyrus. *Brain Res.* 1997;757(1):119-132. doi:10.1016/S0006-8993(97)00170-4.
169. Povlishock JT, Katz DI. Update of neuropathology and neurological recovery after traumatic brain injury. *J Head Trauma Rehabil.* 2005;20(1):76-94. doi:10.1097/00001199-200501000-00008.
170. Hunt RF, Scheff SW, Smith BN. Regionally localized recurrent excitation in the dentate gyrus of a cortical contusion model of posttraumatic epilepsy. *J Neurophysiol.* 2010;103(3):1490-1500. doi:10.1152/jn.00957.2009.
171. Gaetz M. The neurophysiology of brain injury. *Clin Neurophysiol.* 2004;115(1):4-18. doi:10.1016/S1388-2457(03)00258-X.
172. Cohen AS, Pfister BJ, Schwarzbach E, Sean Grady M, Goforth PB, Satin LS. Injury-induced alterations in CNS electrophysiology. *Prog Brain Res.* 2007;161:143-169. doi:10.1016/S0079-6123(06)61010-8.
173. Cantu D, Walker K, Andersen L, et al. Traumatic brain injury increases cortical glutamate network activity by compromising GABAergic control. *Cereb Cortex.* 2015;25(8):2306-2320. doi:10.1093/cercor/bhu041.
174. Greer J, Hånell A, Mcginn M, Povlishock J. Mild traumatic brain injury in the mouse induces axotomy primarily within the axon initial segment. *Acta Neuropathol.* 2013;126(1):59-74. doi:10.1007/s00401-013-1119-4.
175. LaPlaca MC, Simon CM, Prado GR, Cullen DK. CNS injury biomechanics and experimental models. *Prog Brain Res.* 2007;161:13-26. doi:10.1016/S0079-6123(06)61002-9.
176. Granacher, Jr. RP. *Traumatic Brain Injury: Methods for Clinical and Forensic Neuropsychiatric Assessment.* Boca Raton, FL: CRC Press; 2003.
177. Namjoshi DR, Good C, Cheng WH, et al. Towards clinical management of traumatic brain injury: a review of models and mechanisms from a biomechanical perspective. *Dis Model Mech.* 2013;6(6):1325-1338. doi:10.1242/dmm.011320.
178. Ding MC, Wang Q, Lo EH, Stanley GB. Cortical Excitation and Inhibition following Focal Traumatic Brain Injury. *J Neurosci.* 2011;31(40):14085-14094.
179. Carron SF, Yan EB, Alwis DS, Rajan R. Differential susceptibility of cortical and subcortical

- inhibitory neurons and astrocytes in the long term following diffuse traumatic brain injury. *J Comp Neurol*. 2016;(1):20-22. doi:10.1002/cne.24014.
180. Büki A, Povlishock JT. All roads lead to disconnection? - Traumatic axonal injury revisited. *Acta Neurochir (Wien)*. 2006;148(2):181-193. doi:10.1007/s00701-005-0674-4.
  181. Corbo J, Tripathi P. Delayed presentation of diffuse axonal injury: A case report. *Ann Emerg Med*. 2004;44(1):57-60. doi:10.1016/j.annemergmed.2003.11.010.
  182. Farkas O, Povlishock JT. Cellular and subcellular change evoked by diffuse traumatic brain injury: a complex web of change extending far beyond focal damage. *Prog Brain Res*. 2007;161:43-59. doi:10.1016/S0079-6123(06)61004-2.
  183. Kelley BJ, Farkas O, Lifshitz J, Povlishock JT. Traumatic axonal injury in the perisomatic domain triggers ultrarapid secondary axotomy and Wallerian degeneration. *Exp Neurol*. 2006;198(2):350-360. doi:10.1016/j.expneurol.2005.12.017.
  184. Pettus EH, Christman CW, Giebel ML, Povlishock JT. Traumatically induced altered membrane permeability: its relationship to traumatically induced reactive axonal change. *J Neurotrauma*. 1994;11(5):507-522. doi:10.1089/neu.1994.11.507.
  185. Carrera E, Tononi G. Diaschisis: Past, present, future. *Brain*. 2014;137(9):2408-2422. doi:10.1093/brain/awu101.
  186. Povlishock JT. Pathobiology of traumatically induced axonal injury in animals and man. *Ann Emerg Med*. 1993;22(6):980-986. doi:10.1016/S0196-0644(05)82738-6.
  187. Alwis DS, Johnstone V, Yan E, Rajan R. Diffuse traumatic brain injury and the sensory brain. *Clin Exp Pharmacol Physiol*. 2013;40(7). doi:10.1111/1440-1681.12100.
  188. Allitt BJ, Iva P, Yan EB, Rajan R. Hypo-excitation across all cortical laminae defines intermediate stages of cortical neuronal dysfunction in diffuse traumatic brain injury. *Neuroscience*. 2016;334. doi:10.1016/j.neuroscience.2016.08.018.
  189. Nudo RJ. Recovery after brain injury: mechanisms and principles. *Front Hum Neurosci*. 2013;7(December):1-14. doi:10.3389/fnhum.2013.00887.
  190. Nishibe M, Barbay S, Guggenmos D, Nudo RJ. Reorganization of Motor Cortex after Controlled Cortical Impact in Rats and Implications for Functional Recovery. *J Neurotrauma*. 2010;27(12):2221-2232. doi:10.1089/neu.2010.1456.
  191. Guerriero RM, Gize CC, Rotenberg A, Geurriero RM, Giza CC, Rotenberg A. Glutamate and GABA imbalance following traumatic brain injury. *Curr Neurol Neurosci Rep*. 2015;15(5):1-20. doi:10.1007/s11910-015-0545-1.Glutamate.
  192. Chen Y-H, Huang EY-K, Kuo T-T, Miller J, Chiang Y-H, Hoffer BJ. Impact of Traumatic Brain Injury on Dopaminergic Transmission. *Cell Transplant*. 2017;26(7):1156-1168. doi:10.1177/0963689717714105.
  193. Espinoza TR, Wright DW. The role of progesterone in traumatic brain injury. *J Head Trauma Rehabil*. 2011;26(6):497-499. doi:10.1097/HTR.0b013e31823088fa.
  194. Reid SNM, Juraska JM. Sex differences in the gross size of the rat neocortex. *J Comp Neurol*. 1992;321(3):442-447. doi:10.1002/cne.903210310.
  195. Attella MJ, Nattinville A, Stein DG. Hormonal state affects recovery from frontal cortex lesions in adult female rats. *Behav Neural Biol*. 1987;48(3):352-367. doi:10.1016/S0163-1047(87)90918-6.
  196. Allitt BJ, Johnstone VPA, Richards K, Yan EB, Rajan R. Progesterone Exacerbates Short-Term Effects of Traumatic Brain Injury on Supragranular Responses in Sensory Cortex and Over-Excites Infragranular Responses in the Long Term. *J Neurotrauma*. 2016;33(4). doi:10.1089/neu.2015.3946.
  197. Stein DGG. Progesterone in the treatment of acute traumatic brain injury: a clinical perspective and update. *Neuroscience*. 2011;191:101-106. doi:10.1016/j.neuroscience.2011.04.013.
  198. Gibson CL, Gray LJ, Bath PMW, Murphy SP. Progesterone for the treatment of experimental brain

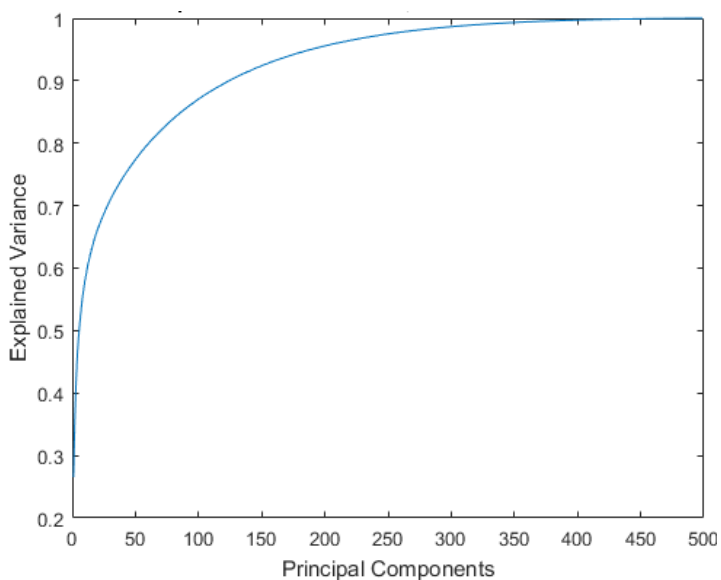
- injury; a systematic review. *Brain*. 2008;131(2):318-328. doi:10.1093/brain/awm183.
199. Xiao G, Wei J, Yan W, Wang W, Lu Z. Improved outcomes from the administration of progesterone for patients with acute severe traumatic brain injury: a randomized controlled trial. *Crit Care*. 2008;12(2):1-10. doi:10.1186/cc6887.
  200. Jia J, Verma S, Nakayama S, et al. Sex differences in neuroprotection provided by inhibition of TRPM2 channels following experimental stroke. *J Cereb Blood Flow Metab*. 2011;31(11):2160-2168. doi:10.1038/jcbfm.2011.77.
  201. Martényi F, Dossenbach M, Mraz K, Metcalfe S. Gender differences in the efficacy of fluoxetine and maprotiline in depressed patients: A double-blind trial of antidepressants with serotonergic or norepinephrinergic reuptake inhibition profile. *Eur Neuropsychopharmacol*. 2001;11(3):227-232. doi:10.1016/S0924-977X(01)00089-X.
  202. Fink G, Sumner BE, McQueen JK, Wilson H, Rosie R. Sex Steroid Control of Mood, Mental State and Memory. *Clin Exp Pharmacol Physiol*. 1998;25(10):764-775. doi:10.1111/j.1440-1681.1998.tb02151.x.
  203. Majewska MD, Harrison NL, Schwartz RD, Barker JL, Paul SM. Steroid hormone metabolites are barbiturate-like modulators of the GABA receptor. *Science (80- )*. 1986;232(4753):1004-1007. doi:10.1126/science.2422758.
  204. Jovanovic H, Lundberg J, Karlsson P, et al. Sex differences in the serotonin 1A receptor and serotonin transporter binding in the human brain measured by PET. *Neuroimage*. 2008;39(3):1408-1419. doi:10.1016/j.neuroimage.2007.10.016.
  205. Alwis DS, Rajan R. Environmental enrichment causes a global potentiation of neuronal responses across stimulus complexity and lamina of sensory cortex. *Front Cell Neurosci*. 2013;(JUL). doi:10.3389/fncel.2013.00124.
  206. Alwis DS, Yan EB, Johnstone V, et al. Environmental enrichment attenuates traumatic brain injury: Induced neuronal hyperexcitability in supragranular layers of sensory cortex. *J Neurotrauma*. 2016;33(11). doi:10.1089/neu.2014.3774.
  207. Bogdanov VB, Middleton NA, Theriot JJ, et al. Susceptibility of Primary Sensory Cortex to Spreading Depolarizations. *J Neurosci*. 2016. doi:10.1523/JNEUROSCI.3694-15.2016.
  208. Maglóczy Z, Halasz P, Vajda J, Czirjak S, Freund TF. Loss of Calbindin-D28K immunoreactivity from dentate granule cells in human temporal lobe epilepsy. *Neuroscience*. 1997;76(2):377-385. doi:S0306-4522(96)00440-X [pii].
  209. Cossart R, Dinocourt C, Hirsch JC, et al. Dendritic but not somatic GABAergic inhibition is decreased in experimental epilepsy. *Nat Neurosci*. 2001;4(1):52-62. doi:10.1038/82900.
  210. Carter DS, Harrison AJ, Falenski KW, Blair RE, DeLorenzo RJ. Long-term decrease in calbindin-D28K expression in the hippocampus of epileptic rats following pilocarpine-induced status epilepticus. *Epilepsy Res*. 2008;79(2-3):213-223. doi:10.1016/j.eplepsyres.2008.02.006.
  211. Knopp A, Frahm C, Fidzinski P, Witte OW, Behr J. Loss of GABAergic neurons in the subiculum and its functional implications in temporal lobe epilepsy. *Brain*. 2008;131(6):1516-1527. doi:10.1093/brain/awn095.
  212. Buriticá E, Villamil L, Guzmán F, Escobar M, García-Cairasco N, Pimienta H. Changes in calcium-binding protein expression in human cortical contusion tissue. *J Neurotrauma*. 2009;26(12):2145-2155.
  213. Tóth K, Ero'ss L, Vajda J, Halász P, Freund TF, Maglóczy Z. Loss and reorganization of calretinin-containing interneurons in the epileptic human hippocampus. *Brain*. 2010;133(9):2763-2777. doi:10.1093/brain/awq149.
  214. Huusko N, Römer C, Ndode-Ekane XE, Lukasiuk K, Pitkänen A. Loss of hippocampal interneurons and epileptogenesis: a comparison of two animal models of acquired epilepsy. *Brain Struct Funct*. 2013;220(1):153-191. doi:10.1007/s00429-013-0644-1.

215. Pang R, Lansdell BJ, Fairhall AL. Dimensionality reduction in neuroscience. *Curr Biol*. 2016;26(14):R656-R660. doi:10.1016/j.cub.2016.05.029.
216. Aljadeff J, Lansdell BJ, Fairhall AL, Kleinfeld D. Analysis of Neuronal Spike Trains, Deconstructed. *Neuron*. 2016;91(2):221-259. doi:10.1016/j.neuron.2016.05.039.
217. McInnes L, Healy J. UMAP: Uniform Manifold Approximation and Projection for Dimension Reduction. 2018:1-18. <http://arxiv.org/abs/1802.03426>.
218. Sporns O. Graph Theory Methods For The Analysis Of Neural Connectivity Patterns. *Neurosci Databases A Pract Guid*. 2003:171-185. doi:10.1007/978-1-4615-1079-6.
219. Bullmore E, Sporns O. Complex brain networks: graph theoretical analysis of structural and functional systems. *Nat Publ Gr*. 2009;10(3):186-198. doi:10.1038/nrn2575.
220. Johnstone VPA, Wright DK, Wong K, O'Brien TJ, Rajan R, Shultz SR. Experimental Traumatic Brain Injury Results in Long-Term Recovery of Functional Responsiveness in Sensory Cortex but Persisting Structural Changes and Sensorimotor, Cognitive, and Emotional Deficits. *J Neurotrauma*. 2015;32(17). doi:10.1089/neu.2014.3785.
221. Yan EB, Johnstone VPA, Alwis DS, Morganti-Kossmann M-C, Rajan R. Characterising effects of impact velocity on brain and behaviour in a model of diffuse traumatic axonal injury. *Neuroscience*. 2013;248. doi:10.1016/j.neuroscience.2013.05.045.
222. Alwis DS, Rajan R. Environmental enrichment and the sensory brain: The role of enrichment in remediating brain injury. *Front Syst Neurosci*. 2014;8(SEP). doi:10.3389/fnsys.2014.00156.
223. Johnstone VPAVPA, Yan EBEB, Alwis DS, Rajan R. Cortical Hypoexcitation Defines Neuronal Responses in the Immediate Aftermath of Traumatic Brain Injury. *PLoS One*. 2013;8(5). doi:10.1371/journal.pone.0063454.
224. Foda MA-E, Marmarou A, Brink W, Foda MA-E, Brink W. A new model of diffuse brain injury in rats: Part I: Pathophysiology and biomechanics. *J Neurosurg*. 1994;80(2):291-300. <http://thejns.org/doi/abs/10.3171/jns.1994.80.2.0291@col.2012.116.issue-6%5Cnhttp://thejns.org/doi/abs/10.3171/jns.1994.80.2.0291@sup.2010.112.issue-2%5Cnhttp://thejns.org/doi/abs/10.3171/jns.1994.80.2.0301>.
225. Hellewell SC, Yan EB, Agyapomaa DA, Bye N, Morganti-Kossmann MC. Post-Traumatic Hypoxia Exacerbates Brain Tissue Damage: Analysis of Axonal Injury and Glial Responses. *J Neurotrauma*. 2010;27(11):1997-2010. doi:10.1089/neu.2009.1245.
226. Yan EB, Johnstone VPA, Alwis DS, Morganti-Kossmann MC, Rajan R. Characterising effects of impact velocity on brain and behaviour in a model of diffuse traumatic axonal injury. *Neuroscience*. 2013;248:17-29. doi:10.1016/j.neuroscience.2013.05.045.
227. Rajan R, Bourke J, Cassell J. A novel stimulus system for applying tactile stimuli to the macrovibrissae in electrophysiological experiments. *J Neurosci Methods*. 2006;157(1):103-117. doi:10.1016/j.jneumeth.2006.04.008.
228. Hartmann MJ, Johnson NJ, Towal RB, Assad C. Behavioral/Systems/Cognitive Mechanical Characteristics of Rat Vibrissae: Resonant Frequencies and Damping in Isolated Whiskers and in the Awake Behaving Animal.
229. Jain R, Kasturi R, Schunck BG. *Machine Vision*. New York: McGraw-Hill; 1995.
230. Beveridge JR, Griffith J, Kohler RR, Hanson AR, Riseman EM. Segmenting images using localized histograms and region merging. *Int J Comput Vis*. 1989;2(3):311-347. doi:10.1007/BF00158168.
231. Haralick RM, Shapiro LG. Image Segmentation Techniques. *Proc SPIE - Int Soc Opt Eng*. 1985;548(November 1984):2-9. doi:10.1016/S0734-189X(85)90153-7.
232. Dijkstra EW. A Note on Two Problems in Connexion with Graphs. *Numer Math*.:269-27.
233. Nencini S, Ivanusic J. Mechanically sensitive A  $\delta$  nociceptors that innervate bone marrow respond to changes in intra-osseous pressure. 2017;13:4399-4415. doi:10.1113/JP273877.

## 5. Appendices

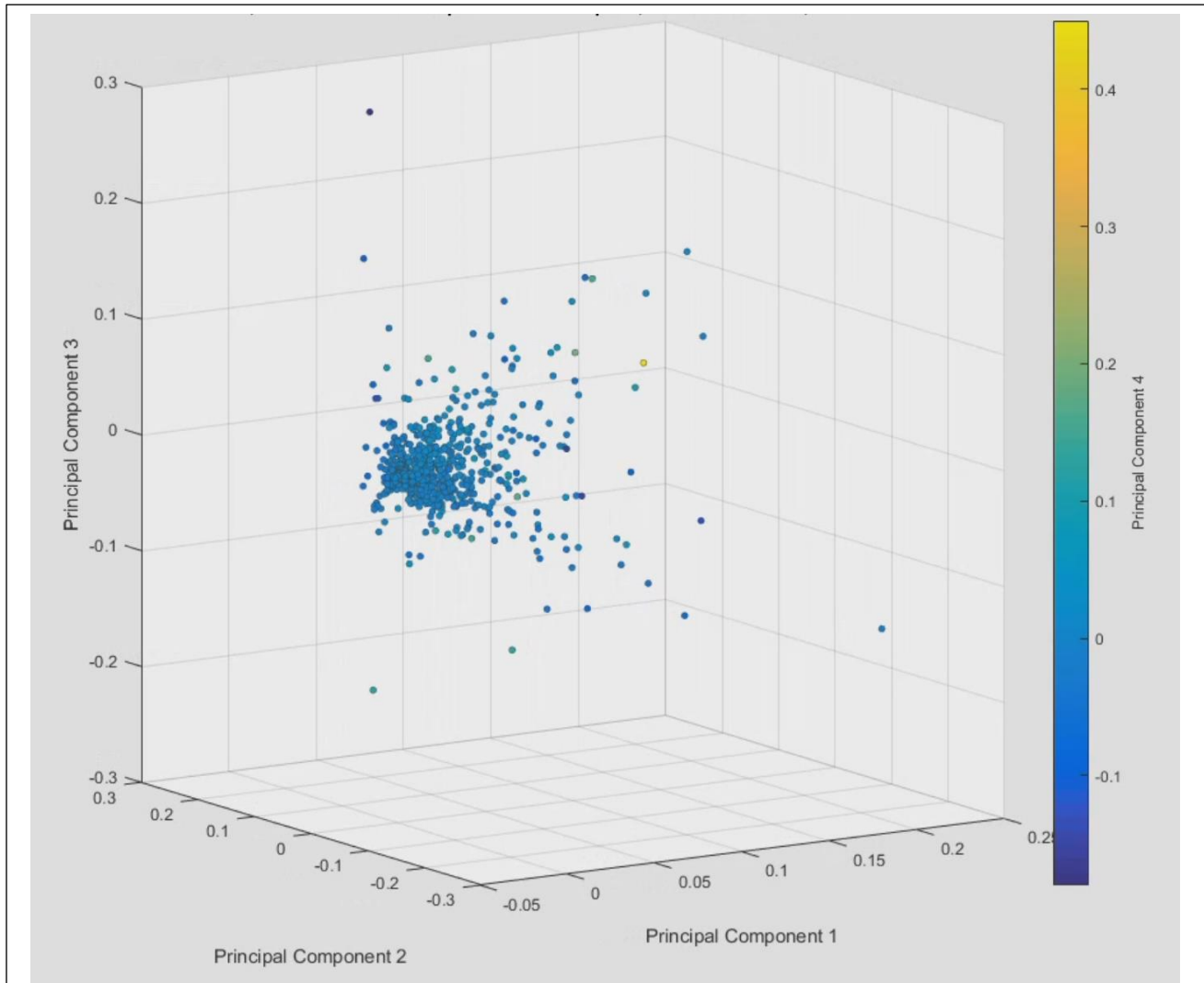
### 5.1 Appendix I - Evaluating PCA as a method for identifying and distinguishing between unit activity patterns

Although the methods employed in this project were capable of identifying and distinguishing between different activity patterns in an accurate way, they did so in rather crude ways insofar as ultimately reducing the complexity of the data to very low dimensional information. For instance, although the local maxima-based method identified units with 0 components (labelled 'non-responders' in the main text), some had an apparent tendency to fire in generally expected response periods, e.g. offset or onset. Yet because their activity was so low, they were not identified by this analysis as having any activity components and labelled a 'non-responder'. As the online units have been hand sorted by experienced experimentalists, we can be reasonably confident of their validity as single units. Therefore, labelling them non-responders them on the basis of relatively weak responses may be short-sighted. Therefore, it may be more appropriate to use a technique which is suitable for identifying and distinguishing between high-dimensional features in and then projecting down into a lower dimension for clustering and visualisation. One such method is PCA, which we will perform and evaluate in this appendix.



**S1.** The cumulative explained variance of the PCA using a segment of online units from layers II and IV ( $n=969$ ). Six PCs were required to reach >50% of explained variance, 42 PCs were required to explain >75% of the variance, 125 PCs were required to explain >90% of the variance, 189 PCs were required to explain >95% of the variance, and 322 PCs were required to explain >99% of the variance. This reveals that despite PCA being a useful tool to reduce the dimensionality of the amplitude-time-firing rate variation for each online unit generally, such reduction is at the expense of a large amount of the original variability, even at very high dimensions.

To perform the PCA, each amplitude-time-firing rate bin was a set element  $i$  in a vector  $V$ , so that  $V = (i_1, i_2, i_3 \dots i_{500})$ . Each vector was then used as a list of 500 features for the PCA analysis, where the 969 online units were evaluated. The cumulative explained variance for all PCs (Figure S1) and the distribution in the first four PCs of each online unit (Figure S2) were calculated.



**S2.** A segment of online units from layers II and IV ( $n=969$ ) plotted in three-dimensional PC space (explaining 41.52% of the total original variance) and shaded according to their values in the fourth PC (explaining an additional 4.52% of the total original variance). In this PC space the units do not appear to be forming local clusters. This may be because there is not a sufficient amount of variance available in this level of PC space or because the PCs used here do not include salient information with respect to unit activity patterns.

One of the hallmarks of PCA is that the PCs are no longer directly interpretable in terms of the original data dimensions. To help establish what information the PCs used in Figure S2 contain, correlation

coefficients (Table S1) and their significance (Table S2) were calculated for the first four PCs, as well as the mean and max firing rates of the online units. Features derived from the graph theoretic analysis (path median times and total distance of all paths) were also included.

**Table S1.** Correlation coefficients (r) of PCs and other features of online units

	P1	P2	P3	Dist	Mean	Max	PC1	PC2	PC3	PC4
P1		0.168	0.143	0.169	-0.286	0.189	0.127	-0.147	-0.063	-0.254
P2	0.168		0.079	0.195	-0.350	0.123	0.008	-0.135	-0.167	-0.296
P3	0.143	0.079		0.087	-0.259	0.086	-0.043	-0.153	-0.119	-0.165
Dist	0.169	0.195	0.087		-0.518	-0.119	-0.205	-0.024	-0.653	-0.436
Mean	-0.286	-0.350	-0.259	-0.518		-0.088	0.002	0.091	0.722	0.843
Max	0.189	0.123	0.086	-0.119	-0.088		0.001	0.014	0.282	0.010
PC1	0.127	0.008	-0.043	-0.205	0.002	0.001		0.001	0.252	0.024
PC2	-0.147	-0.135	-0.153	-0.024	0.091	0.014	0.001		0.016	0.100
PC3	-0.063	-0.167	-0.119	-0.653	0.722	0.282	0.252	0.016		0.773
PC4	-0.254	-0.296	-0.165	-0.436	0.843	0.010	0.024	0.100	0.773	

**Table S2.** Significance of correlation coefficients (p) of PCs and other features of online units

	P1	P2	P3	Dist	Mean	Max	PC1	PC2	PC3	PC4
P1		<b>&lt;0.001</b>	0.048	<b>&lt;0.001</b>						
P2	<b>&lt;0.001</b>		0.014	<b>&lt;0.001</b>	<b>&lt;0.001</b>	<b>&lt;0.001</b>	0.802	<b>&lt;0.001</b>	<b>&lt;0.001</b>	<b>&lt;0.001</b>
P3	<b>&lt;0.001</b>	0.014		<b>&lt;0.001</b>	<b>&lt;0.001</b>	0.007	0.183	<b>&lt;0.001</b>	<b>&lt;0.001</b>	<b>&lt;0.001</b>
Dist	<b>&lt;0.001</b>	<b>&lt;0.001</b>	0.007		<b>&lt;0.001</b>	<b>&lt;0.001</b>	<b>&lt;0.001</b>	0.446	<b>&lt;0.001</b>	<b>&lt;0.001</b>
Mean	<b>&lt;0.001</b>	<b>&lt;0.001</b>	<b>&lt;0.001</b>	<b>&lt;0.001</b>		0.006	0.941	0.005	<b>&lt;0.001</b>	<b>&lt;0.001</b>
Max	<b>&lt;0.001</b>	<b>&lt;0.001</b>	0.007	<b>&lt;0.001</b>	0.006		0.991	0.665	<b>&lt;0.001</b>	0.756
PC1	<b>&lt;0.001</b>	<b>&lt;0.001</b>	0.183	<b>&lt;0.001</b>	0.941	0.991		0.991	<b>&lt;0.001</b>	0.463
PC2	<b>&lt;0.001</b>	<b>&lt;0.001</b>	<b>&lt;0.001</b>	0.446	0.005	0.665	0.991		0.608	0.002
PC3	0.048	<b>&lt;0.001</b>	<b>&lt;0.001</b>	<b>&lt;0.001</b>	<b>&lt;0.001</b>	<b>&lt;0.001</b>	<b>&lt;0.001</b>	0.608		<b>&lt;0.001</b>
PC4	<b>&lt;0.001</b>	<b>&lt;0.001</b>	<b>&lt;0.001</b>	<b>&lt;0.001</b>	<b>&lt;0.001</b>	0.756	0.463	0.002	<b>&lt;0.001</b>	

As can be expected from PCA, which attempts to make each successive PC orthogonal and thus maximize the independence of each PC, the PCs, while they correlate with each other to some degree,

are the features which correlate with the least other features in Tables S1 and S2. It is noteworthy that the first PC, which accounts alone for 26.54% of the total original variance in the raw data, is significantly correlated with only the timing of the first shortest path (P1), but not the second (P2) or third (P3) shortest path – whereas PCs 2-4 do significantly correlate with the timings of the shortest paths.

Also of interest is the fact that P1, P2, and P3 are all significantly correlated with each other. This is reassuring, since we expect that because patterned unit activity clusters rely on regularity in inhibition and excitation, each major component of activity should be occurring in time with a regular relationship to other major components of activity. P2 and P3 are significantly correlated but by an order of magnitude less than each other pair of path median times. This is also reassuring, since we expect (in a 50ms analysis window) for there to be a limited number of 1ms bin major activity components, as identified by the shortest paths. Two such components occurring within a 50ms window is reasonable, but three or more will be rarer, and thus should only be correlated when such a third component is real (or where a major activity component spreads across successive 2ms bins).

Although there is no clear indication of clustering or separation of the online units in Figure S2, it is still worth checking to see if units from different conditions are noticeably separable. In Figure S3, units from our primary layers of interest, layers II and IV, are plotted in new three-dimensional PC space (calculated from just those data) and shaded by condition – Sham or TBI. Here, in fact, there appears to some level of clustering or separation between Sham and TBI, but not much; TBI units appear more frequent at higher scores of PC1 and potentially in some regions with higher scores of PC3. However, since we are only testing the first three PCs here, and there could be differences in the distributions of any of the 419 PCs in this PC space, one- and two-sample Kolmogorov-Smirnov tests were conducted to compare the Sham vs. TBI distributions in this new PC space for significant differences (Figure S5). Two-way Kolmogorov-Smirnov tests may help reveal which PCs are salient for the separation of Sham and TBI units and therefore provide better clustering agreement in these PC spaces.

Also, to directly test how well the PCs in Figure S3 could cluster Sham and TBI units, k-means clustering with 50 replications using an online-update phase was conducted (Figure S4, where  $k=2$ , representing Sham and TBI) was conducted.

**L2 & L4 online units plotted in PCA space, Contact stimulus, Sham (blue) + TBI (red)**

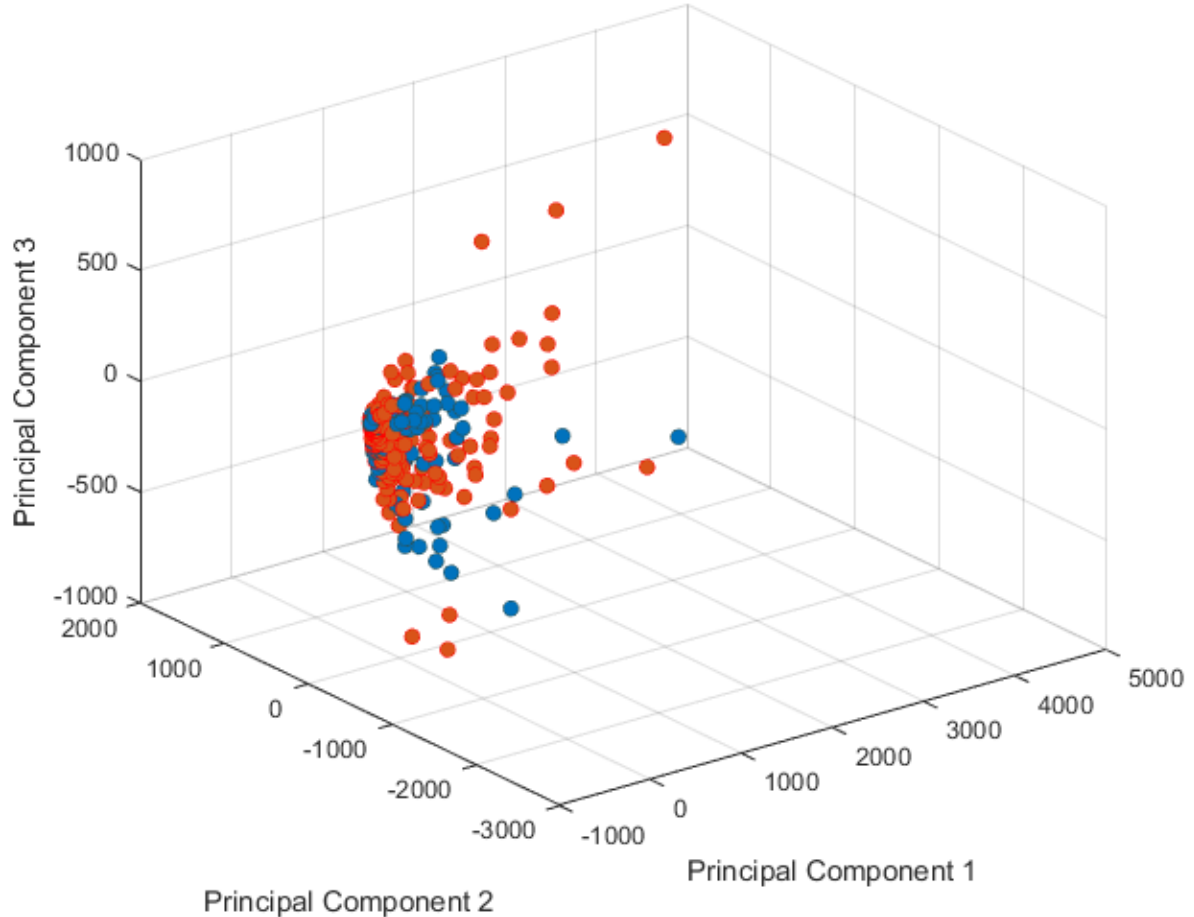


**Figure S3.** All online units from layers II and IV (n=420) plotted in new three-dimensional PC space (explaining 44.57% of the total original variance) and shaded by condition: Sham (n=168; blue) and TBI (n=252; red). Unlike in Figure S2, in this PC space the units do appear to be forming limited local clusters, and according to health status. However, the data is generally still not easily separable and other PCs might make these groups more separable; these PCs may represent an insufficient amount of variance or components of the original variance that is simply not as salient or important for distinguishing between Sham and TBI conditions as other PCs.

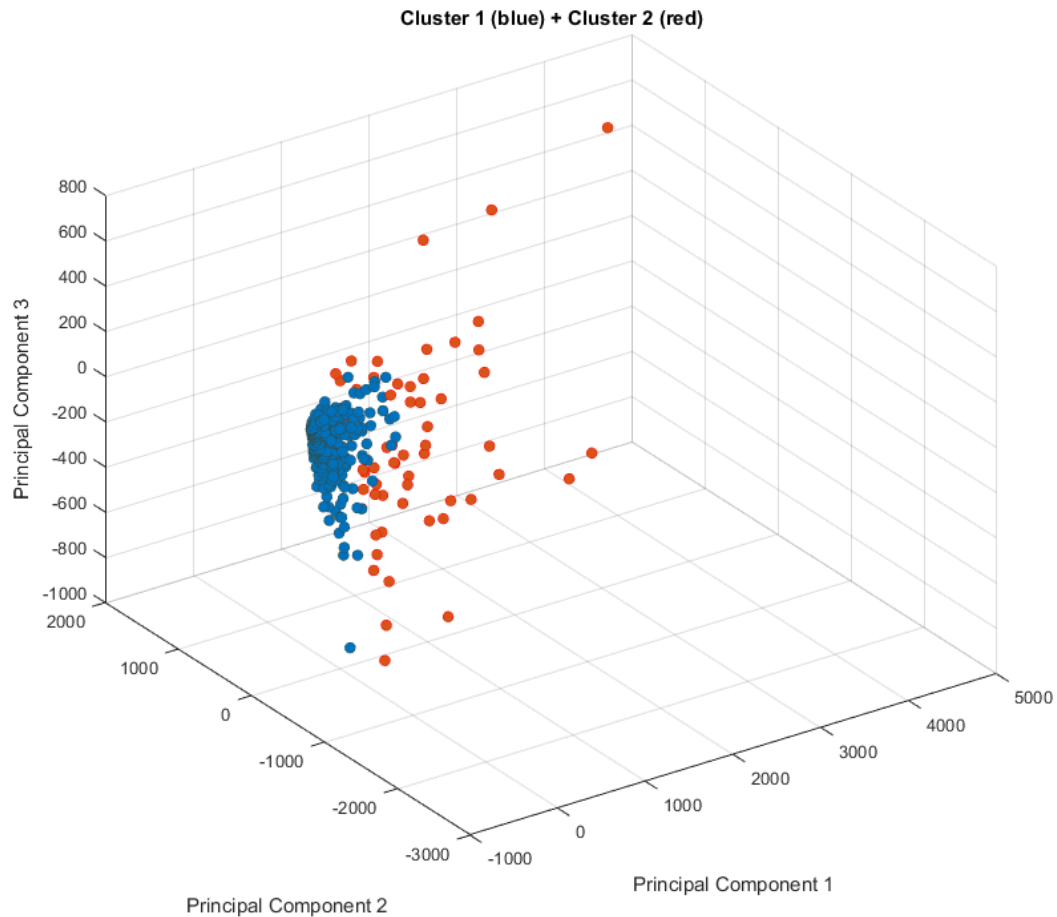
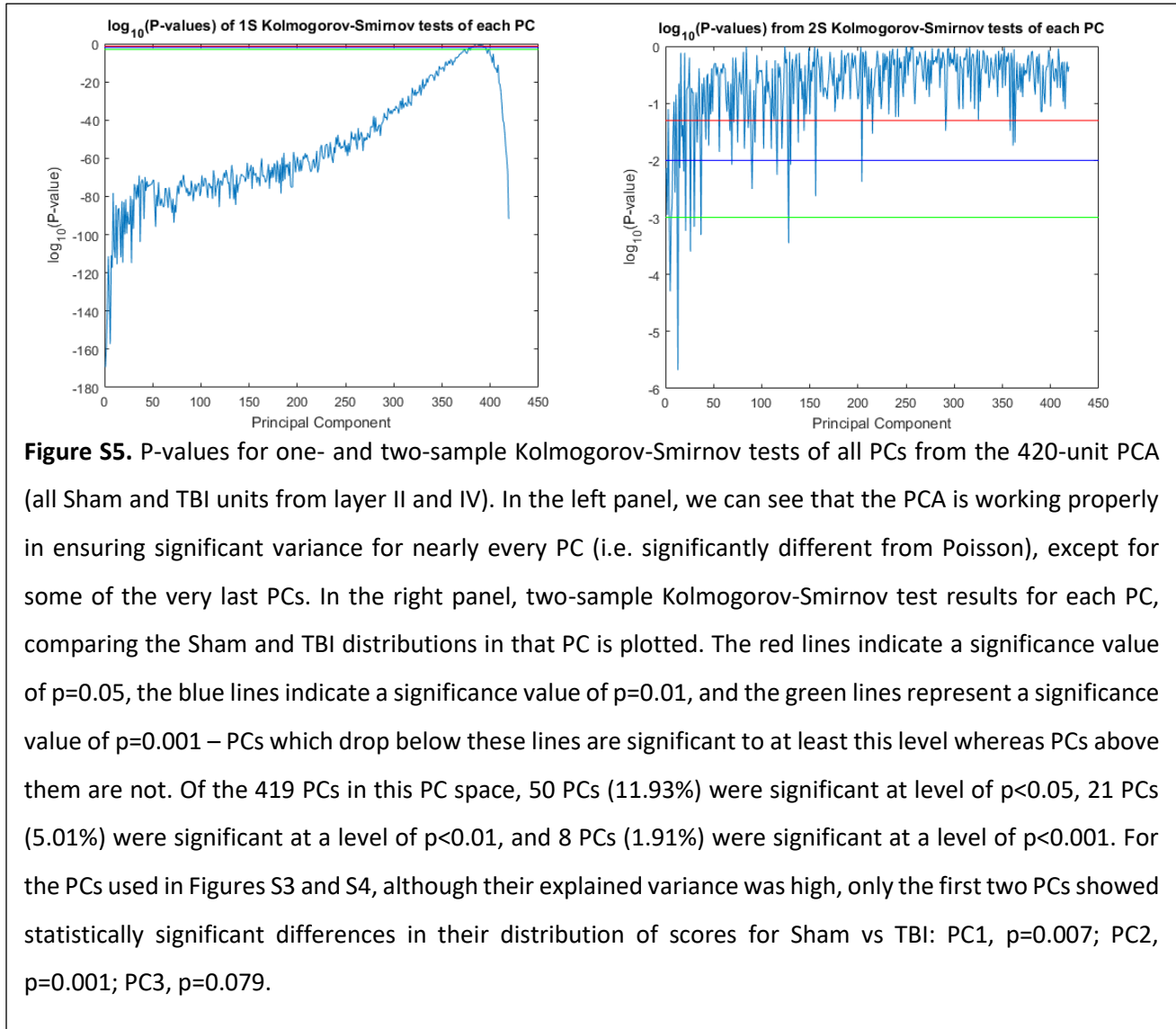


**Figure S4.** All online units from layers II and IV (n=420) plotted in three-dimensional PC space and clustered using k-means, where k=2. Cohen's kappa coefficient = 0.017. The Pearson correlation coefficient between the cluster assignments and the ground truth = 0.023 (p=0.634).

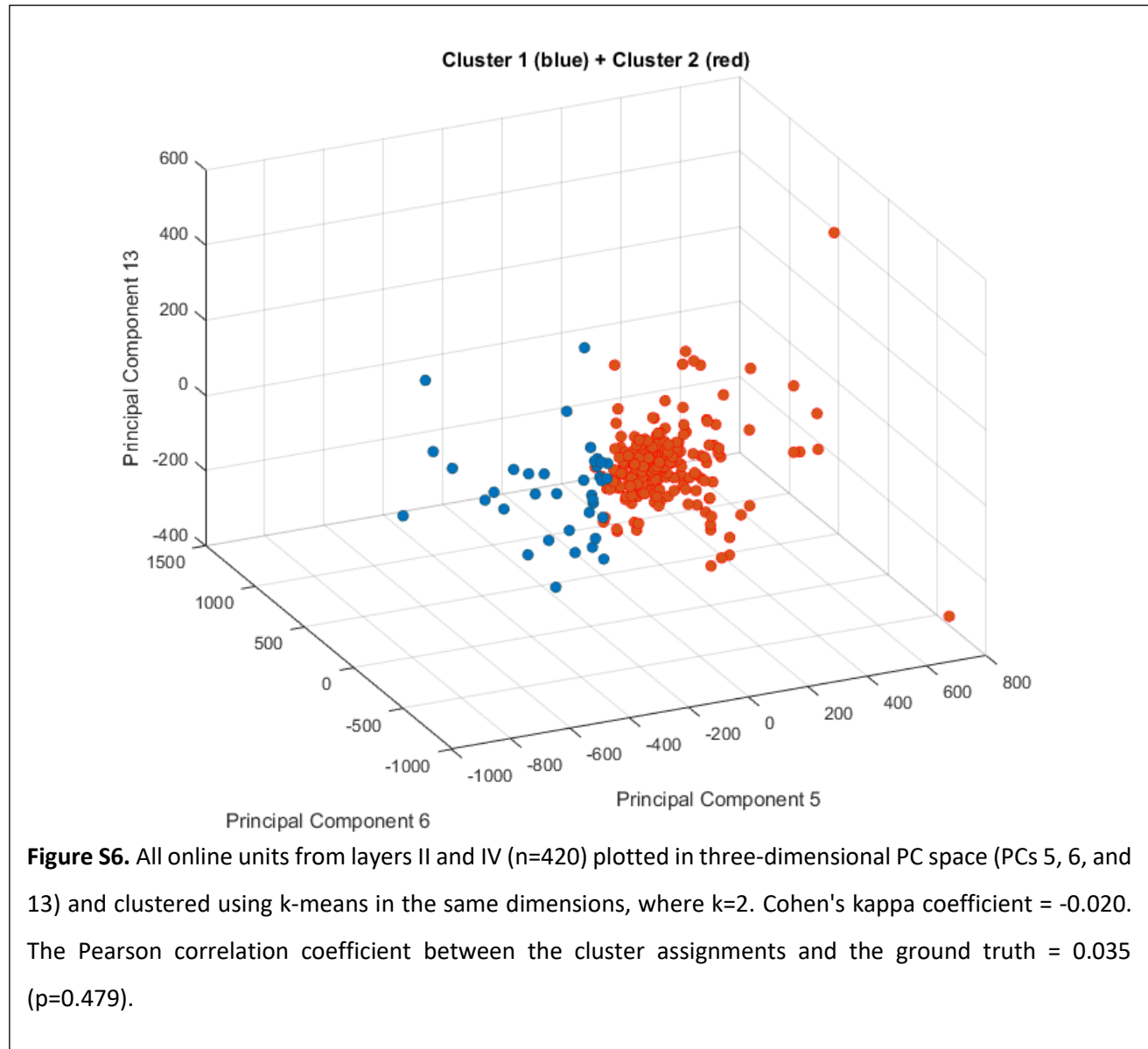
Since the clustering in the new PC space did not perform well (Figure S4; Cohen's kappa coefficient = 0.017), Figure S5 gives us some potential important insights on which other PCs may hold more salient components of variability for the goal of separating Sham and TBI units. shows that while each PC is distributed significantly differently to a Poisson distribution, a minority (n=65; 13%) of the PC distributions are significantly different (p<0.05) between the Sham and TBI conditions. This indicates that while the PCA is doing its job in identifying variance amongst the online units, the vast majority of this variance is not

useful for distinguishing between Sham and TBI conditions or their differing patterns of activity. However, this helps us identify potential PCs of interest for the purposes of future clustering, as mentioned above.



So far, while PCA has reliably reduced the dimensions of the raw firing rate data, it has done so at a cost of salient variability in the context of separating Sham and TBI units from one another. These problems might be solved by including more PCA dimensions, however doing so comes at a cost of transparency and clarity, as well as making later analyses more complicated. To avoid this “curse of dimensionality” problem (which PCA is traditionally employed to solve in the first instance), we will attempt another clustering in the PC space, but this time choose PCs which show the most significant different distributions differences between Sham and TBI according to the two-sample Kolmogorov-Smirnov tests. These PCs are

(in decreasing order of explained variability) PC5 ( $p=5.06 \times 10^{-5}$ ), PC6 ( $p=9.39 \times 10^{-4}$ ), and PC13 ( $p=2.10 \times 10^{-6}$ ). The resultant clustering is shown in Figure S6.



Unfortunately, and although the separability seems visually clearer in Figure S6, the clustering agreement metrics based on the results from clustering with PCs 5, 6, and 13 were only marginally better than those for PCs 1, 2, and 3 (Cohen's kappa coefficient difference =  $0.003$ ; Pearson correlation coefficient difference =  $0.012$  ( $p$ -value difference =  $-0.155$ ), despite each of these PCs being highly significantly different in their distributions of Sham and TBI units. This is still an impressive result, since PCs 5, 6, and 13 collectively account for only 7.27% of the total original variance whereas PCs 1, 2, and 3

collectively account for 44.57% of the total original variance. This highlights very strongly, then, that it is a specific and complex subset of the overall unit activity variability on a raw scale which accounts for the differences between Sham and TBI units. One last method to attempt, but which is not plottable, is to perform the clustering with more than three PCs. Table S3 presents the clustering results for higher numbers of PC dimensions using k-means clustering, where  $k=2$ , and all clustering is repeated 50 times.

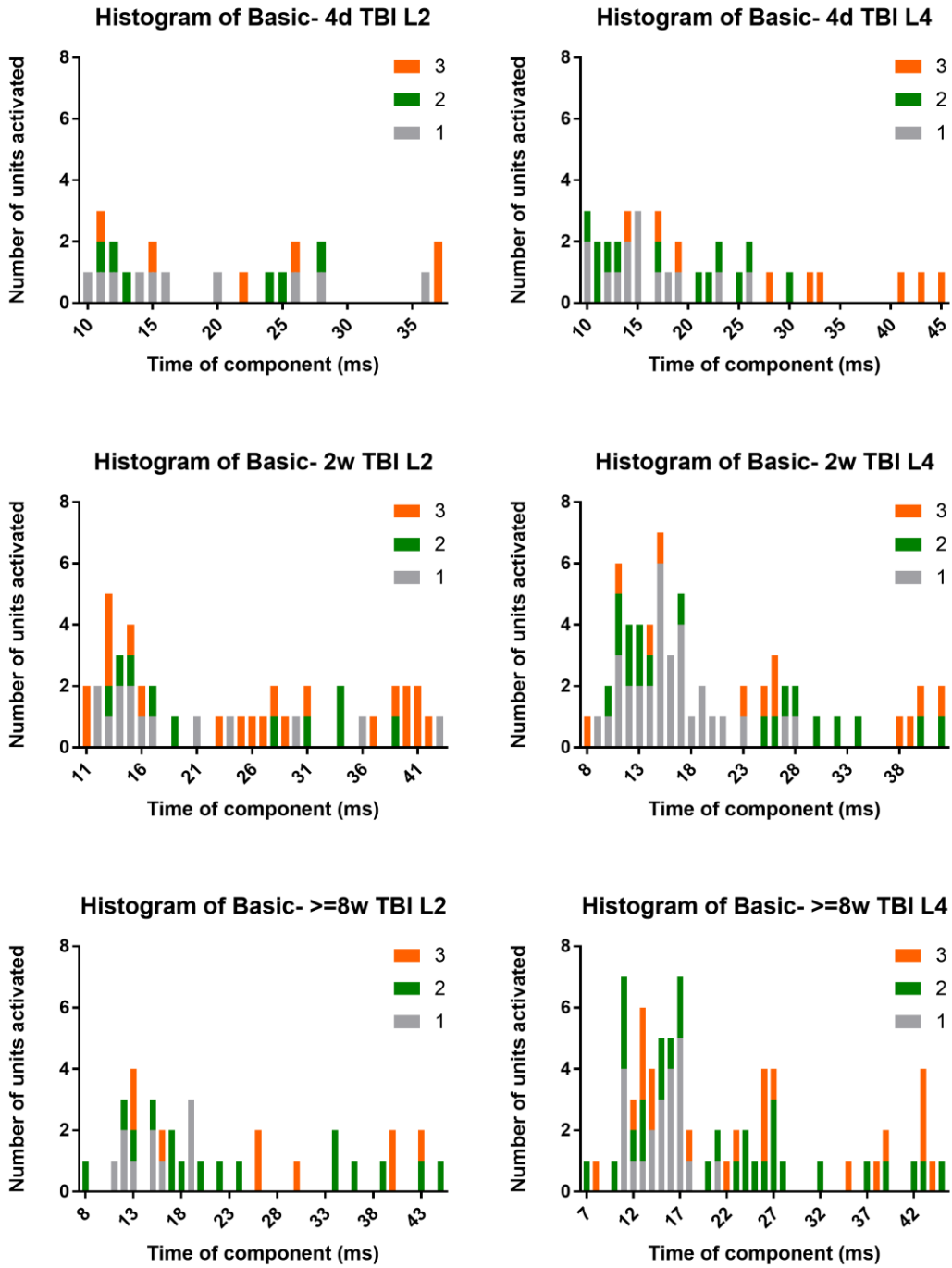
<b>Table S3.</b> Evaluation of high-dimensional clustering results for successfully distinguishing between Sham and TBI units.			
<i>PCs used</i>	<i>Total explained variance</i>	<i>Cohen's <math>\kappa</math> coefficient</i>	<i>Pearson's <math>R</math> (<math>p</math>-value)</i>
PC1-PC5	55.36%	0.002	0.003 ( $p=0.960$ )
PC1-PC10	62.44%	0.011	0.016 ( $p=0.742$ )
PC1-PC15	67.55%	0.011	0.016 ( $p=0.742$ )
PC1-PC20	70.31%	0.007	-0.009 ( $p=0.849$ )
PC1-PC25	73.13%	0.007	0.009 ( $p=0.849$ )
PC1-PC50	82.75%	0.011	0.016 ( $p=0.742$ )
PC1-PC100	91.83%	0.007	-0.009 ( $p=0.849$ )
PC1-PC200	98.31%	0.007	-0.009 ( $p=0.849$ )
8PCs with highly significant ( $p<0.001$ ) two-sample KS tests (see Figure S6)	9.24%	0.024	-0.042 ( $p=0.387$ )
29PCs with very significant ( $p<0.01$ ) two-sample KS tests (see Figure S6)	98.42%	0.011	0.016 ( $p=0.742$ )
79PCs with significant ( $p<0.05$ ) two-sample KS tests (see Figure S6)	99.78%	0.015	-0.024 ( $p=0.631$ )

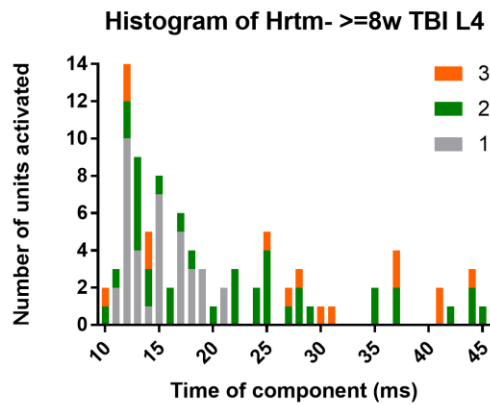
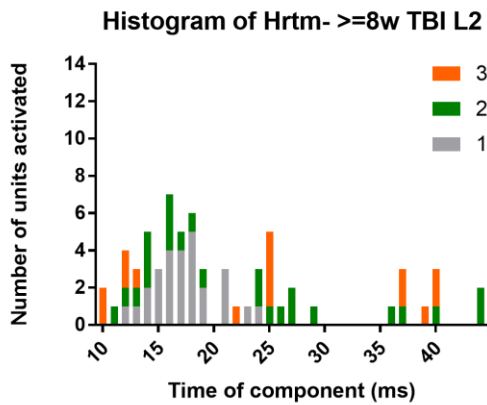
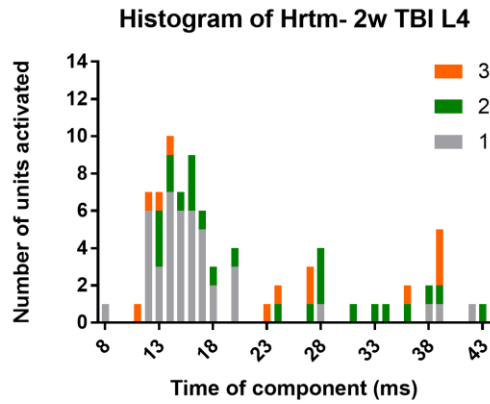
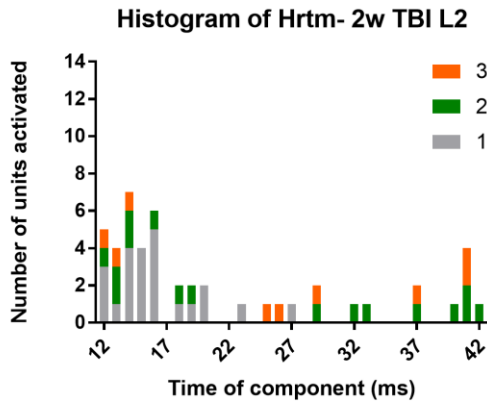
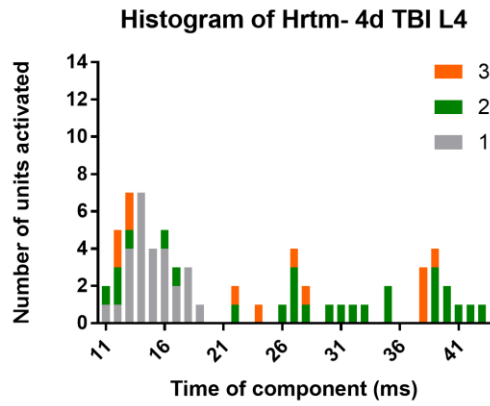
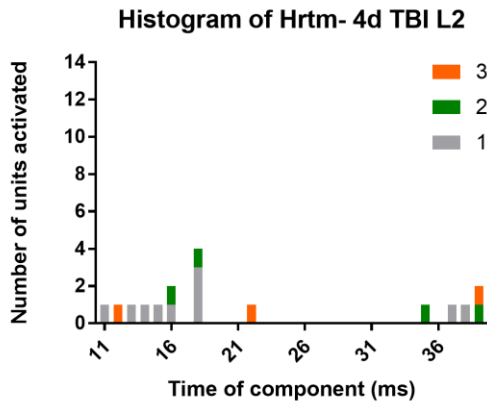
The best separations of Sham and TBI units were found for combinations of high-dimensional PC space where scores for Sham and TBI units in the individual PCs had been shown previously (see Figure S4) to be significantly differently distributed according to two-sample Kolmogorov-Smirnov tests.

However, even the best of these results had low agreement (Cohen's  $\kappa$  coefficient = 0.024) and correlation (-0.042,  $p=0.387$ ) with the ground truth categories of Sham and TBI units. This suggests that despite PCA identifying some regions of the high-dimensional variability space in raw unit activities which have significantly different scores for Sham and TBI units, such PCs – calculated from the raw activities alone (without the prior identification and statistical description of features) – are insufficient to reliably separate Sham and TBI unit activities.

This, combined with the fact that the PCs are difficult to interpret, led to our decision not to base the main unit activity pattern analyses on PCA but rather the combination of the local maxima-based method and graph theoretic method described in the main text.

## 5.2 Appendix II – Time distributions of peak-based TBI components





## 5.1 Appendix III – MATLAB implementation of graph theoretic analysis

```
function [G] = graph_of_2d_array(unit);
% creates an unweighted graph of a 2d array with starting node and ending
nodes, connected to
% the first and last rows of the array, respectively (for purposes of Dijks-
tra's algorithm)

% create adjacency matrix with nodes = elems of matrix, and connect all
% numerical neighbours and up/down and diagonally (per heatmap matrix)
elems = numel(unit);
dims = size(unit);
row_scale = dims(1)/dims(2)*100;
col_scale = dims(2)/dims(1);
graph_conn = zeros(elems) + diag([repmat(row_scale,elems-1,1)],1) +
diag([repmat(row_scale,elems-1,1)],-1) + diag([repmat(row_scale*col_scale,el-
ems-50,1)],50) + diag([repmat(row_scale*col_scale,elems-50,1)],-50) +
diag([repmat(row_scale*4,elems-49,1)],49) + diag([repmat(row_scale*4,elems-
49,1)],-49) + diag([repmat(row_scale*4,elems-51,1)],51) + diag([rep-
mat(row_scale*4,elems-51,1)],-51);

% remove edges joining opposite sides of matrix ('cut the cylinder')
unit_dims = size(unit);
for K = unit_dims(1):unit_dims(1):elems
graph_conn(K,K+1) = 0; % remove end-to-end joining, e.g. if unit_dims(1)=
50, then remove 50-51
graph_conn(K+1,K) = 0;
try
graph_conn(K-49,K-50) = 0; % (mirror)
graph_conn(K-50,K-49) = 0;
graph_conn(K+1,K-50) = 0; % remove end-to-end diagonals,
% e.g. if unit_dims(1)= 50, then remove 101-50
graph_conn(K-50,K+1) = 0;
graph_conn(K,K-49) = 0; % (mirror)
graph_conn(K-49,K) = 0;
catch
fprintf('Error cutting 'cylinder' graph for this unit')
continue
end
end

graph_conn(1,50) = 0; graph_conn(50,1) = 0;
graph_conn = graph_conn(1:elems,1:elems); % remove phantom nodes

% create start and end nodes
start_node = elems+1;
end_node = elems+2;
graph_conn(start_node,1:unit_dims(1)) = 1; % start node
graph_conn(1:unit_dims(1),start_node) = 1;
graph_conn(end_node,elems-unit_dims(1):elems) = 1; % end node
graph_conn(elems-unit_dims(1):elems,end_node) = 1;

% make directed graph
G = digraph(graph_conn);

end
```

```

sets = {'L4-Hartmann-sham','L4-Basic-sham','L4-Basic-tbi','L2-Hartmann-
sham','L2-Hartmann-tbi','L2-Basic-sham','L2-Basic-tbi'};

for set = 1:length(sets)
    data = sets{1,set};
    dashes = strfind(data,'-');
    layer = data(1:2);
    health = data(dashes(2)+1:end);
    type = data(dashes(1)+1:dashes(2)-1);

    events = eval([layer,health,'EventSummary_',type]);
    name_col = set;
    figDir = ['figures\'',layer,'\'];

    for K = 1:length(events(:,1,1))
        unit = events(K, :, :);
        unit = squeeze(unit);
        unit = unit*20;
        len = numel(unit);

        try
            % create graph and weight edges
            [G] = graph_of_2d_array(unit);
            plot(G) % optional
            weights = abs(unit/max(max(unit)) - 1) * 100; % normalise
            weights(weights==0) = 1; % turn 0s into 1s
            weights = reshape(weights,1,len);

            % assign weights to graph
            dest_nodes_list = G.Edges.EndNodes(:,2);
            for node = 1:len
                G.Edges.Weight(dest_nodes_list==node) = weights(node);
            end

            % use Dijkstra's algorithm to find shortest path
            [path1,d1] = shortestpath(G,len+1,len+2,'method','positive');

            % find 'second' shortest path
            weights(path1(2:end-1)) = path1(2:end-1) + 1000; % add arb large
            weights to nodes from 'first' shortest path
            for node = 1:len
                G.Edges.Weight(dest_nodes_list==node) = weights(node);
            end
            [path2,d2] = shortestpath(G,len+1,len+2,'method','positive'); %
            find path

            % find 'third' shortest path
            weights(path2(2:end-1)) = path2(2:end-1) + 1000; % add arb large
            weights to nodes from 'second' shortest path
            for node = 1:len
                G.Edges.Weight(dest_nodes_list==node) = weights(node);
            end
            [path3,d3] = shortestpath(G,len+1,len+2,'method','positive'); %
            find path
        end
    end
end

```

```
    paths1{set,K,:} = path1;
    paths2{set,K,:} = path2;
    paths3{set,K,:} = path3;

    dists1(set,K,:) = d1;
    dists2(set,K,:) = d2;
    dists3(set,K,:) = d3;
catch
    fprintf(['Error for: set ',set,', unit ',num2str(K)])
    continue
end

end

clear weights

end

dijkstra_analysis = {{paths1,paths2,paths3},{dists1,dists2,dists3}};
```